# Late Quaternary Paleoseismology of the West Valley Fault Zone—Insights from the Baileys Lake Trench Site

by Michael D. Hylland[1], Christopher B. DuRoss[1], Greg N. McDonald[1], Susan S. Olig[2],
Charles G. Oviatt[3], Shannon A. Mahan[4], Anthony J. Crone[5], and Stephen F. Personius[4]

[1] Utah Geological Survey, Salt Lake City, Utah
[2] URS Corporation, Oakland, California
[3] Kansas State University, Manhattan, Kansas
[4] U.S. Geological Survey, Denver, Colorado
[5] U.S. Geological Survey, retired

# CONTENTS

# FIGURES

## TABLES

## PLATE

# Late Quaternary Paleoseismology of the West Valley Fault Zone—Insights from the Baileys Lake Trench Site

*by Michael D. Hylland, Christopher B. DuRoss, Greg N. McDonald, Susan S. Olig, Charles G. Oviatt, Shannon A. Mahan, Anthony J. Crone, and Stephen F. Personius*

## ABSTRACT

The West Valley fault zone (WVFZ) and the Salt Lake City segment (SLCS) of the Wasatch fault zone comprise Holocene-active normal faults that bound an intrabasin graben in northern Salt Lake Valley, Utah, and have evidence of recurrent, large-magnitude (M ~6–7) surface-faulting earthquakes. Despite significant progress in our understanding of earthquake hazards along the Wasatch Front, outstanding research questions in Salt Lake Valley include the timing, displacement, and recurrence of Holocene earthquakes on the WVFZ and northern SLCS, and whether the WVFZ is seismically independent of, or moves coseismically with, the SLCS. To improve paleoseismic data for the WVFZ and better understand the seismogenic relation between the WVFZ and SLCS, we conducted a fault-trench investigation at the Baileys Lake site and compared earthquake timing and displacement data with data from the SLCS, including new data from the Penrose Drive site on the northern SLCS.

The Baileys Lake site is near the northern end of the westernmost traces of the WVFZ, collectively referred to as the Granger fault. At this site, we excavated three trenches across two small (<1-m-high) east-facing fault scarps. At least four surface-faulting earthquakes postdate deposition of Lake Bonneville highstand clay at ~19 ka: earthquake BL4 occurred at $15.7 \pm 3.4$ ka (2σ), and was a sublacustrine event (Provo phase); BL3 occurred at $13.0 \pm 1.1$ ka, after Lake Bonneville's regression to very low levels and before transgression of the Gilbert-episode lake across the site; and BL2 and BL1 occurred at $12.3 \pm 1.1$ ka (during the Gilbert episode) and $5.5 \pm 0.8$ ka (post-Gilbert), respectively. Average per-event vertical displacement for the Granger fault at the Baileys Lake site is $0.5 \pm 0.1$ m. Combining the Baileys Lake data with previous paleoseismic data yields a paleoearthquake chronology comprising six late Quaternary earthquakes for the WVFZ as a whole (W1–W6): five on the Granger fault and one (W2) on the Taylorsville fault (eastern trace of the WVFZ). Mean recurrence over different time intervals ranges from 3.6 to 5.4 kyr for the Granger fault, and from 2.0 to 3.6 kyr for the WVFZ as a whole. The variability in recurrence intervals may result from differences in surface-faulting activity on the numerous strands that make up the fault zone, as well as from a paleo-seismic record that is likely incomplete due to the small number of sites where earthquake timing has been documented.

Several WVFZ earthquakes have times that are similar to those of SLCS earthquakes. Specifically, the mean earthquake times and two-sigma ranges for WVFZ earthquakes W1, W2, W3, W4, and W6 are similar to those of SLCS earthquakes S1, S2, S4, S8, and S9, respectively. Earthquake W5 lacks a clear temporal association with a SLCS earthquake. However, W5 occurred in the latest Pleistocene (~13 ka), a period in which the SLCS record may be incomplete. Although earthquake-timing uncertainties preclude determining an unequivocal coseismic link between the WVFZ and SLCS, our results suggest that large earthquakes on the WVFZ that are coseismic with or triggered by fault movement on the SLCS have a higher likelihood than WVFZ earthquakes that occur completely independent of movement on the SLCS. When considered together with mechanical and geometric models of the fault system, the paleoseismic data support a high likelihood for synchronous rupture of the WVFZ with the SLCS.

## INTRODUCTION

### Purpose and Scope

The West Valley fault zone (WVFZ) and the Salt Lake City segment (SLCS) of the Wasatch fault zone comprise Holocene-active normal faults that together form an intrabasin graben in the northern part of Salt Lake Valley (figures 1, 2, and 3). These faults trend through the most densely populated part of Utah and have evidence of recurrent, large-magnitude (M ~6–7) surface-faulting earthquakes, but because of urbanization, have received limited paleoseismic study. At the time of this investigation there were significant questions regarding the paleoseismic histories of both faults, including (1) the timing of Holocene earthquakes on the WVFZ and northern SLCS (previous SLCS paleoseismic data were limited to the southern of three subsections of the fault segment), (2) the timing, recurrence, and displacement of mid-Holocene to latest Pleistocene earthquakes on both faults, and (3) whether the WVFZ is seismically independent of or ruptures coseismically with
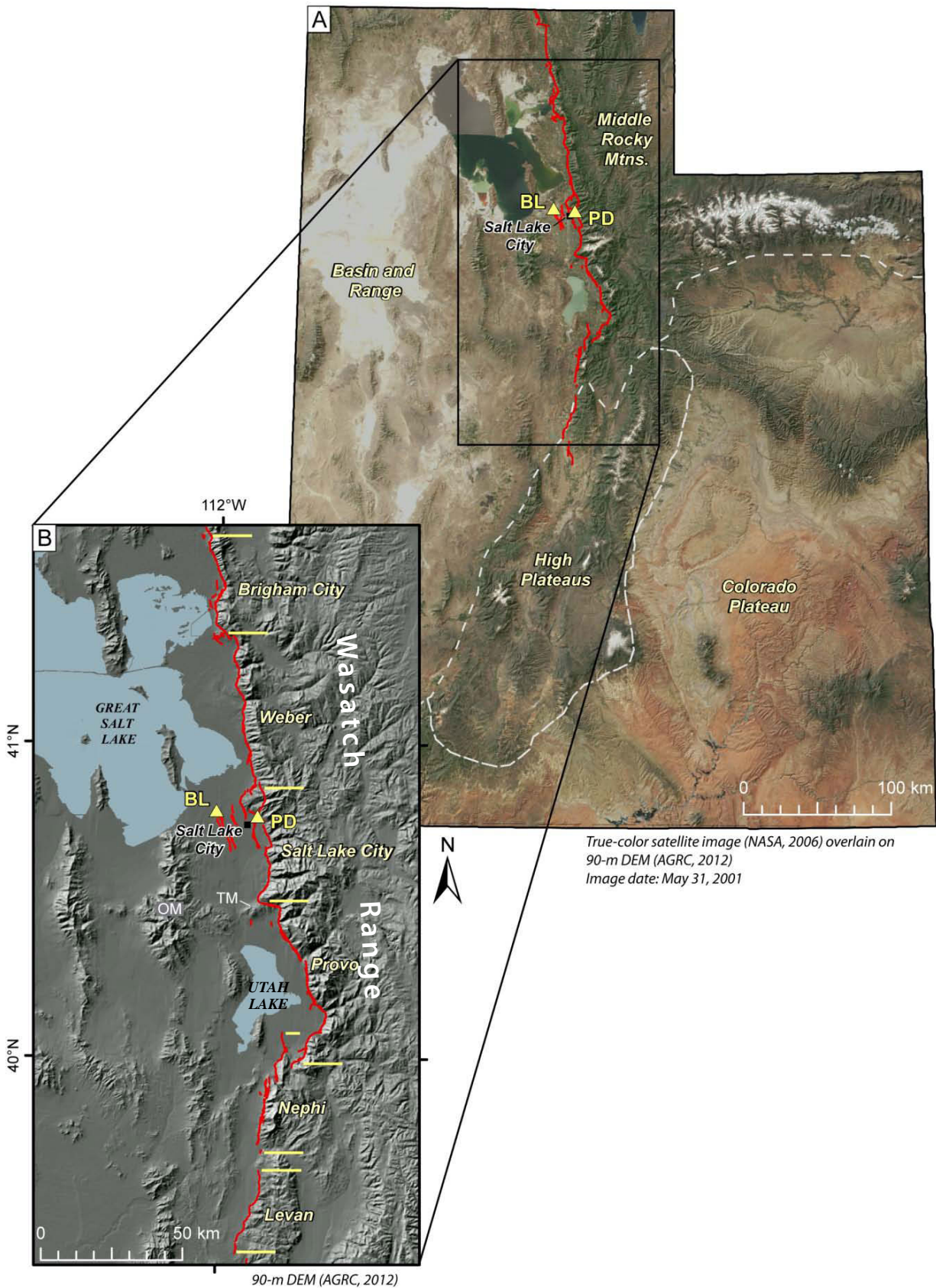
*Figure 1. Regional setting of the Wasatch and West Valley fault zones. A. Physiographic provinces of Utah, and the Wasatch and West Valley fault zones (red lines). BL, Baileys Lake trench site on the West Valley fault zone (this study); PD, Penrose Drive trench site on the Wasatch fault zone (DuRoss and others, 2014). B. Central segments of the Wasatch fault zone, and West Valley fault zone west of the Salt Lake City segment, showing locations of the Baileys Lake and Penrose Drive trench sites. OM, Oquirrh Mountains; TM, Traverse Mountains. Fault traces from Black and others (2003).*

the SLCS. Understanding these fault characteristics is necessary for quantifying the seismic hazard of the central Wasatch Front.

To improve the quality and resolution of paleoseismic data for the WVFZ and SLCS, as well as our understanding of the seismogenic relation between them, the Utah Geological Survey (UGS) and USGS conducted fault-trench investigations at two sites—one on the WVFZ (Baileys Lake site) and one on the SLCS (Penrose Drive site) (figures 2 and 3). These investigations included (1) detailed topographic and geologic mapping of the trench sites, (2) scarp profiling, (3) excavating five trenches—three at Baileys Lake and two at Penrose Drive, (4) mapping the trench-wall exposures in detail, (5) sampling organic remains and fine-grained detrital sediment for radiocarbon and luminescence dating, respectively, (6) developing probabilistic models of earthquake times using Ox-Cal software, and (7) determining earthquake chronologies, vertical displacement, recurrence, and fault slip rate.

This report presents data and results from the Baileys Lake site. Data and results from the Penrose Drive site on the SLCS are presented in the companion report (DuRoss and others, 2014) in this UGS Special Study. These two reports supersede the initial release of the study results in a Final Technical Report to the USGS (DuRoss and Hylland, 2012). Together, the new data from the Baileys Lake and Penrose Drive sites improve our understanding of earthquake behavior and interaction on the WVFZ and SLCS, and ultimately allow for a more accurate assessment of earthquake probabilities and hazard for the central Wasatch Front.

## Geologic Setting

Salt Lake Valley occupies one of several north-south trending grabens at the eastern margin of the actively extending Basin and Range Province. The Wasatch Range and Oquirrh Mountains bound the valley on the east and west, respectively; Great Salt Lake lies to the north, and the east-west trending Traverse Mountains separate Salt Lake Valley from Utah Valley to the south (figure 1). Two Quaternary geologic features that have been particularly important in producing the modern physiography of the region are the Wasatch fault zone and late Pleistocene Lake Bonneville.

The Wasatch fault zone is the longest active normal-slip fault in the western United States and the most active fault in Utah, forming the structural boundary between the actively extending Basin and Range Province and the relatively more stable Middle Rocky Mountain and Colorado Plateau provinces. Extending 350 km from southern Idaho to central Utah, the Wasatch fault zone comprises 10 segments, each of which is thought to be seismogenically independent (Swan and others, 1980; Schwartz and Coppersmith, 1984; Machette and others, 1992; Wheeler and Krystinik, 1992). The SLCS, one of the central five segments
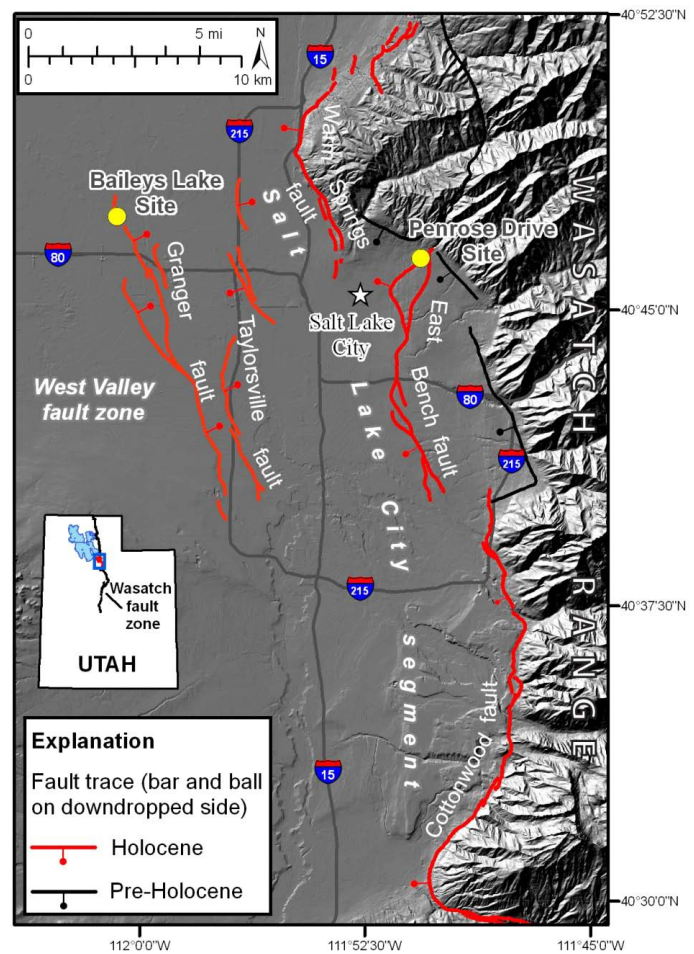


*Figure 2. The West Valley fault zone comprises two strands on the floor of northern Salt Lake Valley: the Granger and Taylorsville faults. The Salt Lake City segment, one of the central, most active segments of the Wasatch fault zone, comprises three strands along the base of the Wasatch Range: the Warm Springs, East Bench, and Cottonwood faults. In 2010, the UGS conducted fault trenching studies at the Baileys Lake site at the north end of the Granger fault (this study), and also at the Penrose Drive site at the north end of the East Bench fault (DuRoss and others, 2014).*

of the Wasatch fault zone that have evidence of repeated Holocene earthquakes (Machette and others, 1992), generally forms the eastern margin of Salt Lake Valley. Since the mid-Holocene (~6.5 ka), surface-faulting earthquakes on individual segments of the Wasatch fault zone have occurred on average every 1300–2500 years, and average vertical slip rates range from about 0.5 to 2.2 mm/yr (Machette and others, 1992; Friedrich and others, 2003; Lund, 2005).

Climatic conditions during the Pleistocene were conducive to the episodic formation of pluvial lakes in the eastern Great Basin, and Lake Bonneville was the most recent and largest of these (Gilbert, 1890). Details of Lake Bonneville's history are the subjects of ongoing research, but the general record of the rise and fall of the lake is well established. As summarized by Currey (1990) and Oviatt and others (1992) and recently updated by Godsey and others (2005, 2011), Oviatt and others

(2005), Benson and others (2011), and Miller and others (2013), the Bonneville lake cycle began around 30 ka. Over time, the lake rose and eventually reached its highest level at the Bonneville shoreline (~1550 m [5090 ft]) shortly before 18 ka. At the Bonneville highstand level, lake water overflowed the Bonneville basin threshold at Zenda in southeastern Idaho, spilling into the Snake–Columbia River drainage basin.

The Zenda threshold failed catastrophically at about 18 ka, resulting in a rapid drop in lake level of approximately 110 m during the Bonneville Flood (O'Connor, 1993). The lake level stabilized when erosional downcutting was impeded by a bedrock-controlled threshold at Red Rock Pass, about 2.5 km south of Zenda, or possibly about 9 km farther south near Swan Lake (Janecke and Oaks, 2011). Lake Bonneville remained at or near this level until about 15 or 16 ka (Godsey and others, 2005, 2011; Miller and others, 2013), forming the Provo shoreline (~1450 m [4760 ft]).

A climatic change to warmer and drier conditions caused the lake to regress rapidly from the Provo shoreline to near desiccation levels by the end of the Pleistocene (Eardley, 1962; Currey and others, 1988b; Currey, 1990). A small rise in lake level to an elevation of 1295 m (4250 ft) marked the Gilbert episode, which culminated around

11.6 ka (Oviatt and others, 2005; Oviatt, 2014), after which the lake regressed to near modern Great Salt Lake levels (historical average elevation 1280 m [4200 ft]). As a whole, the remarkable stratigraphic and geomorphic records of Lake Bonneville have proven extremely valuable in reconstructing paleoseismic histories of faults in the Bonneville basin, particularly along the central segments of the Wasatch fault zone.

On the floor of northern Salt Lake Valley, the WVFZ consists of intrabasin normal faults that span an area about 16 km long by 1–6 km wide (figure 2). The two subparallel, northwest-trending main traces of the fault zone and their associated subsidiary traces are known as the Granger fault (western traces) and Taylorsville fault (eastern traces). Both faults have scarps on post-Bonneville lake cycle (latest Pleistocene to Holocene) lacustrine and alluvial deposits, and previous paleoseismic studies have documented multiple Holocene surface-faulting earthquakes (Keaton and others, 1987; Keaton and Currey, 1989). The scarps are typically about 0.5–1.5 m high, but have a maximum height of 6 m near the southern end of the Granger fault. Scarps on the Granger fault face east, and scarps on the Taylorsville fault face both east and west. As a whole, the WVFZ is considered to be an antithetic structure to the west-dipping SLCS, with the SLCS acting as the master or controlling fault (figure 3).
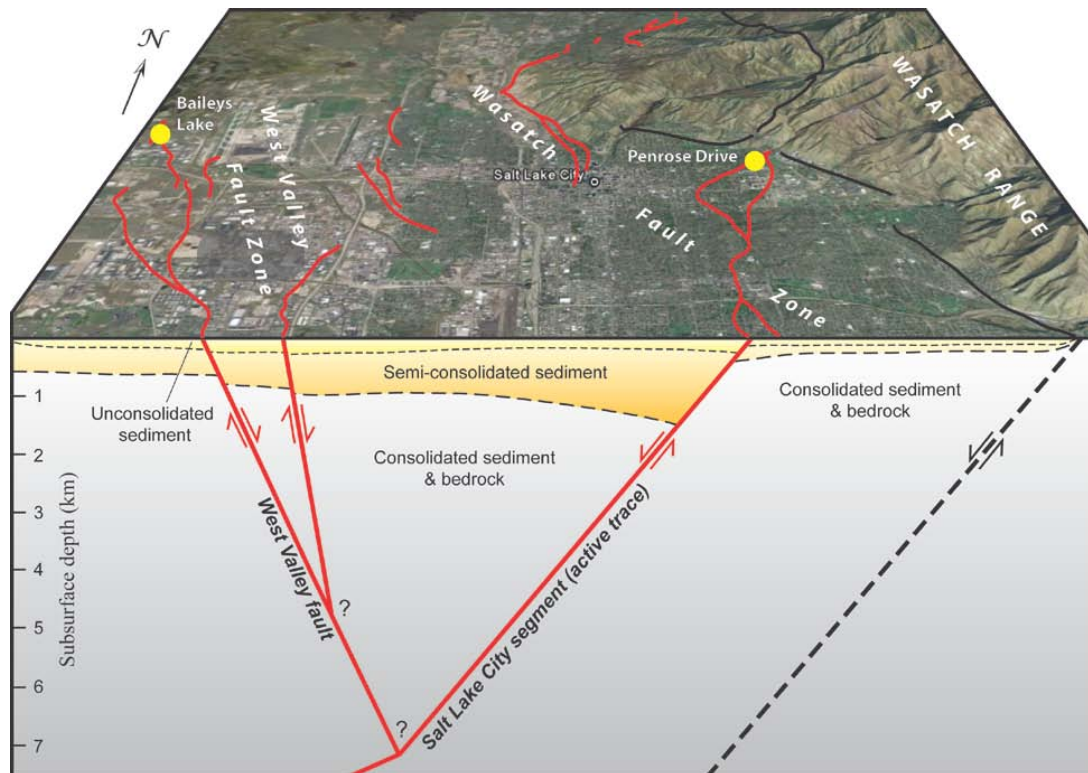


**Figure 3.** *Generalized schematic diagram of likely subsurface geometry of the Wasatch–West Valley fault system, based largely on figure 1 of Bruhn and Schultz (1996). The West Valley fault zone is antithetic to the west-dipping Salt Lake City segment (master fault), forming an intrabasin graben in northern Salt Lake Valley. Mapped fault traces from Black and others (2003), superimposed on a Google Earth image. Map scale varies; no vertical exaggeration implied.*

## Previous Studies of the West Valley Fault Zone

Previous studies have constrained the long-term (140 kyr) cumulative displacement and slip rate for the WVFZ, but timing and displacement data for individual surface-faulting earthquakes have been lacking. Previous detailed paleoseismic investigations of the WVFZ include those of Keaton and others (1987) and Keaton and Currey (1989) (figure 4). On the Granger fault, Keaton and others (1987) investigated two sites on the southern part of the fault where they excavated two trenches, drilled 10 boreholes, and supplemented these data with 1:24,000-scale geomorphic mapping of key sites on both the Granger and Taylorsville faults. Their study also included thermoluminescence (four samples) and amino acid racemization (three samples) dating of mostly pre-Bonneville-cycle lacustrine deposits. In a follow-up study, Keaton and Currey (1989) drilled a total of 24 boreholes at three sites on the northern part of the Granger fault. The trenches revealed discrete, planar faulting, but yielded no individual earthquake timing data and only minimum values of per-event displacement. The boreholes indicated cumulative vertical displacements of 0.7–3 m offset on "post-Bonneville" (<12 ka) deposits, 5–7 m of offset on Bonneville lake-cycle deposits (12–28 ka), and 13–14 m of offset on a paleosol developed on Cutler Dam (pre-Bonneville) lake-cycle deposits (60 ± 20 ka). Significantly, Keaton and others (1987) found no evidence of differential displacements within Bonneville lake-cycle sediments in their boreholes near the south end

of the Granger fault, which they interpreted as indicating a period of tectonic quiescence on this part of the fault during Lake Bonneville time. On the Taylorsville fault, Keaton and others (1987) excavated four trenches at two locations near the middle and at the south end of the fault. These trenches showed evidence for mostly monoclinal folding with minor discrete faulting in near-surface sediments. At the site near the middle of the fault, Keaton and others (1987) determined that post-Gilbert deposits (<12 ka) were vertically offset 1.2–1.5 m by a single surface-faulting earthquake.

Two trenches excavated by consultants have yielded useful earthquake timing data for the WVFZ where the UGS was able to sample organic sediment for radiocarbon dating (figure 4). A trench on the Granger fault yielded a radiocarbon age that suggests a surface-faulting earthquake occurred around 1.4 ka (unpublished UGS data; appendix H), and a trench on the Taylorsville fault yielded radiocarbon ages that suggest a surface-faulting earthquake occurred around 2.2 ka (Solomon, 1998; appendix H). The dating results suggest a similarity in the times of these WVFZ earthquakes and the two most recent surface-faulting earthquakes on the SLCS (around 1.3 and 2.2 ka; see DuRoss and others, 2014). However, these trenches were open only briefly, precluding detailed logging, so the geologic context of the samples is not well defined. Because of this, as well as the nature of the radiocarbon ages (apparent mean residence time [AMRT] ages from bulk-soil
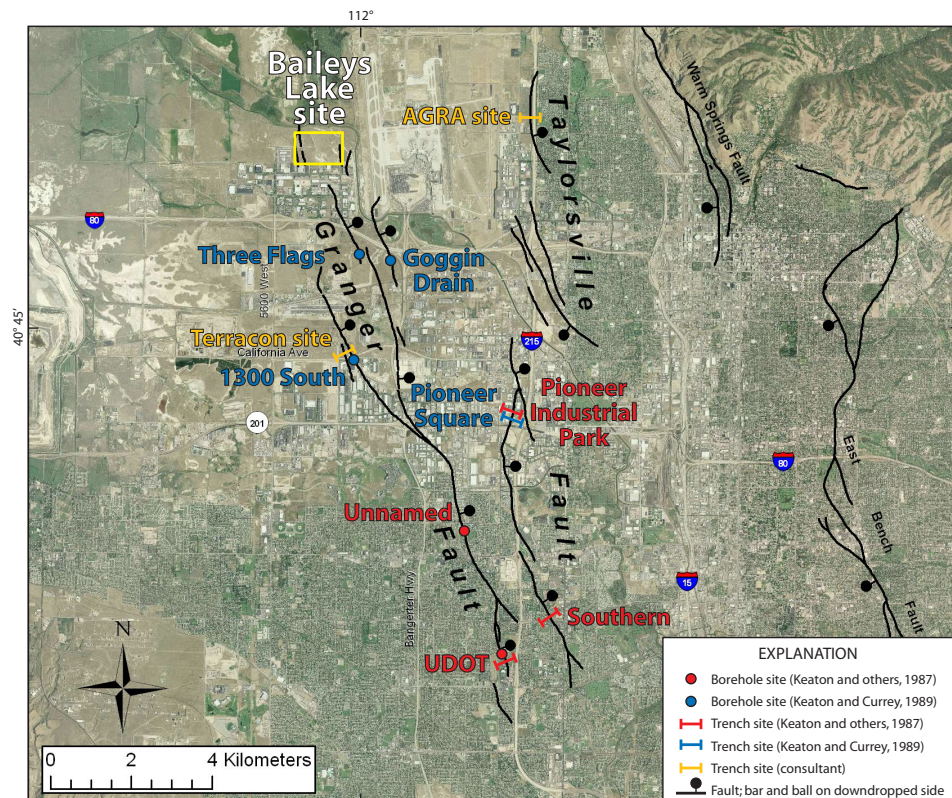


**Figure 4.** *Locations of West Valley fault zone borehole and trench sites evaluated by paleoseismic investigations of Keaton and others (1987) and Keaton and Currey (1989), and the Baileys Lake trench site (this study; see figure 5). Also shown are locations of consultants' trenches that yielded earthquake timing information. Base is high-resolution (1 ft) orthophoto (2009; National Agriculture Imagery Program).*

samples), relatively large uncertainty exists in the relation between the radiocarbon ages and earthquake timing.

## OVERVIEW AND METHODS

Units of measurement in this report are generally in the metric (SI) system; however, we report shoreline elevations in terms of both meters and feet above mean sea level (AMSL) to facilitate their use with USGS 7.5-minute quadrangle maps. Elevations of shorelines near the Baileys Lake site have not been adjusted for isostatic rebound, as most or all of the rebound associated with the regression of Lake Bonneville would have taken place by the time these basin-floor shorelines formed (e.g., Oviatt and others, 1992; Miller and others, 2013). All ages in this report are in calendar-calibrated kilo-annum (thousand years; ka). Lastly, the rise and fall of lake water during the Gilbert episode has been variously assigned as the latest and lowest lake-level rise of Lake Bonneville (e.g., Oviatt, 1997; Oviatt and others, 2001) or the earliest and highest lake-level rise of Great Salt Lake (e.g., Currey, 1990; Oviatt and others, 1992, 2005). Herein, we follow the convention of Oviatt (2014) and consider the Gilbert to be a separate lake episode in the Bonneville basin—it was about 1500 yr younger than the post-Provo-shoreline regression of Lake Bonneville, but was higher and less saline than Holocene Great Salt Lake.

### Trench Investigations

We identified potential trench sites using (1) fault-trace and surficial-geologic mapping by Keaton and others (1987), Keaton and Currey (1989), Personius and Scott (1992), and S.S. Olig (written communication, June 2008); (2) our interpretation of 1937 (Agricultural Stabilization and Conservation Service, 1937) and 1970s (low-sun-angle) aerial photographs (Cluff and others, 1970; included in Bowman and others, 2009) and 2006–2009 orthophotography from the National Agricultural Imagery Program (NAIP) (U.S. Department of Agriculture [USDA], 2012; Utah Automated Geographic Reference Center [AGRC], 2012); (3) 2006 1- and 2-m-posting LiDAR data for Salt Lake Valley (AGRC, 2012); and (4) our own field reconnaissance. Discussions and analyses of WVFZ and SLCS paleoseismic data by the Utah Quaternary Fault Parameters Working Group (UQFPWG; e.g., Lund, 2005, 2007) helped guide our decisions regarding trench-site locations. Of several possible sites on the WVFZ, we selected the Baileys Lake site as our preferred trench site because of the relatively undisturbed nature of fault scarps at the site, the potential to document evidence for earthquakes of different ages associated with two different scarps, and access considerations.

The Baileys Lake site, named for a nearby wetland area, is a 0.8-km[2] parcel of vacant Salt Lake City-owned land immediately west of the Salt Lake City International Airport and near the northern end of the mapped trace of the Granger fault. In the vicinity of the site, the Granger fault comprises four subparallel strands that offset fine-grained Lake Bonneville and post-Bonneville deposits (figure 5; plate 1). However, scarps associated with the two easternmost strands are modified by human disturbance and post-faulting erosion and are in restricted and difficult-to-access areas, so we trenched only the two western traces. Although the Baileys Lake site is crossed by a drainage canal, power lines, natural gas and petroleum pipelines, and associated service roads, and has extensive areas of fill, significant portions of the two scarps that cross the site remain unmodified.

We excavated three trenches at the Baileys Lake site in September 2010 to expose fault-related sediments and document vertical displacement on the two traces of the Granger fault at the site. Two trenches crossed the westernmost scarp: a 44-m-long northern trench—designated the West(N) trench—and 10 m to the south, a 21-m-long, parallel, southern trench—designated the West(S) trench. The third trench—designated the East trench—was a 52-m-long trench excavated across the scarp about 0.5 km to the east of the two western trenches (figure 5). Because the site is on the floor of the Great Salt Lake basin, shallow groundwater was a logistical concern for trenching. For planning purposes, we installed two piezometers at the site and monitored groundwater levels on a monthly basis for a year prior to trenching (data available at http://geology.utah.gov/databases/groundwater/site.php?site_id=50). Maximum depth to groundwater ranged from 3.2 to 3.4 m below the ground surface. This depth is lower than typical historical groundwater levels in this area, and was likely a direct reflection of the low level of nearby Great Salt Lake. At the time of our trenching, Great Salt Lake was near its historical lowstand, having a surface elevation of approximately 1278 m based on USGS gage data (Utah Water Science Center: ut.water.usgs.gov/greatsaltlake/elevations/). Our piezometer data provided us with target depths to keep the trench floors above the potentiometric groundwater surface, and helped avoid trench flooding and caving problems. The West(N) trench was about 2 m deep whereas the West(S) trench was locally deepened to 3.3 m to maximize exposure of the fault zone. Shallow groundwater limited the depth of the East trench to 1.5 m.

We used a total station (Trimble TTS 500) to map the trench-wall exposures by measuring the positions of markers (e.g., nails and flagging) along the upper and lower limits of the trench wall and projecting those points to a vertical plane that represented the average orientation of the trench wall. The total station and averaged vertical plane were then used to set up a 1-m square grid on the trench wall, which we used as a reference grid to construct 1:20-scale photomosaics. The fine-grained nature of the exposed deposits and the fine detail visible on the photomosaics allowed us to map stratigraphic contacts and structure on clear acetate overlays using the photomosaics as a base. We mapped the north-facing wall of the West(S) trench, the entire north-facing wall and middle part (area of fault zone) of the south-facing wall of the West(N) trench, and the north-facing wall of the East trench. Plate 1 shows maps and photomosaics of the exposures with a single
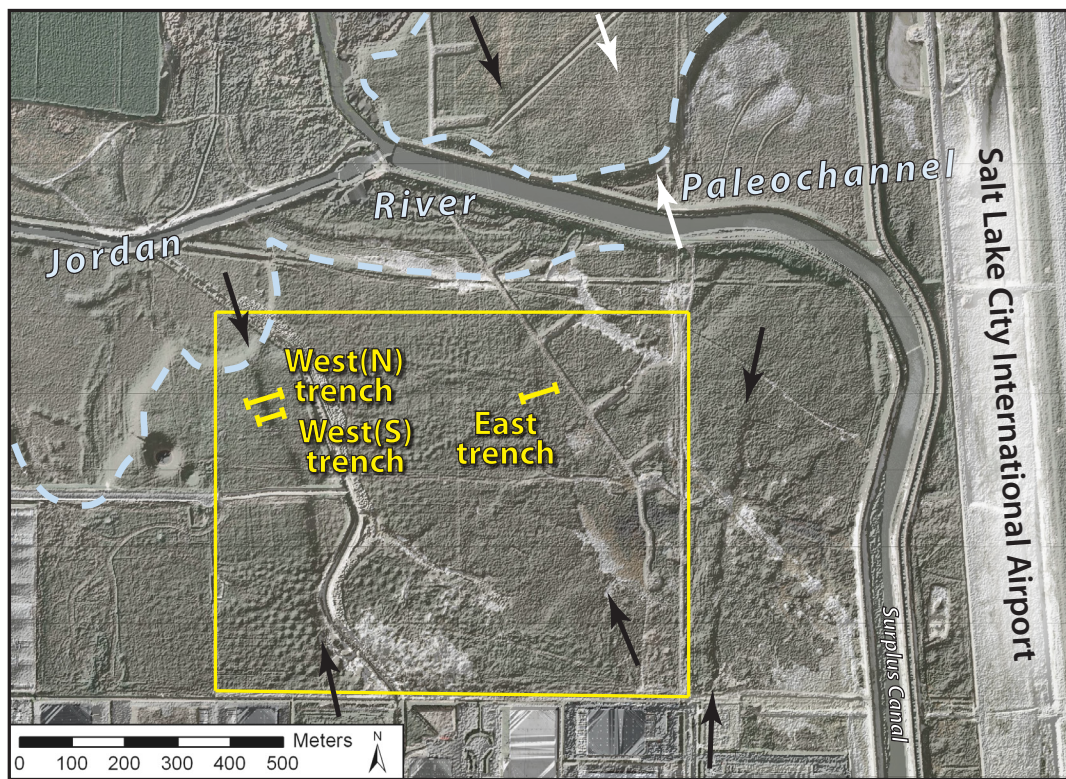
**Figure 5.** *The Granger fault in the vicinity of the Baileys Lake site (yellow box) comprises three east-facing fault scarps (black arrows) and one west-facing scarp (white arrows). With the exception of the westernmost scarp, the fault scarps are geomorphically very subtle and have vertical offsets of just a few tens of centimeters. For this study, we trenched the two east-facing scarps that cross the site, excavating two trenches across the larger western scarp and one trench across the smaller eastern scarp. Base image is combined high-resolution (1 m) orthophoto (2009) and LiDAR data (2006, 2-m posting, illuminated from the northwest), both from Utah Automated Geographic Reference Center.*

coordinate system for the West(N) and West(S) trenches and a different coordinate system for the East trench, referenced herein using horizontal (h-) and vertical (v-) meter marks. Stratigraphic units and pedogenic soils are described in appendices A and B and summarized on plate 1.

## Numerical Dating

### Radiocarbon Dating

We sampled lacustrine, wetland, and scarp-colluvial deposits as well as buried soil A-horizon sediment for radiocarbon ($^{14}$C) dating to estimate deposit and soil ages and provide limits on the timing of paleoearthquakes (appendices C and D). For discussions of common sources of uncertainty in radiocarbon dating and paleoseismic studies, see Trumbore (2000), Nelson and others (2006), and DuRoss and others (2011). At the Baileys Lake site, we collected bulk-sediment samples and dated (using accelerator mass spectrometry [AMS]) a total of seven charcoal samples consisting of discrete fragments separated from the bulk samples. The charcoal separation was conducted by PaleoResearch Institute (Golden, Colorado), who also attempted to identify the separated charcoal fragments to increase the likelihood of dating locally derived charcoal (e.g., phreatophytes) rather than non-local (detrital) charcoal (e.g., conifer species transported from the basin margins). Locally

derived charcoal fragments are more likely burned in-place or very near the location where they are sampled, and therefore are less likely to have an inherited, older age (Puseman and Cummings, 2005). Six of the seven charcoal samples from the Baileys Lake site only produced collections of small, unidentifiable charcoal fragments, and the seventh sample (BL-R5) lacked datable organic material (appendix C). The individual charcoal fragments from each bulk sample were combined into samples of at least ~0.5 mg, which then yielded composite charcoal ages.

We submitted the charcoal samples to the National Ocean Sciences Accelerator Mass Spectrometry (NOSAMS) Facility of the Woods Hole Oceanographic Institution (Woods Hole, Massachusetts) for AMS radiocarbon dating. In our text discussions, the radiocarbon age results are reported as the mean and two-sigma ($2\sigma$) uncertainty rounded to the nearest century in thousands of calendar years before 1950 using the Reimer and others (2009) terrestrial calibration curve applied in OxCal calibration software (Bronk Ramsey, 1995, 2001, 2009).

### Luminescence Dating

We collected 16 samples to estimate burial ages of lacustrine, loess, and paleosol sediment using optically stimulated lumi-

nescence (OSL) dating (appendix E). OSL dating relies on the cumulative dose of in situ natural radiation in sediment to estimate the time when the sediment was last exposed to sunlight during erosion and transport before final deposition (Huntley and others, 1985). Ideally, the sunlight exposure was sufficiently long (about 10 minutes) during erosion and transport to fully reset or "zero" any preexisting luminescence signal in the grains, and thus the luminescence age should represent the time when the sediment was deposited (Aitken, 1994). If the sediment's exposure to sunlight was not long enough (e.g., because of rapid deposition, a short travel path, or filtered light in turbid water) to fully reset the luminescence signal, the sediment may retain an inherited signal (Forman and others, 1991; Duller, 2008) and OSL dating will produce an overestimated (maximum) age for the deposit. In contrast, underestimated (minimum) ages result if the luminescence signal becomes saturated, where the signal does not increase despite continued exposure of the sediment to radiation (Duller, 2008). Saturation results in a maximum age limit for OSL dating of ~75–300 ka, depending on the radiation dose rate and mineral dated (Rhodes, 2011).

Luminescence dating of the Baileys Lake samples included OSL ages on quartz grains (quartz OSL) as well as infrared-stimulated luminescence (IRSL) ages on feldspar grains, measured as a check of the OSL ages. We consider the quartz OSL ages to be more reliable because the IRSL signal takes longer to "zero" than the OSL signal—after sunlight-exposure times of about tens of seconds to minutes, there is a 1–2 order-of-magnitude difference in the remaining OSL and IRSL luminescence signals (Duller, 2008). However, OSL and IRSL ages that overlap within error limits provide an additional degree of confidence that partial bleaching (insufficient sunlight exposure) is not a problem in the sediments.

Our luminescence samples were processed at the USGS Luminescence Dating Laboratory (Denver, Colorado). A portable gamma-ray spectrometer was not available at the time of our field sampling, so background radiation from potassium, uranium, and thorium isotopes, as well as moisture content representative of field conditions, was measured in the laboratory. To correct for the amount of time the sediment was below the water table and thereby improve accuracy of the luminescence ages, we estimated a water-saturation history for the sampled sediment using the Lake Bonneville hydrograph of Oviatt (1997) and the Great Salt Lake hydrograph of Murchison (1989), adjusted using our groundwater monitoring data from the site (see discussion in Hylland and others, 2012). Appendix E presents the OSL ages as the mean and one-sigma uncertainty rounded to the nearest decade; where discussed in the text, however, the error is doubled ($2\sigma$ rounded to the nearest century) for continuity with the calendar-calibrated radiocarbon ages and the modeling of earthquake times using OxCal. In discussing the OSL ages, we report the ages in thousands of calendar years before the sample processing date (2011) and do not adjust for the 61-year difference in

the processing date versus the reference standard for $^{14}C$ (1950); this difference is minor compared to the large OSL age uncertainties (generally about 1–5 kyr at $2\sigma$), and is accounted for in OxCal modeling of earthquake times.

## OxCal Modeling Methods

To evaluate earthquake timing and associated uncertainties, we used OxCal radiocarbon calibration and analysis software (version 4.1.7; Bronk Ramsey, 1995, 2001, 2009; using the IntCal09 calibration curve of Reimer and others, 2009). OxCal probabilistically models the timing of undated events (e.g., earthquakes) by weighting the time distributions of chronological constraints (e.g., radiocarbon and luminescence ages and historical constraints) included in a stratigraphic model (Bronk Ramsey, 2008). The program generates a probability density function (PDF) for each event in the model—i.e., the likelihood that an earthquake occurred at a particular time—using the chronologic and stratigraphic constraints and a Markov Chain Monte Carlo sampling method (Bronk Ramsey, 2008). For more detailed discussions of the application of OxCal modeling to paleoseismic data, see Lienkaemper and Bronk Ramsey (2009) and DuRoss and others (2011).

The OxCal depositional model for the Baileys Lake site (appendix G) uses stratigraphic ordering information, radiocarbon and OSL ages, and a historical constraint that no large surface-faulting earthquakes ($\geq$M ~6.5) have occurred since 1847, to define the time distributions of earthquakes identified at the site. We correlated depositional units between trenches and constructed a single OxCal model. Where necessary, we removed numerical-age outliers using geologic judgment (knowledge of sediments, soils, and sample contexts), the degree of inconsistency with other ages in the model for comparable deposits (e.g., stratigraphically inverted ages), and an agreement index between the original (unmodeled) and modeled numerical ages (Bronk Ramsey, 1995, 2008). Similarly, we constructed two additional OxCal models to determine earthquake times based on available radiocarbon ages from consultants' trenches (appendix H). We report earthquake time ranges as the mean and two-sigma uncertainty in thousands of calendar years B.P. rounded to the nearest century.

## Biostratigraphic Dating

In addition to the numerical dating described above, we used ostracode biostratigraphy to provide a relative temporal framework for the Lake Bonneville deposits at the Baileys Lake site. The taxonomic nomenclature used herein follows that of R.M. Forester (USGS), who with other researchers has identified faunal assemblages that are useful in stratigraphic correlation to the various phases of the well-documented Bonneville lake cycle (Spencer and oth-

ers, 1984; Forester, 1987; Thompson and others, 1990; see also Oviatt, 1991). Ostracode identifications and interpretations are summarized in appendix F.

# BAILEYS LAKE TRENCH SITE

## Surface Faulting and Geology

The Baileys Lake site is at the northern end of the Granger fault, and is crossed by two parallel scarps that trend about N. 10° W. and are about 0.5 km apart. The nearly flat site lies at an elevation of 1285 to 1288 m (figure 6), which coincides with the elevation of the Holocene highstand of Great Salt Lake (approximately 2–3 ka) as estimated by Currey and others (1988a; 1287 m [4221 ft]) and Murchison (1989; 1287 m [4223 ft]). However, we found no clear geomorphic or stratigraphic evidence of the Holocene highstand at this site (Hylland and others, 2011). The site is approximately 9 m below the elevation of the Gilbert shoreline at the Magna Spit (Currey, 1982; Murchison, 1989), which is about 8 km south of the Baileys Lake site. An east-west trending paleochannel of the Jordan River crosses the northern part of the site, and this channel was likely occupied around the time of the Holocene highstand of Great Salt Lake (Murchison, 1989) (figure 5). The active channel of the Jordan River has since migrated 6 km eastward, possibly due to tectonic tilting and subsidence associated with normal faulting along the SLCS (Keaton, 1987).

Geologic deposits at the Baileys Lake site consist of fine-grained lacustrine sediment of Lake Bonneville overlain by Holocene loess, playa clays, and minor sandy alluvium. Soils on these deposits are alkali to saline (Woodward and others, 1974). Miller (1980) mapped the surficial deposits in the vicinity of the Baileys Lake site as consisting mostly of fine-grained Holocene deltaic deposits; where present, these deposits may be associated with a "late Gilbert paleodelta" (Murchison, 1989). Eolian erosion of the fine-grained surficial deposits has locally created shallow topographic depressions, or deflation basins, which in turn become ephemeral ponds during periods of high water table and/or after rainstorms or snowmelt. Sandy, fine-grained alluvium is present on the floor of the Jordan River paleochannel where it crosses the site.

## Granger Fault Scarps and Surface Offset

The two fault scarps that cross the Baileys Lake site are part of the distributed system of fault traces that characterize the northern half of the Granger fault. Both scarps are east facing. The larger western scarp has about 0.9 m of vertical surface offset based on projections of the upper and lower ground surfaces along a northeast-trending profile (figure 7). The Jordan River paleochannel truncates the western scarp, and the scarp does not continue immedi-
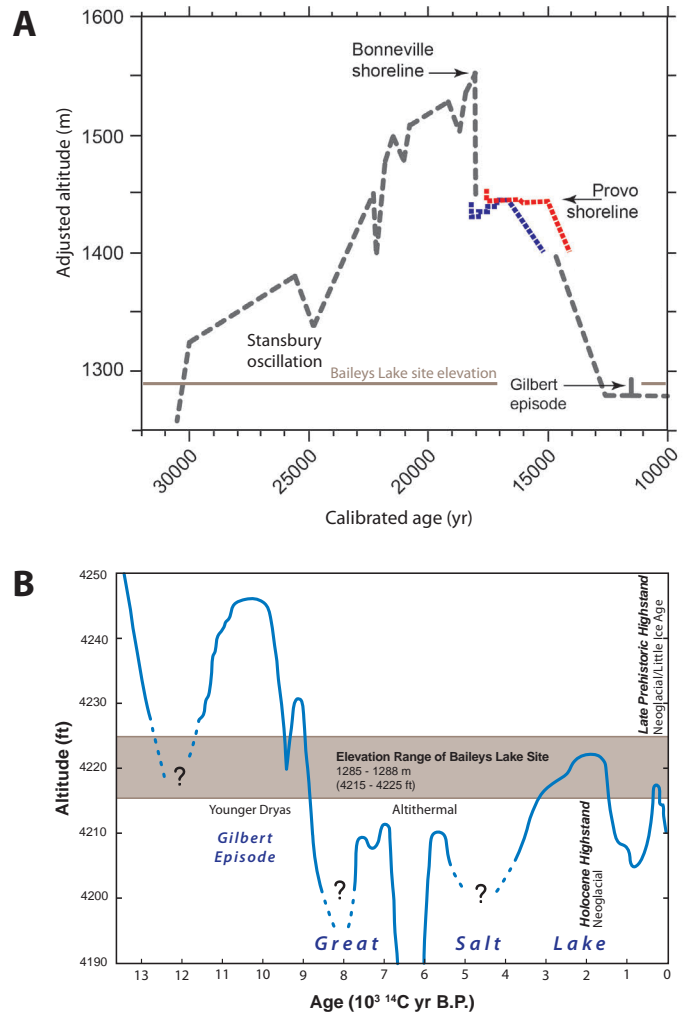


**Figure 6.** *Lake Bonneville and Great Salt Lake hydrographs showing relation of water depth to elevation of the Baileys Lake site. A. Lake Bonneville hydrograph showing lake-level changes in the Bonneville basin since about 30 ka (modified from Reheis and others, in press). Altitudes adjusted for differential isostatic rebound. Red and blue lines are from Miller and others (2013) and indicate two datasets related to the Provo shoreline. B. Great Salt Lake hydrograph (from Murchison, 1989) showing lake-level changes in the Great Salt Lake basin since about 12 ka, and associated climate intervals and stadials (after Hylland and others, 2012). Although Murchison (1989) and Currey and others (1988a) estimated Great Salt Lake reached a level of about 1287 m (4221–4223 ft) in the late Holocene, we found no geomorphic or stratigraphic evidence of this late Holocene highstand at the Baileys Lake site. Also, data from the northeastern shore of Great Salt Lake indicate that the culmination of the Gilbert episode was relatively short-lived, possibly lasting just a few centuries at most (Oviatt and others, 2005; Oviatt, 2014).*

ately north of the paleochannel. About 1.5 km to the northwest, however, several geomorphically subtle, east-facing scarps lie on-trend with the western scarp, and these are likely fault scarps as opposed to fluvial scarps (McKean and Hylland, 2013). Development in the Salt Lake International Center industrial area obscures the western scarp south of the Baileys Lake site, but pre-development aerial photography indicates the fault trace connects with the 0.5-
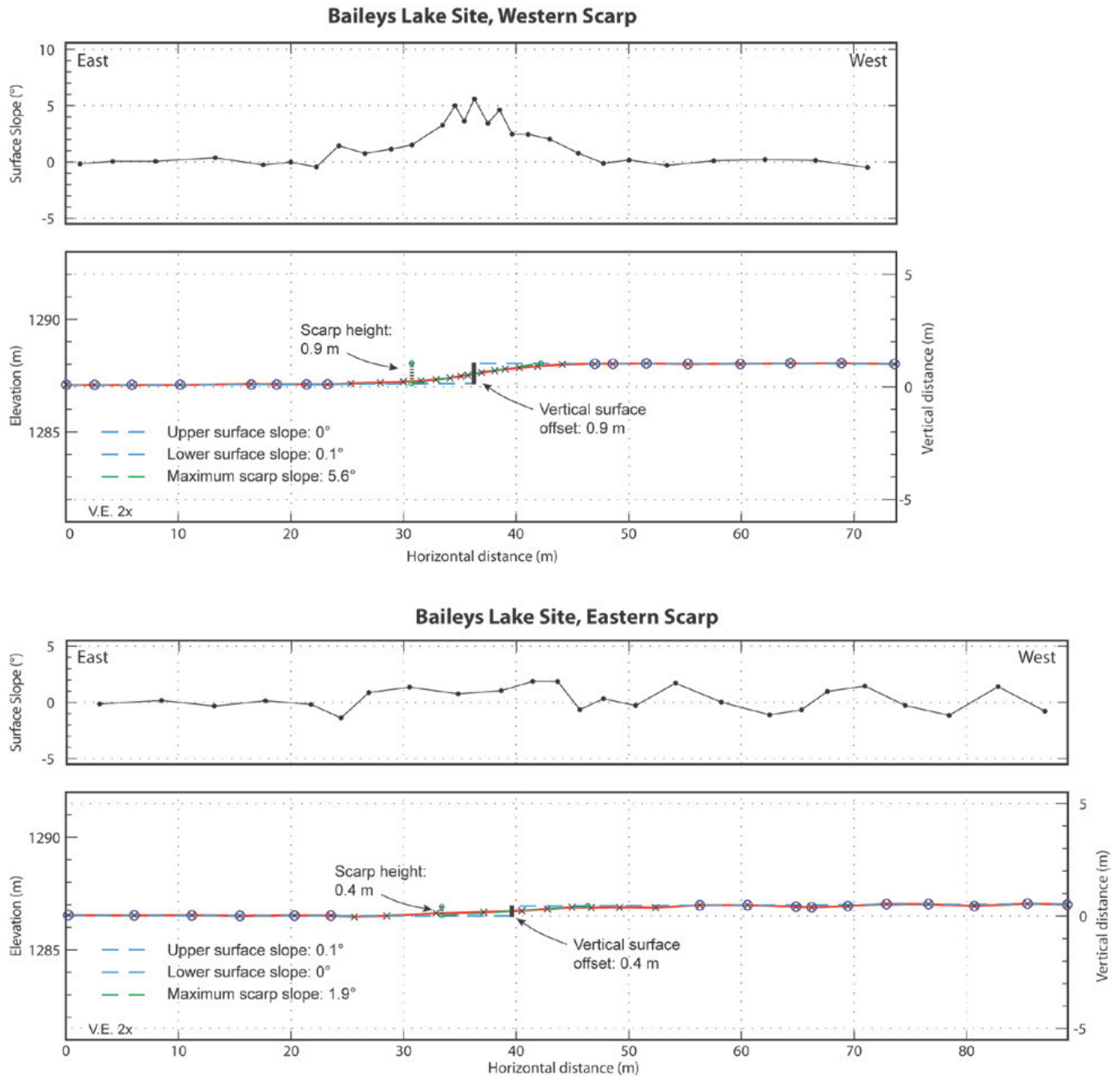
**Figure 7.** *Scarp profiles and surface slope plots across the western and eastern fault scarps at the Baileys Lake site; profile locations shown on plate 1. Profile points (X's) measured using high-precision GPS (August 31, 2010). Elevation is relative to mean sea level, vertical distance is relative to minimum surface elevation along each profile. Blue circles indicate profile points used to determine upper and lower surface slopes. Scarp height is the vertical distance between the intersections of the maximum scarp slope with the upper and lower surface-slope projections (green circles). Vertical exaggeration = 2x.*

to 0.8-m-high, east-facing scarp at the Three Flags local-ity (see figure 4) of Keaton and Currey (1989) approxi-mately 3 km to the south (McKean and Hylland, 2013). The smaller eastern scarp is geomorphically very subtle, and a northeast-trending scarp profile indicates about 0.4 m of vertical surface offset (figure 7). The northern con-tinuation of the eastern scarp is locally obscured by ser-vice roads and a canal that occupies the Jordan River pa-leochannel (figure 5), but a short segment of this scarp is apparent immediately north of the canal. Development in

the Salt Lake International Center industrial area obscures the eastern scarp south of the Baileys Lake site.

As noted above, two other fault scarps lie near the eastern boundary of the Baileys Lake site (figure 5). We identified an extremely subtle scarp on the north side of the Jordan River paleochannel during our review of the LiDAR data. This scarp faces west, forming a graben with the eastern trenched scarp, and likely extended southward but was de-stroyed by the service road along the eastern boundary of

the Baileys Lake site (McKean and Hylland, 2013). The other scarp lies just east of the Baileys Lake site, is east facing, and has been modified by human disturbance and post-faulting erosion.

## Trench Stratigraphy and Structure

Collectively, our three trenches at the Baileys Lake site exposed five distinct packages of sediment: (1) pre-Bonneville wetland/alluvial-marsh deposits, (2) Bonneville lacustrine deposits, (3) Gilbert-episode lacustrine deposits, (4) post-Gilbert loess, and (5) scarp-derived colluvium (colluvial wedges). The exposed stratigraphy correlates very well between the trenches, so we describe the stratigraphy for the site as a whole. The following stratigraphic discussion is modified from Hylland and others (2012). See plate 1 for maps and photomosaics of the exposed stratigraphy, and appendix A for descriptions of the stratigraphic units.

### Pre-Bonneville Wetland/Alluvial-Marsh Deposits

We exposed pre-Bonneville deposits (unit 1) only in the footwall of the West(S) trench, where we excavated the trench to the maximum depth allowed by the water table. These deposits consist of massive to laminated, gray to brown clay with thin interbeds of white, fine-grained sand. The clay contains charophyte stem encrustations and decayed root filaments, *Scirpus*-type (bulrush) seed fragments, and fragmented and carbonate-coated ostracodes (*Candona rawsoni*). Numerous small fragments of oxidized clay scattered throughout the lower part of the exposure indicate local burrowing. Collectively, the sedimentology and organic material indicate deposition in a wetland or alluvial-marsh environment. Charcoal from the upper part of the unit yielded an age of $35.8 \pm 0.8$ ka (BL-R4).

### Bonneville Lacustrine Deposits

A nearly complete section of Lake Bonneville deposits overlies the pre-Bonneville wetland/alluvial-marsh deposits (figure 8). The Lake Bonneville section at the Baileys Lake trench site is 2.5–4.0 m thick, similar to thicknesses of the Bonneville section measured in basin-floor outcrops elsewhere in the northern Bonneville basin (Oviatt and Miller, 1997), in nearby basin-floor boreholes (e.g., Eardley and others, 1973, as reinterpreted by Oviatt and others, 1999; Spencer and others, 1984; Balch and others, 2005; Oviatt and Thompson, 2005, and unpublished data), and as imaged in high-resolution lake-floor seismic-reflection profiles (Colman and others, 2002).

**Transgressive phase:** The basal part of the Lake Bonneville section consists of a 0.8-m-thick sequence of ripple-laminated, locally cross-bedded silty sand with clay interbeds (unit 2a). This unit contains gastropod shell fragments and ostracodes (*C. rawsoni, Limnocythere staplini, and Cytherissa lacustris*) and generally fines upward into a 0.5-m-thick bed of massive

greenish clay containing the ostracodes *L. staplini, L. ceriotuberosa, and Candona caudata*(?). The ostracode assemblage is consistent with the early transgressive phase of the Bonneville lake cycle (e.g., Spencer and others, 1984; Forester, 1987; Thompson and others, 1990), as are OSL ages ranging from $31.6 \pm 3.3$ ka (BL-L1) to $31.0 \pm 3.9$ ka (BL-L16).

The middle part of the Lake Bonneville section consists of 1.8 m of massive, gray to reddish-brown clay with thin interbeds of silt and fine sand (units 2b, 2c, 2d, and 2e). These sediments represent deep-water deposition during the transgressive phase of the Bonneville lake cycle. The sedimentary character of the silt and sand interbeds varies and likely results from both depositional and post-depositional processes. All of the interbeds have abrupt contacts with the enclosing clay, and some exhibit basal flame structures and numerous tabular clay clasts suspended in graded sand and silt. In some places, the clay clasts are isolated and are likely rip-up clasts transported and deposited with the sand and silt, and in other places groupings of clasts are subhorizontal and appear to be fragments of formerly intact clay stringers (figure 9). The sharp basal contacts, graded bedding, and possible rip-up clasts suggest sudden, rapid pulses of coarser-grained sedimentation in a depositional environment otherwise dominated by clay (i.e., quiet and/or deep water). We interpret the interbeds as turbidites associated with the episodic influx of silt and sand; possible mechanisms of turbidite deposition include strong flood-stage river discharge, delta-front slumping, and destabilization of lake-margin deposits by lake-level fluctuations or earthquakes. Similar interbeds within the deep-water Bonneville clays elsewhere in the Bonneville basin have also been interpreted as turbidites (e.g., Oviatt and others, 2005). The thickest interbed at the Baileys Lake site (20 cm; unit 2d) is also the most sand rich, and is a composite interbed containing disrupted (disturbed, but not transported) clay stringers. We attribute the bedding disruption to fluidization as the result of earthquake-induced liquefaction.

The clay beds of the middle part of the Lake Bonneville section contain the ostracodes *L. staplini, L. ceriotuberosa, C. caudata*(?), and *C. adunca*, and the assemblage in the uppermost part of the section (unit 2e) is consistent with the mid- to late-transgressive phase of the Bonneville lake cycle (e.g., Spencer and others, 1984; Forester, 1987; Thompson and others, 1990). The silt interbeds yielded OSL ages ranging from $24.4 \pm 5.0$ ka (BL-L3) at the base of unit 2c to $19.3 \pm 0.8$ ka (BL-L7) in unit 2e.

The top of the deep-water clay sequence (top of unit 2e) is marked by a nearly planar contact (figure 10) that is overlain by a thin (generally <2 cm), fine-grained breccia layer consisting of sand and small (<1 mm thick) carbonate fragments; for logging purposes, this breccia layer is included as the basal part of unit 3. Beneath the contact, unit 2e displays open, upright folds, the tops of which are truncated at the contact; we observed this relation in both the western and eastern trenches. We hypothesize that the folding and truncation were
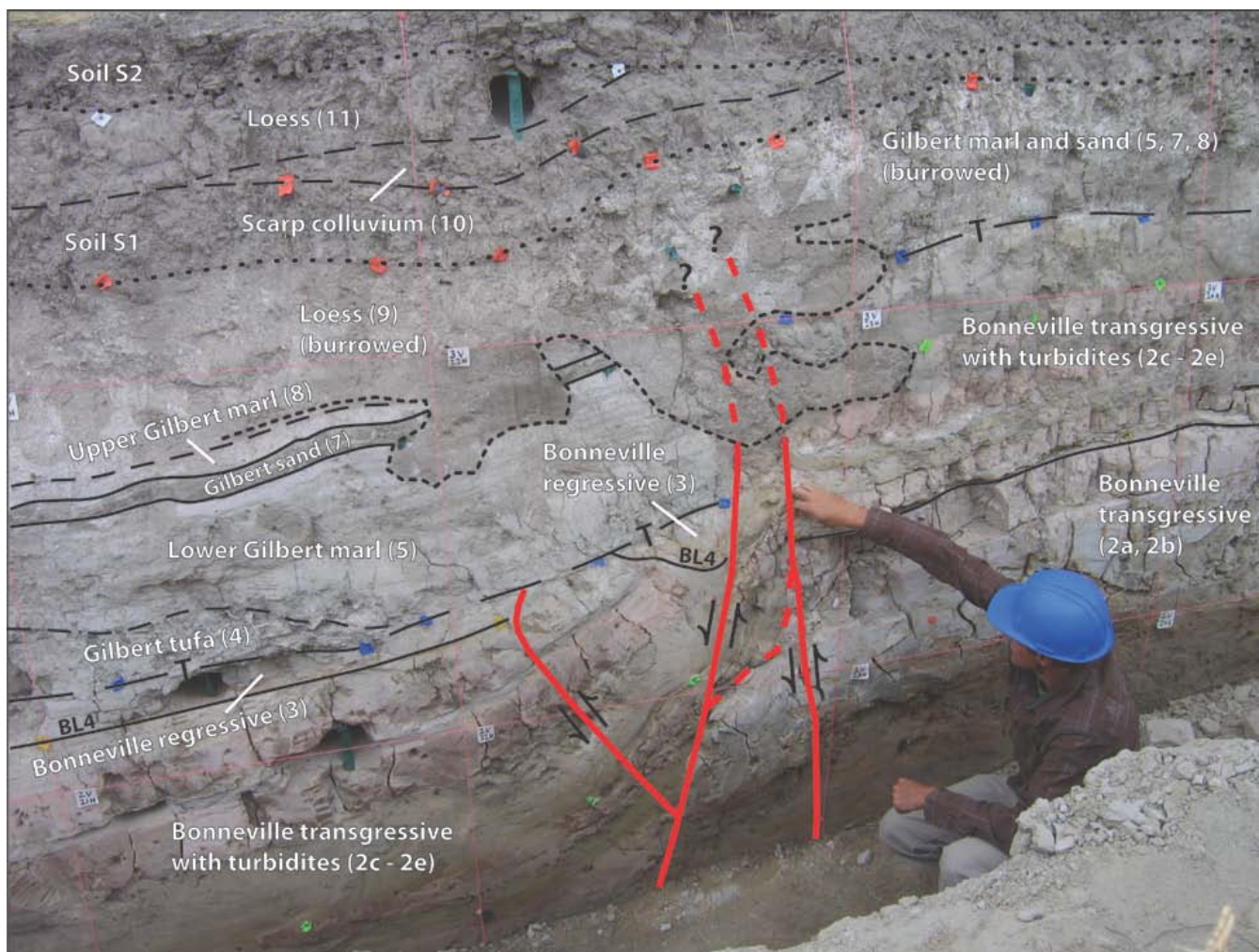
*Figure 8. Fault-zone exposure in the south wall of the Baileys Lake West(N) trench, showing nearly complete Lake Bonneville section (see Hylland and others, 2012). Unit numbers given in parentheses; see appendix A for unit descriptions and appendix B for descriptions of pedogenic soils. We interpret contact labeled "BL4" as an event horizon associated with earthquake BL4 (see "Chronology of Surface-Faulting Earthquakes" section in text). T indicates erosional unconformity with overlying (mostly very thin) tufa deposit; in the fault footwall, this unconformity has removed Bonneville regressive deposits (unit 3) as well as the BL4 event horizon. Upper two dotted lines mark base of soil A horizons; lower dotted line delineates extensive burrowing that obscures stratigraphic and structural relations in the upper part of the exposure. Grid-line spacing is 1 m.*

nearly contemporaneous and associated with a single earthquake on the Granger fault—the folding resulting from disturbance of the lake-floor deposits by strong ground shaking during earthquake BL4 (see "Chronology of Surface-Faulting Earthquakes" below), and the truncation occurring immediately after the earthquake and resulting from subaqueous erosion associated with strong lake-bottom currents triggered by fault-related offset of the lake floor. Also at the top of unit 2e, vertical fractures penetrate downward to about 10 cm below the upper contact, and the reddish-brown clay of unit 2e has been chemically reduced to a greenish-gray color in the vicinity of the fractures (figure 10). Many of these fractures extend upward through the overlying Bonneville regressive deposits (unit 3). Hylland and others (2012) interpreted the fractures to be desiccation cracks that formed after the regressive phase of Lake Bonneville, when the sediment column dried out during the lake's lowstand prior to the Gilbert transgression.

**Regressive phase:** The transgressive, deep-water clay sequence is overlain by finely laminated, greenish clay with silt and sand (unit 3) (figures 10 and 11). This unit averages about 40 cm thick but ranges from 2 to 60 cm thick, the variability resulting from an overlying erosional unconformity (discussed below under "Gilbert-Episode Deposits"). Ostracodes in this unit include *L. ceriotuberosa, C. caudata*(?), *C. adunca*, and *C. lacustris*; many are broken and unidentifiable fragments, suggesting reworking from older deposits. This assemblage indicates deposition during the regressive phase of the Bonneville lake cycle, while the Provo shoreline was forming or during the immediate post-Provo regressive phase (very early in the post-Provo regressive phase of the lake) (e.g., Oviatt and Miller, 1997). OSL ages of 14.1 ± 1.6 ka (BL-L8) and 13.0 ± 1.2 ka (BL-L9) likewise indicate deposition during late Provo-shoreline time and/or during the post-Provo regressive phase.
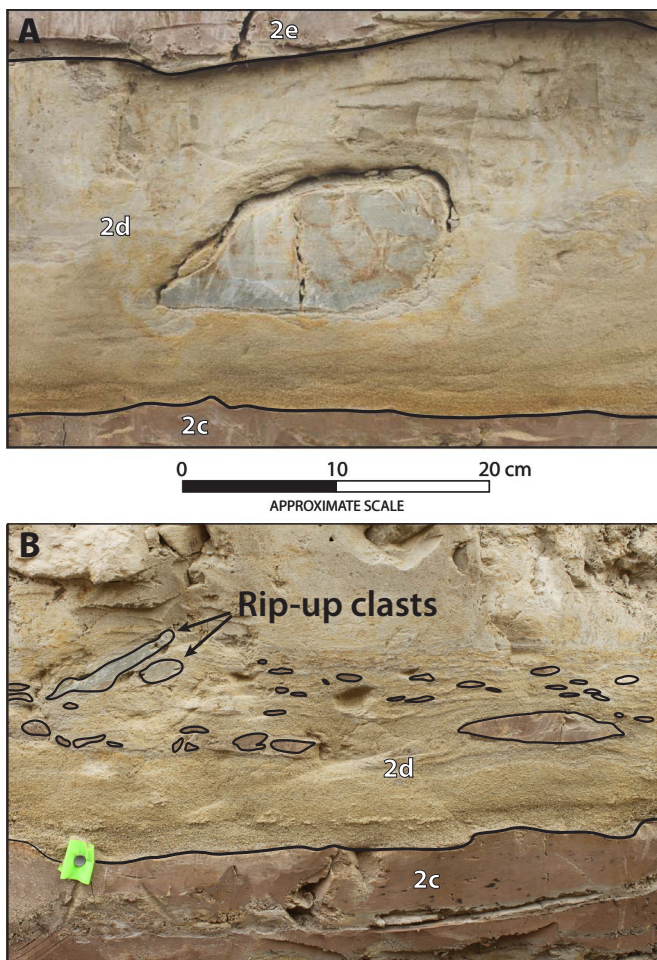
*Figure 9. Sedimentology of the thickest and most sand-rich turbidite interbed (unit 2d) within the deep-water transgressive Bonneville clays exposed in the Baileys Lake trenches. A. Greenish-gray clay rip-up clast suspended in sand and silt matrix, exposed in the south wall of the West(N) trench (h-20.2 m, v-1.5 m). Turbidite bed grades from medium sand at the base to silt at the top. B. Greenish-gray rip-up clasts (transported) and disrupted reddish-brown clay stringers (disturbed, but not transported) suspended in sand and silt matrix, exposed in the south wall of the West(S) trench (h-23.4 m, v-1.5 m); clast boundaries outlined to highlight shape and orientation.*

## Gilbert-Episode Deposits

The Bonneville regressive deposits are overlain by a sequence of lacustrine deposits comprising, from bottom to top, a layer consisting mostly of tufa (unit 4), a laminated marl (unit 5), a thin bed of dark-gray sand (unit 7), and an upper, thin bed of laminated marl (unit 8) (figure 11). The tufa layer, which also includes clay, silt, and fine to coarse sand, consists mostly of a "hash" of broken (reworked) tufa fragments, but locally the tufa comprises intact, in situ pods or "mats" as much as several tens of centimeters thick. The tufa was deposited on an undulating unconformity; laminae in the silty clay beneath the unconformity are cut by the unconformity, whereas laminae in the marl above the tufa conformably drape the underlying topography. In the western trenches, the unconformity

cuts down-section only into unit 3 on the hanging wall of the fault, but it has completely stripped unit 3 and most of unit 2e from the footwall. The tufa is present in all of the trenches, indicating persistence across the site. We interpret the tufa as having formed in the shorezone when lake water transgressed across the site during the Gilbert episode; the shorezone must have remained at the elevation of the tufa deposit (approximately 1286–1287 m [4219–4222 ft]) for a sufficient duration to allow accumulation of precipitated calcium carbonate. Alternatively, the tufa deposition may be related to spring flow immediately prior to the Gilbert transgression (Hylland and others, 2012).

Carbonate-rich, laminated clay and silt (marl; unit 5) conformably overlies the tufa. The laminated marl was deposited during the Gilbert episode based on the presence of unidentifiable, carbonate-coated ostracode fragments (reworked) and an OSL age of 12.5 ± 1.8 ka (BL-L13). The marl is in turn overlain by a distinctive, thin (<10 cm), dark-gray, medium to coarse sand composed predominantly of subangular quartz grains (unit 7; figure 11). The sand is massive to thinly bedded, has an abrupt lower contact with the underlying marl, and locally comprises one or more graded beds. The sand is present in all of the trenches, although it generally thins westward and is difficult to identify on the footwall side of the western trenches. In the East trench, the sand grades laterally to silt in the western part of the trench (facies change at h-38; plate 1). The sand yielded an OSL age of 11.5 ± 5.2 ka (BL-L14) (the large uncertainty in the age results from a relatively small number of aliquots measured). A <15-cm-thick unit of carbonate-rich, finely laminated clay and silt (marl; unit 8) overlies the dark sand, and is very similar to the marl that underlies the sand.

The OSL age of the unit 7 sand, its stratigraphic position between two lacustrine marls, and its abrupt lower contact indicate that the sand likely formed in a shorezone that crossed the site during a second transgression of the Gilbert episode (Hylland and others, 2012), similar to the double transgression interpreted by Oviatt and others (2005) in Gilbert-age deposits on the northeastern shore of Great Salt Lake (Public Shooting Grounds site). The thin lacustrine marl (unit 8) overlying the shorezone sand appears to represent deeper-water deposition during higher levels of the Gilbert episode, which culminated at about 11.6 ka (Oviatt and others, 2005; Oviatt, 2014).

## Post-Gilbert Loess

The Gilbert lacustrine sequence is overlain primarily by deposits of massive silt and clay (loess; units 9 and 11) (figure 8) that have a cumulative thickness of 0.4–1.0 m. The lower loess (unit 9) has a moderate degree of soil carbonate development (up to stage II; after Machette [1985] and Birkeland and others [1991]). A soil A horizon (soil unit S2) is developed in the top of the upper loess (unit 11) at the modern ground surface, and a buried paleosol with blocky to prismatic structure (weakly developed Bt horizon; soil unit S1) was evident in the western trench exposures about 0.4 m below the ground
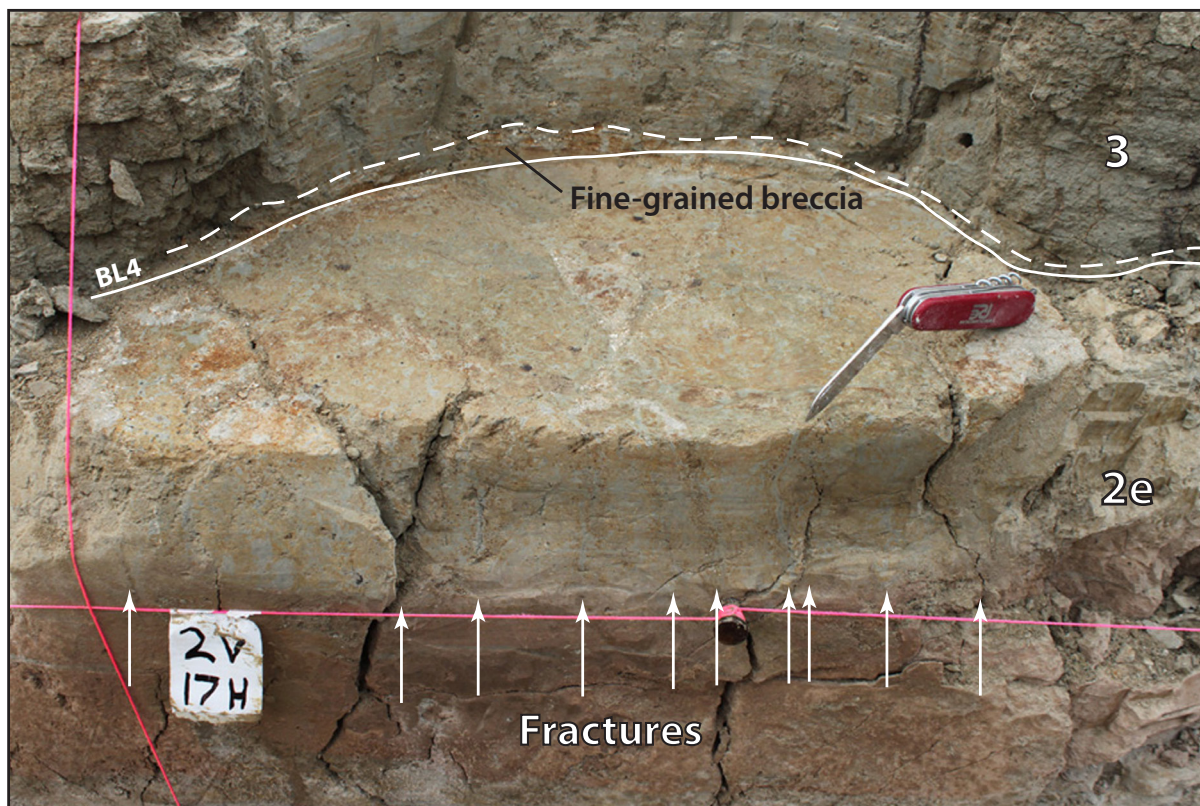
*Figure 10. Exhumed surface of the planar contact (solid white line) between reddish-brown, massive, Bonneville transgressive clay (unit 2e) and overlying greenish, laminated, Bonneville regressive clay and silt (unit 3), exposed in the West(S) trench. A thin, fine-grained breccia containing small carbonate fragments immediately overlies the planar contact, which we interpret as an event horizon associated with earthquake BL4 (see "Chronology of Surface-Faulting Earthquakes" section in text). Vertical fractures extend downward about 10 cm into the top of unit 2e and appear to control the depth to which the clay has been chemically reduced to a gray color.*

surface. The loess (unit 9) below soil S1 yielded an OSL age of 12.5 ± 1.4 ka (BL-L11); because this unit overlies Gilbert-episode deposits, its true age must be near the young end of the two-sigma uncertainty range. The loess (unit 11) above soil S1 yielded an OSL age of 3.2 ± 0.5 ka (BL-L10). Charcoal from soil S1 yielded an age of 6.2 ± 0.1 ka (BL-R1), and the soil matrix yielded an OSL age of 6.0 ± 1.0 ka (BL-L12).

## Scarp-Derived Colluvium

Scarp-derived colluvium comprises two separate colluvial wedges (units 6 and 10; figure 12), each providing evidence for a surface-faulting earthquake on the Granger fault. The colluvial units, which have different thicknesses and wedge-shaped geometries, are both overlain by loess deposits (units 9 and 11) which in turn have pedogenic soil horizons developed on them. We observed the two colluvial wedges only in the West(N) trench; pervasive burrowing obscured stratigraphic details in the upper part of the fault zone in the West(S) trench, and the lack of surface rupture in the East trench precluded colluvial-wedge formation there (see "Granger Fault—Eastern Trace" below). The youngest colluvial wedge (unit 10) is not faulted, whereas the older wedge (unit 6) has been faulted

down-to-the-east along the western trace of the Granger fault.

Unit 6—the oldest scarp colluvium—is a distinct, layered mixture of colluvium and organic-rich sediment (figure 12). The colluvium consists of disaggregated, fine-gravel to sand-size fragments of clay, silt, and sand derived from unit 5; the source of the organic-rich, fine-grained "soil stringers" is uncertain. The sediment layers are inclined at about 30°. However, units 7 and 8 (and therefore also unit 6) appear to have been warped in the hanging wall by the most recent surface-faulting earthquake such that they dip eastward 7°–11° more steeply within about 2 m of the fault zone; therefore, the original depositional dip of the colluvial-wedge sediments was likely about 19°–23°. We interpret the distinctive fabric of the scarp colluvium as resulting from sloughing of wet scarp-face material as the scarp eroded back over a relatively short period of time. Because unit 6 is both underlain and overlain by Gilbert-episode marl, the scarp colluvium must have been deposited during a time of low lake level between the two Gilbert-episode transgressions (see discussion above; Oviatt and others, 2005; Hylland and others, 2012). Unit 6 tapers from 0.5 to 0 m thick over a horizontal distance of about
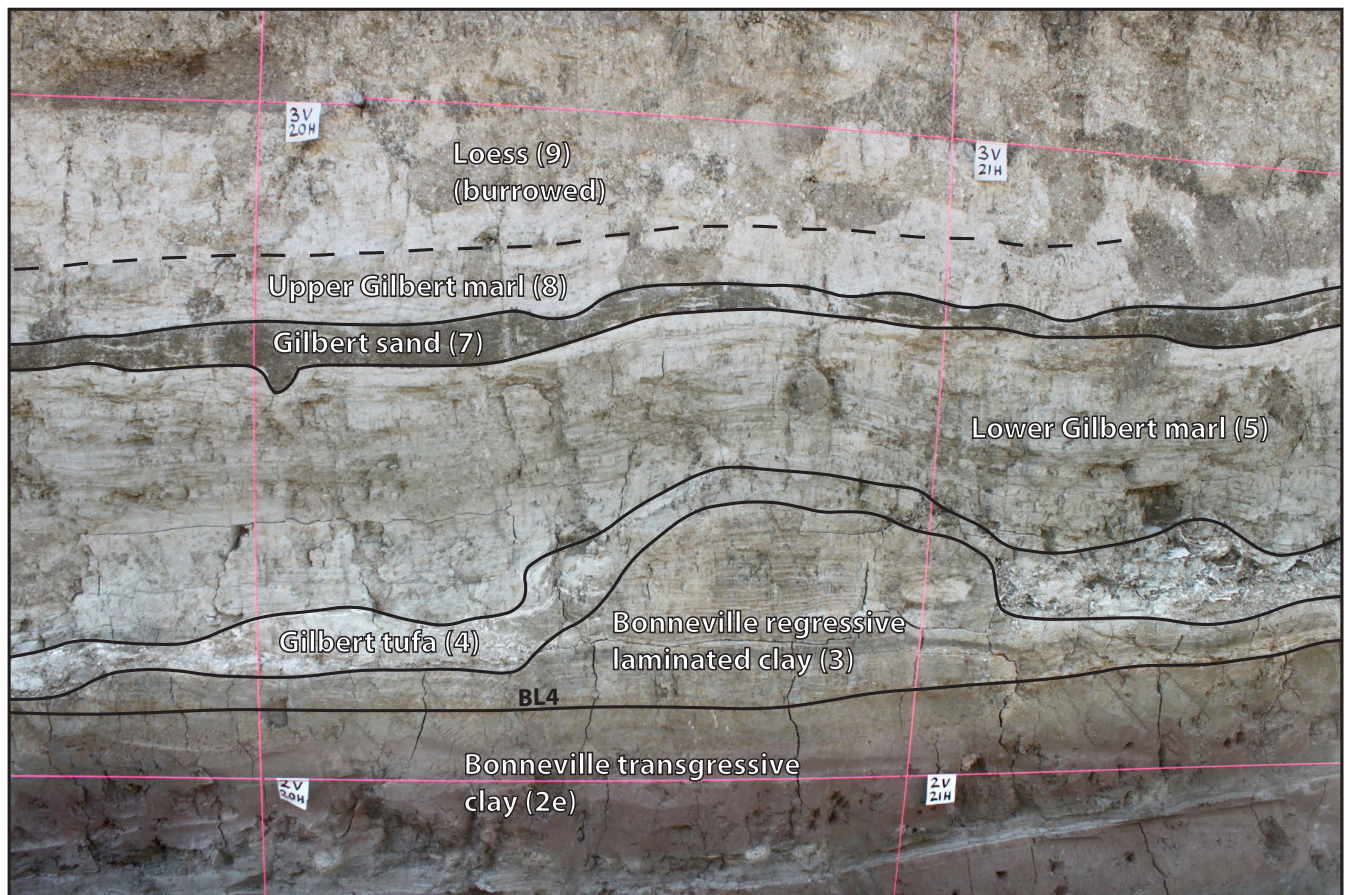
**Figure 11.** *Gilbert-episode stratigraphic section (units 4, 5, 7, and 8) exposed in the West(N) trench. Unit numbers given in parentheses; see appendix A for unit descriptions. Laminated Bonneville regressive clay is cut by a transgression-related unconformity at the base of the Gilbert tufa, whereas units above the tufa conformably drape the underlying topography. The dark-gray Gilbert shorezone sand likely represents a second Gilbert-episode transgression across the site. We interpret the contact labeled "BL4" as an event horizon associated with earthquake BL4 (see "Chronology of Surface-Faulting Earthquakes" section in text). Grid-line spacing is 1 m.*

0.8 m, and the toe of the wedge may grade into the Gilbert shorezone sand (unit 7), although this relation is obscured by burrowing and overprinting by soil carbonate development (stage II). Burrowing is also evident within the colluvial wedge itself. Two subsamples of unidentifiable charcoal from the colluvium yielded ages of 0.6 ± 0.1 ka (BL-R2-1) and 1.7 ± 0.1 ka (BL-R2-2); based on the ages of overlying deposits, these radiocarbon ages are much too young and likely indicate contamination from young organic material associated with burrowing. We observed this colluvial wedge only in the north wall of the West(N) trench; pervasive burrowing apparently obliterated this deposit in the south wall.

Unit 10—the youngest scarp colluvium—consists of granular (sand and fine gravel) soil blocks derived from unit S1 that bury an eroded scarp free face (figure 12). Unit 10 is massive, with no apparent depositional fabric, and tapers from 17 to 0 cm thick over a horizontal distance of about 1.8 m. Two subsamples of unidentifiable charcoal from the colluvium yielded ages of 4.3 ± 0.1 ka (BL-R3-1) and 4.8 ± 0.1 ka (BL-R3-2). This colluvial wedge was most dis-

tinct in the north wall of the West(N) trench, but could also be recognized in the south wall.

## Granger Fault

**Western trace:** In the two western trenches, the western trace of the Granger fault is a relatively narrow zone of steeply dipping, anastomosing fault planes within a broader zone of warping (plate 1). Based on measurements across the two trenches, the main fault zone strikes approximately N. 5° W. and comprises several well-defined, subparallel fault planes having an average apparent eastward dip of 80°–85° in a 10- to 40-cm-thick zone. However, the faults generally steepen toward the ground surface, and locally are vertical to west dipping (75°–85°). At least part of the west dip may be due to rotation associated with the broader down-to-the-east warping, which spans a zone 2 m wide at the West(S) trench and 7 m wide at the West(N) trench. We were able to delineate individual geologic units within the fault zone in the West(N) trench, and offset of these units shows that most of the fault displacement occurred on the eastern bounding fault of the main fault zone. In the West(S) trench, the faulted strata are
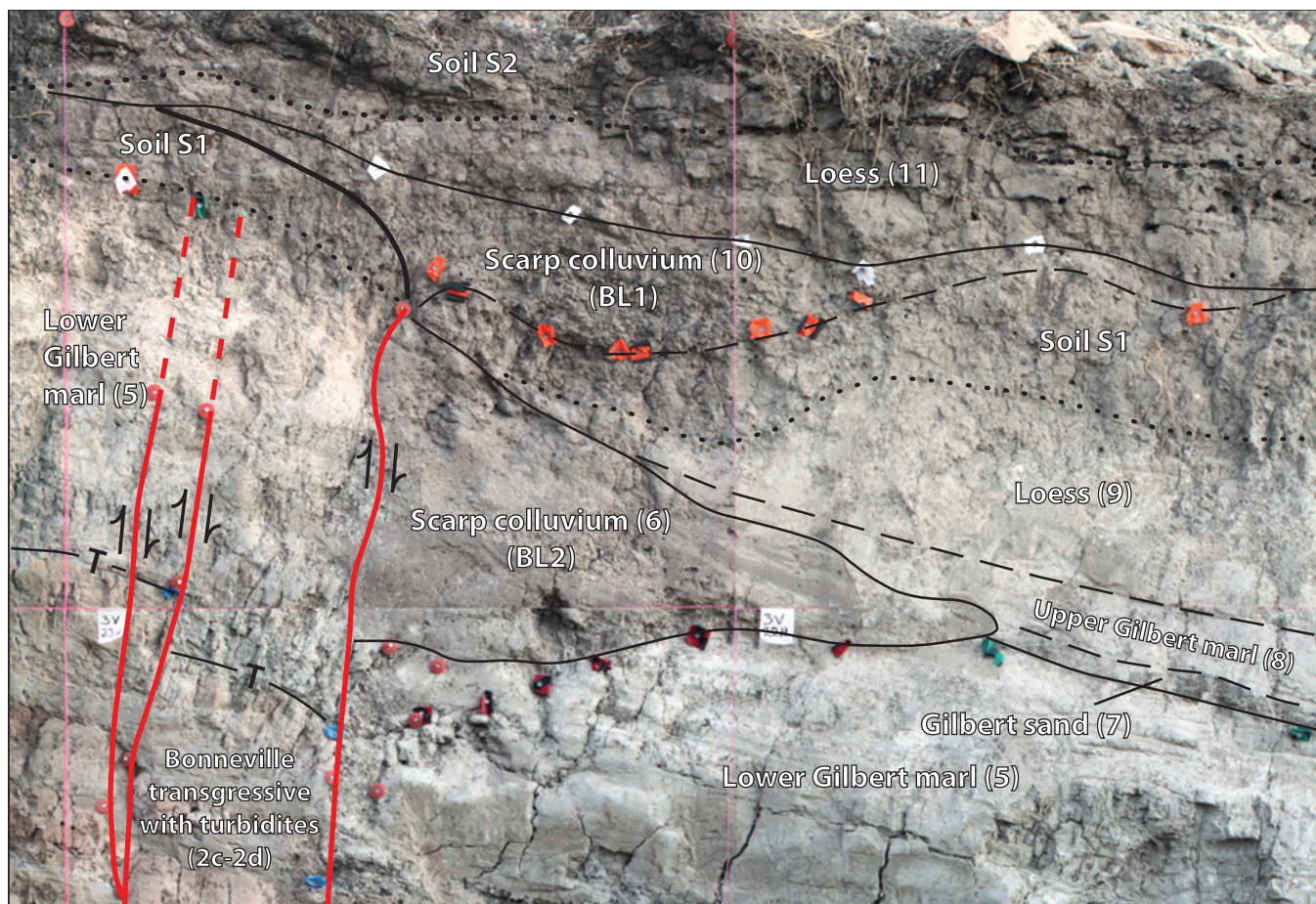
***Figure 12.*** *Fault-zone exposure in the north wall of the Baileys Lake West(N) trench, showing deposits of scarp-derived colluvium (units 6 and 10) associated with the two most recent surface-faulting earthquakes (BL1 and BL2). Unit numbers given in parentheses; see appendix A for unit descriptions and appendix B for descriptions of pedogenic soils. Dotted lines indicate base of modern soil (S2) and buried paleosol (S1); heavy black line indicates buried fault-scarp free face. T indicates erosional unconformity with overlying (mostly very thin) tufa deposit. Gridline spacing is 1 m.*

more intensely sheared and we could not delineate individual units within the fault zone.

Several west-dipping fault planes are present within about 1 m east of the main fault zone. Based on the exposure in the south wall of the West(N) trench (plate 1), these faults are splays of the eastern bounding fault of the main fault zone. The splay faults generally dip 60°–75° west but are locally vertical to steeply east dipping, and have apparent reverse displacements of about 5 cm. Unlike the faults that form the main fault zone, which offset post-Bonneville deposits up to and including the mid-Holocene-age paleosol (unit S1) as apparent in the north wall of the West(N) trench (plate 1), the splay faults only displace strata older than unit 4 (Gilbert tufa), and therefore predate the Gilbert lake transgression.

Faulting on the western trace of the Granger fault at the Baileys Lake site has produced both monoclinal folding and discrete shear on fault planes. The oldest fault-related deformation exposed in the trenches is monoclinal folding of the Bonneville transgressive deposits (unit 2). As apparent in the south wall of

the West(N) trench (h-21 to 22.7; plate 1), these deposits are folded to a greater degree than any of the younger deposits, indicating a deformational event older than the warping that affected the younger deposits. Combined with the absence of any scarp-derived colluvium associated with the older deformation, the folding indicates a sublacustrine event that deformed plastically and produced monoclinal folding but no surface rupture. Higher in the stratigraphic section, the two wedges of scarp-derived colluvium (units 6 and 10) are evidence of two later subaerial faulting events that produced surface rupture.

The presence of correlative strata across the fault zone allowed us to measure vertical displacement (throw) for different time periods, although erosion, burrowing, and soil development limit the number of useful marker horizons in the upper part of the trenches. By projecting the average footwall and hanging-wall dips of the basal contact of the Gilbert shorezone sand (unit 7), we measured 0.7–0.9 m of displacement across the fault zone in the West(S) trench and 0.9–1.1 m of displacement in the West(N) trench. This gives a latest Pleistocene–Holocene (post-13 ka) throw of 0.9 ± 0.2 m. By projecting the average footwall

and hanging-wall dips of the basal contact of the Bonneville clay with turbidites (unit 2c), we measured 1.7–2.0 m of displacement across the fault zone in the West(S) trench and 1.8–2.0 m of displacement in the West(N) trench. This gives a throw of 1.9 ± 0.2 m since about 24 ka (OSL sample BL-L3).

Dividing the cumulative vertical displacement by four faulting events (see "Chronology of Surface-Faulting Earthquakes" below) yields an average per-event displacement of 0.5 ± 0.1 m (2σ). The maximum thickness of the oldest colluvial wedge (unit 6), 0.5 m, is the same as the calculated per-event displacement, but the maximum thickness of the youngest colluvial wedge (unit 10), 0.17 m, is much less than the calculated per-event displacement. The thinness of the youngest wedge could reflect smaller vertical displacement in the corresponding surface-faulting event. However, as noted above, vertical displacement across the western trace of the Granger fault at the Baileys Lake site includes a component of warping. Exposures on both walls of the West(N) trench (plate 1) indicate that warping of units 7 and 8 (i.e., warping associated with the most recent faulting event) may account for vertical displacement of at least 0.3 m; combining this with the colluvial-wedge thickness results in a total minimum vertical displacement of 0.47 m. Alternatively, net cumulative displacement across the Granger fault in the most recent faulting event may have resulted from coseismic displacement on both the western and eastern traces.

**Eastern trace:** In the East trench, the fault-zone deformation of the eastern trace of the Granger fault is expressed as broad warping across an 8-m-wide deformation zone (h-17 to h-25; plate 1). We observed no discrete shear on fault planes, which would have been readily apparent in the well-stratified Bonneville lacustrine deposits at the base of the trench exposure. The base of the Bonneville regressive deposits (unit 3) was the best horizon for measuring the vertical offset across the warp zone; we projected this planar contact across the warp zone and measured 0.5 ± 0.1 m of offset. Geologic unit boundaries above unit 3 are much less planar, and are particularly convoluted near the middle of the warp zone. The disruption of the Holocene section in this trench was likely caused by ground oscillation accompanying liquefaction of the relatively sandy deposits above the Bonneville clays. The combination of liquefaction-related deformation, burrowing, and overprinting by stage II soil carbonate development made it difficult to determine if post-Bonneville deposits are warped the same amount as the Bonneville deposits.

The warping on the eastern trace of the Granger fault may indicate that either a small vertical displacement has occurred on this fault strand, and/or fault movement occurred when the water table was high and the fine-grained deposits were saturated and deformed plastically. Although we cannot be certain of the number of events responsible for this small amount of warping, we attribute it to a single post-Bonneville (Holocene) earthquake.

## Paleoseismology of the Baileys Lake Site

### Chronology of Surface-Faulting Earthquakes

At the Baileys Lake site, at least four large earthquakes associated with movement on the Granger fault occurred after deposition of Lake Bonneville highstand clay (unit 2e) at about 19 ka (figures 13 and 14; table 1). We found evidence for four earthquakes (BL1 through BL4) on the western trace of the fault and at least one earthquake on the eastern trace. As discussed above, although the amount of vertical offset (0.5 ± 0.1 m) across the eastern-trace warp zone is consistent with the average per-event vertical displacement across the western-trace fault zone, we cannot unequivocally attribute the eastern deformation to a single event. Also, the lack of data to narrowly constrain the time of the eastern deformation precludes correlation with faulting on the western trace. The time of the eastern deformation can only be defined as post-Bonneville (Holocene).

The two oldest earthquakes (BL4 and BL3) documented in the western trenches are based on structural and stratigraphic relations within the pre-Gilbert lacustrine section, whereas the two youngest earthquakes (BL2 and BL1) are based on scarp-colluvial deposits. Earthquake timing is based on OxCal modeling (appendix G).

Earthquake BL4 occurred at 15.7 ± 3.4 ka and is based on (1) the pronounced monoclinal folding of the Bonneville transgressive deposits (unit 2) in the fault zone (i.e., folded to a greater degree than overlying units), (2) the internal deformation in units 2d and 2e that is likely related to liquefaction, (3) the subaqueous erosion surface at the top of unit 2e, and (4) the thin breccia layer that immediately overlies the erosion surface at the top of unit 2e. The modeled earthquake time (around the time of occupation of the Provo shoreline) is consistent with the style of deformation (folding vs. fault-plane shear) and the lack of associated scarp-derived colluvium, which indicate a sublacustrine event. Also, the structural and stratigraphic relations (as described in the following paragraph) indicate BL4 occurred prior to deposition of Bonneville regressive deposits (unit 3) around 14 ka. An OSL age of 19.3 ± 0.8 ka (BL-L7) from a turbidite near the top of the Bonneville transgressive sequence provides a maximum limit on the earthquake time, and an OSL age of 14.1 ± 1.6 ka (BL-L8) from the base of unit 3 provides a relatively close minimum limit.

The four observations listed above that provide the basis for earthquake BL4 suggest the following scenario. Upward propagation of fault rupture formed a subaqueous scarp (characterized by monoclinal folding of Bonneville transgressive deposits) on the floor of Lake Bonneville. Strong ground shaking that accompanied the fault rupture triggered liquefaction in the sandy, relatively thick turbidite bed of unit 2d, and fluidization of this bed resulted in internal deformation (stretching and disruption of clay
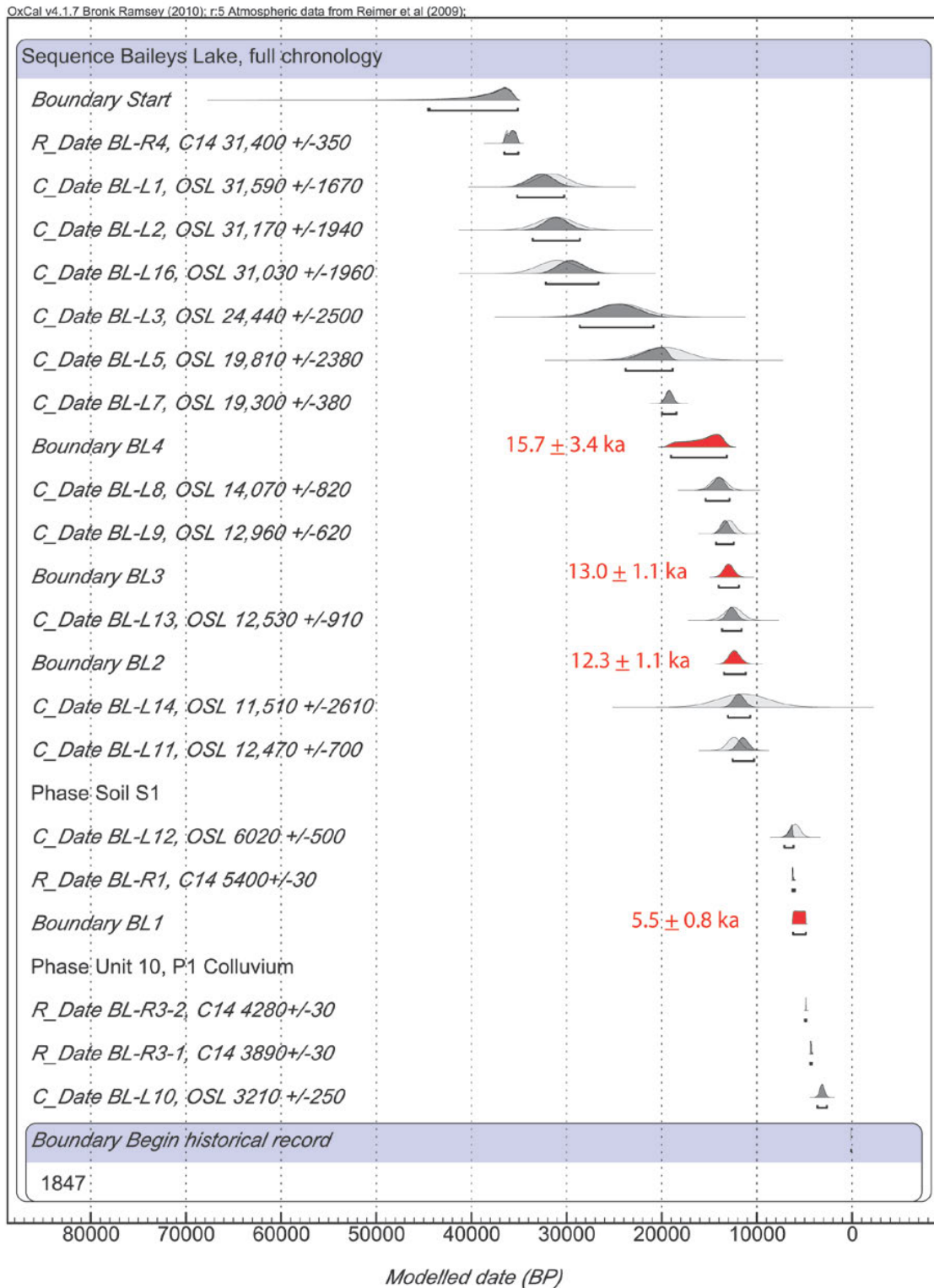
*Figure 13.* *OxCal model for the Baileys Lake site, showing stratigraphic ordering of radiocarbon and luminescence ages (appendices D and E) and probability density functions (PDFs) for the timing of earthquakes BL1–BL4 (red). Appendix G presents a summary table of the model output. The model includes **C_Date** for luminescence ages, **R_Date** for radiocarbon ages, **Phase** for groups of ages where the relative stratigraphic ordering is unknown, and **Boundary** for undated events (e.g., earthquake BL1); see DuRoss and others (2011) for a general discussion of OxCal modeling applied to paleoseismic studies. Model constructed using OxCal version 4.1.7 (Bronk Ramsey, 2009) and the IntCal09 radiocarbon calibration curve (Reimer and others, 2009). Brackets below PDFs indicate 2σ time ranges.*
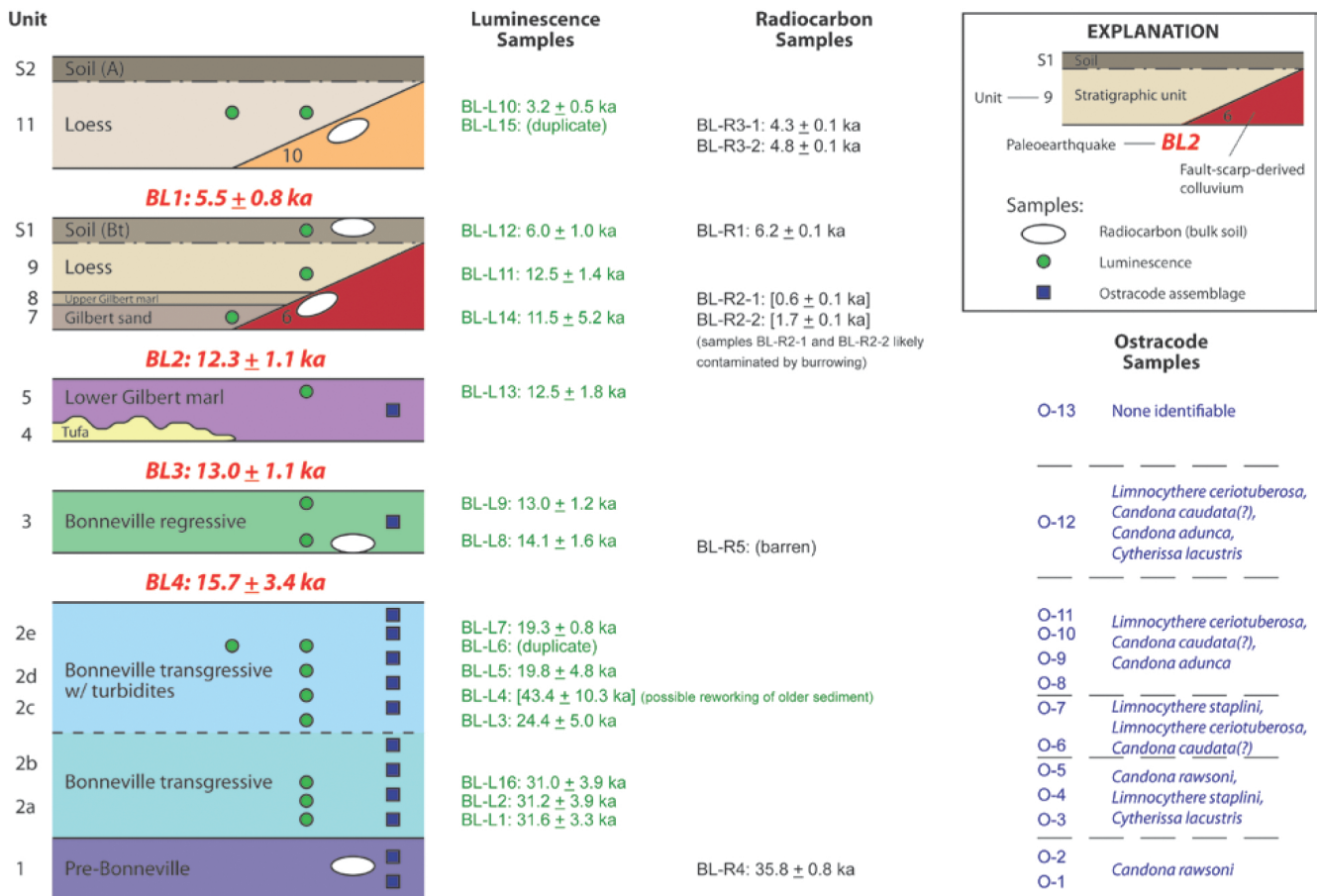
**Figure 14.** *Chronostratigraphic summary for the Baileys Lake site, showing timing of earthquakes BL1 through BL4 as modeled in OxCal (see figure 13 and appendix G). Earthquake times and all numerical ages are reported with 2σ uncertainty; brackets indicate age out of stratigraphic order (within uncertainty limits)—note that these ages were not used as constraints in the OxCal modeling. Refer to appendices C and D (radiocarbon ages), appendix E (luminescence ages), and appendix F (ostracode identification and interpretation) for details.*

**Table 1.** *Summary of Baileys Lake earthquake timing and displacement data.*

| Event[1] | Mean[2] (ka) | ±2σ[2] (kyr) | 5%[2] (ka) | 95%[2] (ka) | Displacement[3] (m) | Unit[4] |
|---|---|---|---|---|---|---|
| BL1 | 5.54 | 0.80 | 4.86 | 6.19 | 0.4–0.6 | 10 |
| BL2 | 12.34 | 1.14 | 11.17 | 13.47 | 0.4–0.6 | 6 |
| BL3 | 12.96 | 1.06 | 11.88 | 14.02 | 0.4–0.6 | – |
| BL4 | 15.70 | 3.38 | 13.16 | 19.05 | 0.4–0.6 | – |

[1] Earthquake identified at the Baileys Lake site and modeled in OxCal (figure 13; appendix G).
[2] Mean earthquake times, 2σ ranges, and 5th–95th percentile ranges based on the OxCal model (appendix G).
[3] Per-event vertical displacement. Range based on average displacement, colluvial-wedge thickness data, and amount of warping associated with BL1 (see discussion in text).
[4] Trench-log unit for scarp-derived colluvium associated with the earthquake (plate 1; appendix A).

stringers) as well as upright, open folds in the overlying unit 2e; these folds lie well beyond the fault deformation zone—for example, h-8 to h-9 in the West(N) trench, and the western half of the East trench (plate 1). The erosion surface at the top of unit 2e (observed in both the western and eastern trenches) truncates the open folds; this erosion also dramatically thinned unit 2e near the fault—for example, h-22.6, v-2.4, West(N) trench (plate 1)—indicating that a scarp produced by the monoclinal folding was present at the time of the erosional event. We hypothesize that the erosion occurred immediately after scarp formation during BL4 (i.e., the erosion surface is an event horizon associated with BL4), and was produced by strong lake-bottom currents that resulted from vertical offset of the lake floor. These currents were likely also responsible for transporting carbonate fragments to the site, which were deposited in the thin breccia layer that accumulated on top of the erosion surface as sediment eventually settled out of the turbid (post-earthquake) lake water. Collectively, the liquefaction in unit 2d, folding in unit 2e, subaqueous erosion at the top of unit 2e, and the breccia at the base of unit 3 resemble features of seismites that have been

described from the Dead Sea rift basin (e.g., Marco and Agnon, 1995, 2005; Agnon and others, 2006), and we interpret this stratigraphic sequence as a seismite associated with earthquake BL4.

The timing of BL4 is likely responsible for the apparent absence of a stratigraphic signature of the Bonneville Flood (~18 ka) in the Lake Bonneville section at the Baileys Lake site. Any stratigraphic evidence for the flood that might have existed would have been destroyed as the sediments at the top of the transgressive sequence were disturbed and redistributed during strong ground shaking and then eroded by the ensuing strong lake-bottom currents. Alternatively, Hylland and others (2012) noted that the two-sigma timing range (12.3–19.1 ka) of BL4 overlaps the time of the flood, so an earthquake (possibly a WVFZ–SLCS coseismic event) coincident with the flood cannot be ruled out.

Earthquake BL3 occurred at 13.0 ± 1.1 ka, prior to transgression of the Gilbert-episode lake across the site, and is based on two structural and stratigraphic relations: (1) A small block of Bonneville regressive marl (unit 3) is preserved in the hanging wall within the fault zone at h-22.6, v-2.5, West(N) trench (plate 1). Along with units 2e and 2d, the marl has been tightly folded by fault movement subsequent to the monoclinal folding of BL4. The tight folding does not involve, and therefore predates, the basal Gilbert erosional unconformity and the overlying Gilbert marl (unit 5). (2) A splay fault cuts unit 3 and older deposits, and is in turn truncated by the basal Gilbert unconformity; see h-22.2, v-2.3, West(N) trench (plate 1). Therefore, the fault movement postdates deposition of the Bonneville regressive marl and predates the Gilbert transgression. An OSL age of 13.0 ± 1.2 ka (BL-L9) provides a close maximum limit on the earthquake time, and an OSL age of 12.5 ± 1.8 ka (BL-L13) provides a minimum limit. BL3 occurred around the time that Lake Bonneville reached near-desiccation levels; the presence of fault-plane shear (i.e., brittle deformation) suggests that the lacustrine sediments may not have been saturated, and the faulting may have been a subaerial event. However, no scarp-derived colluvium associated with this earthquake is apparent in the trench exposures. If a colluvial wedge had formed, it likely was eroded during transgression of the Gilbert-episode lake across the site.

Earthquake BL2 occurred at 12.3 ± 1.1 ka and is based on a wedge of scarp-derived colluvium (unit 6) that accumulated between Gilbert marl depositional episodes (units 5 and 8) and before deposition of early Holocene loess (unit 9). An OSL age of 12.5 ± 1.8 ka (BL-L13) provides a relatively close maximum limit on the earthquake time, and OSL ages of 11.5 ± 5.2 ka (BL-L14) and 12.5 ± 1.4 ka (BL-L11) provide minimum limits. The distinctive sedimentary texture of the colluvial wedge (suggesting wet depositional conditions) is consistent with the earthquake occurring around the time of the Gilbert lake cycle, probably when the lake was below the elevation of the site and just prior to the second Gilbert

transgression. As noted above ("Scarp-Derived Colluvium" section), the stratigraphic relation between the colluvial wedge and Gilbert shorezone sand (unit 7) is unclear, and the radiocarbon ages for organic sediment from the colluvial wedge are unreliable, but the two units may be roughly contemporaneous.

Earthquake BL1—the most recent earthquake—occurred at 5.5 ± 0.8 ka. Evidence for BL1 includes unfaulted scarp colluvium (unit 10) and an eroded fault free face, fault offset of the BL2 scarp colluvium, and warping of post-BL2 deposits (e.g., unit 8). Unit 10 overlies soil S1, which yielded ages of 6.0 ± 1.0 ka (BL-L12) and 6.2 ± 0.1 ka (BL-R1); these ages provide a close maximum limit on the time of BL1. Unit 10 colluvium yielded ages of 4.3 ± 0.1 ka (BL-R3-1) and 4.8 ± 0.1 ka (BL-R3-2), which provide a close minimum limit on earthquake timing.

## Earthquake Recurrence and Fault Slip Rate

We calculated recurrence intervals between individual Baileys Lake earthquakes (inter-event recurrence) and over several earthquake cycles (mean recurrence). Using the mean earthquake times, inter-event recurrence intervals for the Granger fault at the Baileys Lake site vary from 0.7 kyr for BL3–BL2 to 6.8 kyr for BL2–BL1 (table 2). Using the three intervals between BL4 and BL1, the mean post-Bonneville highstand recurrence interval for the Granger fault at the Baileys Lake site is 3.4 kyr. The mean Holocene recurrence interval is about 6 kyr (two earthquakes in about 12 kyr).

Because of the uncertainty in amount of displacement associated with earthquake BL1, we calculate only open-ended vertical slip rates for the Granger fault at the Baileys Lake site. The post-Bonneville highstand slip rate is about 0.09–0.12 mm/yr based on 1.7–2.1 m of displacement in 18 kyr, and the Holocene slip rate is about 0.06–0.09 mm/yr based on 0.7–1.1 m of displacement in about 12 kyr.

# PALEOSEISMOLOGY OF THE WEST VALLEY FAULT ZONE

## Correlation of Earthquakes

Fault-trench data document at least six large earthquakes on the WVFZ—five on the Granger fault and one on the Taylorsville fault—since the time of the Lake Bonneville highstand around 18 ka. The data are for the four (or more) earthquakes identified at the Baileys Lake site, and two earthquakes identified in consultants' trenches excavated as part of pre-development fault-setback investigations required by local governments (discussed further in the "Earthquake Timing and Recurrence" section below; see also appendix H). By comparison, Keaton and others (1987) and Keaton and Currey (1989) postulated one to five post-Bonneville highstand earthquakes at various individual sites on the WVFZ, and six to seven earthquakes on the

**Table 2.** *Chronology and recurrence of surface-faulting earthquakes at the Baileys Lake site.*

| Baileys Lake Earthquake | Earthquake Time (ka) | Chronology (ka) | Inter-event RI[1] (kyr) |
|---|---|---|---|
| BL1 | 5.5 ± 0.8 | **5.5** (4.7–6.3) | – |
| BL2 | 12.3 ± 1.1 | **12.3** (11.2–13.4) | BL2–BL1: **6.8** (4.9–8.7) |
| BL3 | 13.0 ± 1.1 | **13.0** (11.9–14.1) | BL3–BL2: **0.7** (0–2.9) |
| BL4 | 15.7 ± 3.4 | **15.7** (12.3–19.1) | BL4–BL3: **2.7** (0–7.2) |

| Interval | Elapsed Time (kyr) | No. Intervals | Mean RI[2] (kyr) | Notes |
|---|---|---|---|---|
| BL3–BL1 | 7.5 | 2 | 3.8 | post-Provo shoreline (<14 ka) |
| BL4–BL1 | 10.2 | 3 | 3.4 | post-Bonneville highstand (<18 ka) |

[1] Recurrence interval (RI) calculated from mean earthquake times (bold), with minimum and maximum recurrence intervals calculated from 2σ ranges of earthquake times; RI = 0 results from overlapping 2σ ranges.

[2] Recurrence interval calculated from elapsed time between earthquakes (based on mean earthquake times) divided by number of inter-event time intervals.

WVFZ as a whole. However, the numbers of earthquakes determined in those two studies were primarily from geomorphic observations, total stratigraphic offset documented in boreholes, and an estimated average per-event vertical displacement of 1.2–1.5 m that was based on cross-cutting geomorphic relations and a single vertical displacement measurement from a trench exposure at the Pioneer Industrial Park site (figure 4; Keaton and others, 1987). Given the average per-event vertical displacement of the Baileys Lake earthquakes of 0.5 ± 0.1 m, and the single-event displacement from a consultant's trench on the northern part of the Taylorsville fault of 0.5–0.7 m (Solomon, 1998; unpublished UGS data), a displacement of 1.2–1.5 m may be more representative of maximum displacement than average displacement. Interestingly, two-dimensional boundary-element modeling by Bruhn and Schultz (1996) showed that, on average, net slip and surface offset on antithetic faults was about 20–30 percent of the net slip on an underlying listric master fault. Applying this reduction factor to SLCS displacements ranging from 0.8 to 2.2 m (DuRoss and others, 2014) predicts WVFZ displacements on the order of 0.2–0.7 m. Finally, because Keaton and others (1987) and Keaton and Currey (1989) were unable to more precisely determine the times of individual earthquakes, we cannot directly correlate their earthquakes, the Baileys Lake earthquakes, and the earthquakes documented in consultants' trenches.

## Earthquake Timing and Recurrence

Because of the distributed nature of surface faulting across the WVFZ, a complete chronology of latest Quaternary earthquakes likely cannot be obtained from a single site. Keaton and others (1987) and Keaton and Currey (1989) demonstrated considerable differences, both east-to-west and north-to-south, in the possible number of earthquakes at different sites (i.e., between the Granger and Taylorsville faults and along the strike of the Granger fault, respectively). A relatively complete earthquake record could only be obtained by paleoseismic studies at numerous sites on both the Granger and Taylorsville

faults, and given the restrictions associated with site access, scarp modification related to development activities, and shallow groundwater, a complete record may never be obtained. Accordingly, the chronologies we present here for the Granger fault and WVFZ as a whole are incomplete (i.e., preliminary).

Table 3 shows a preliminary chronology of large earthquakes on the Granger fault, developed from our Baileys Lake data and earthquake-timing data from a consultant's trench in the middle part of the westernmost trace of the Granger fault (Terracon site; see figure 4 for site location). A bulk-soil sample collected in 1998 by UGS geologists from what was interpreted as scarp-derived colluvium yielded an AMRT radiometric age of 1880 ± 80 ^{14}C yr B.P. (unpublished UGS data). UGS geologists had limited time in the trench and could not prepare a detailed log, so the geologic context of this sample is not well documented; the sample may have come from a soil A horizon buried beneath the colluvial wedge, rather than from the colluvium itself (appendix H). Given the uncertainty as to whether the age of the sampled sediment provides a minimum or maximum limit on earthquake timing, we constructed two OxCal models (appendix H) to account for both possibilities and use the mean of the two modeled earthquake times (1.4 ± 0.7 ka) for this earthquake.

The range of inter-event recurrence intervals for the five Granger-fault earthquakes is the same as for the Baileys Lake site: 0.7–6.8 kyr (tables 2 and 3). The variability in inter-event recurrence undoubtedly reflects differences in surface-faulting activity on different strands of the fault, as suggested by the apparent difference in timing of the most recent earthquake at the Terracon site with that at the Baileys Lake site (earthquake BL1). Mean recurrence intervals range from 3.6 to 5.4 kyr, but again, the earthquake chronology for the Granger fault is likely incomplete and actual mean recurrence intervals are likely shorter. Keaton and others (1987) and Keaton and Currey (1989) calculated average recurrence estimates of

2.6–14 kyr for the Granger fault. However, as discussed above, these recurrence estimates are based on an assumed number of faulting events within a given time period, so their estimates have large uncertainties.

Table 4 shows a preliminary chronology of surface-faulting earthquakes for the WVFZ as a whole, developed from our Baileys Lake data, the Terracon site data, and earthquake-timing data from a consultant's trench at the northern end of the Taylorsville fault (AGRA site; see figure 4 for site location). In 1997, UGS geologists collected two bulk-soil samples from the AGRA trench: a sample of crack-fill sediment/fault-zone colluvium yielded an AMRT age of 2350 ± 80 ^{14}C yr B.P., and a sample from sag pond deposits beneath a possible colluvial wedge yielded an AMRT age of 2520 ± 70 ^{14}C yr B.P. (unpublished UGS data). Solomon (1998) reported the earthquake time as ~2.2 ka (the average of the two calendar-calibrated ages), and our OxCal model yielded a similar result (2.2 ± 0.2 ka; appendix H).

**Table 3.** *Preliminary chronology and recurrence of surface-faulting earthquakes on the Granger fault.*

| Granger Fault Earthquake | Baileys Lake Site (ka) | Terracon Site[1] (ka) | Preliminary Chronology[2] (ka) | Inter-event RI[3] (kyr) |
|---|---|---|---|---|
| G1[4] | – | 1.4 ± 0.7 | **1.4** (0.7–2.1) | – |
| G2 | 5.5 ± 0.8 (BL1) | – | **5.5** (4.7–6.3) | G2–G1: **4.1** (2.6–5.6) |
| G3 | 12.3 ± 1.1 (BL2) | – | **12.3** (11.2–13.4) | G3–G2: **6.8** (4.9–8.7) |
| G4 | 13.0 ± 1.1 (BL3) | – | **13.0** (11.9–14.1) | G4–G3: **0.7** (0–2.9) |
| G5 | 15.7 ± 3.4 (BL4) | – | **15.7** (12.3–19.1) | G5–G4: **2.7** (0–7.2) |

| Interval | Elapsed Time (kyr) | No. Intervals | Mean RI[5] (kyr) | Notes |
|---|---|---|---|---|
| G3–G1 | 10.9 | 2 | 5.4 | latest Pleistocene–Holocene (<13 ka) |
| G4–G1 | 11.6 | 3 | 3.9 | post-Provo shoreline (<14 ka) |
| G5–G1 | 14.3 | 4 | 3.6 | post-Bonneville highstand (<18 ka) |

[1] Earthquake time based on single limiting age (see discussion in text, and appendix H). See figure 4 for site location.
[2] Mean earthquake time and 2σ range; see appendices G and H for OxCal modeling.
[3] Recurrence interval (RI) calculated from mean earthquake times (bold), with minimum and maximum recurrence intervals calculated from 2σ ranges of earthquake times; RI = 0 results from overlapping 2σ ranges.
[4] Earthquake time poorly constrained; see appendix H.
[5] Recurrence interval calculated from elapsed time between earthquakes (based on mean earthquake times) divided by number of inter-event time intervals.

**Table 4.** *Preliminary chronology and recurrence of surface-faulting earthquakes on the West Valley fault zone.*

| WVFZ Earthquake | Granger Fault (ka) | Taylorsville Fault (ka) | Preliminary Chronology[1] (ka) | Inter-event RI[2] (kyr) |
|---|---|---|---|---|
| W1[3] | 1.4 ± 0.7 (Terracon) | – | **1.4** (0.7–2.1) | – |
| W2[3] | – | 2.2 ± 0.2 (AGRA)[4] | **2.2** (2.0–2.4) | W2–W1: **0.8** (0–1.7) |
| W3 | 5.5 ± 0.8 (BL1) | – | **5.5** (4.7–6.3) | W3–W2: **3.3** (2.3–4.4) |
| W4 | 12.3 ± 1.1 (BL2) | – | **12.3** (11.2–13.4) | W4–W3: **6.8** (4.9–8.7) |
| W5 | 13.0 ± 1.1 (BL3) | – | **13.0** (11.9–14.1) | W5–W4: **0.7** (0–2.9) |
| W6 | 15.7 ± 3.4 (BL4) | – | **15.7** (12.3–19.1) | W6–W5: **2.7** (0–7.2) |

| Interval | Elapsed Time (kyr) | No. Intervals | Mean RI[5] (kyr) | Notes |
|---|---|---|---|---|
| W3-W1 | 4.1 | 2 | 2.0 | mid-Holocene (<6 ka) |
| W4-W1 | 10.9 | 3 | 3.6 | latest Pleistocene–Holocene (<13 ka) |
| W5-W1 | 11.6 | 4 | 2.9 | post-Provo shoreline (<14 ka) |
| W6-W1 | 14.3 | 5 | 2.9 | post-Bonneville highstand (<18 ka) |

[1] Mean earthquake time and 2σ range; see appendices G and H for OxCal modeling.
[2] Recurrence interval (RI) calculated from mean earthquake times (bold), with minimum and maximum recurrence intervals calculated from 2σ ranges of earthquake times; RI = 0 results from overlapping 2σ ranges.
[3] Earthquake time poorly constrained; see appendix H.
[4] Earthquake time from Solomon (1998) and unpublished Utah Geological Survey files (see discussion in text, and appendix H). See figure 4 for site location.
[5] Recurrence interval calculated from elapsed time between earthquakes (based on mean earthquake times) divided by number of inter-event time intervals.

The range of inter-event recurrence intervals for the WVFZ as a whole is the same as for the Granger fault (0.7–6.8 kyr), but the mean recurrence intervals range from 2.0 to 3.6 kyr (tables 3 and 4). Again, the variability reflects differences in surface-faulting activity on different strands of the fault zone combined with an incomplete earthquake chronology, and actual mean recurrence intervals are likely shorter. Keaton and others (1987) and Keaton and Currey (1989) reported average recurrence estimates of 1.8–2.2 kyr for the WVFZ as a whole, but these estimates are subject to large uncertainty as discussed above. When the UQFPWG evaluated existing paleoseismic data for the WVFZ in the early 2000s, they considered the available data to be insufficient to estimate preferred and 5th–95th percentile recurrence intervals for the WVFZ (Lund, 2005).

## Slip Rate

The cumulative displacement data obtained by Keaton and others (1987) and Keaton and Currey (1989), combined with the well-documented late Quaternary stratigraphic record of pluvial-lake-cycle and interpluvial sedimentation, allowed them to calculate average slip rates for different time intervals. Their slip rates include 0.03–0.5 mm/yr for the Granger fault over various time intervals within the past 140 kyr, 0.1–0.2 mm/yr for the Taylorsville fault since 12 ka, and 0.5–0.6 mm/yr for the entire WVFZ since 13 ka (table 5). Using these data, the UQFPWG estimated 5th percentile, preferred, and 95th percentile slip rates of 0.1–0.4–0.6 mm/yr for the WVFZ (Lund, 2005). Our calculated slip rates for the Granger fault of 0.09–0.12 mm/yr (post-Bonneville highstand) and 0.06–0.09 mm/yr (Holocene), based on data from the Baileys Lake site, fall within the previously determined range for the fault. Given the small number of events documented in paleoseismic trenching studies and the likelihood of an incomplete paleoseismic record for the WVFZ, we do not attempt to evaluate changes in slip rate over time based on inter-event times and per-event displacements.

## Discussion

Our investigation at the Baileys Lake site improves the late Quaternary earthquake history of the Granger fault, and of the WVFZ as a whole, by providing per-event timing and displacement data for four earthquakes since the Bonneville highstand around 18 ka. Our data, combined with earthquake-timing data from consultants' trenches, provide evidence for six earthquakes on the WVFZ: five on the Granger fault and one on the Taylorsville fault. Inter-event recurrence intervals range from 0.7 to 6.8 kyr for both the Granger fault and the entire WVFZ, and mean recurrence over different time intervals ranges from 3.6 to 5.4 kyr for the Granger fault and 2.0 to 3.6 kyr for the entire WVFZ. The variability in recurrence intervals, similar to that documented by Keaton and others (1987) and Keaton and Currey (1989), likely results from differences in surface-faulting activity on different strands of the fault zone combined with an incomplete earthquake chronology, and actual mean recurrence intervals are likely shorter than those that we report here.

We found evidence at the Baileys Lake site for two earthquakes that occurred during the Bonneville lake cycle: one (BL4) during the early part of the regressive phase of the lake and one (BL3) near the end of the regression. This differs from the findings of Keaton and others (1987), who found no evidence of differential displacements within Bonneville lake-cycle sediments in their boreholes near the south end of the Granger fault. As a result, they interpreted a period of tectonic quiescence on that part of the fault during Lake Bonneville time. Additionally, the timing of the most recent surface-faulting earthquake documented at the Baileys Lake site (BL1) differs substantially from the timing of the most-recent earthquakes documented in consultants' trenches elsewhere on the WVFZ (one on the Granger fault and one on the Taylorsville fault). These differences underscore the spatial and temporal variability of surface faulting across a distributed fault system like the WVFZ, where some strands may rupture in one earthquake and different strands rupture in another earthquake.

Average per-event vertical displacement for the Granger fault at the Baileys Lake site is 0.5 ± 0.1 m. This is similar to the 0.5–0.7 m of displacement measured for a single surface-faulting earthquake documented in a consultant's trench near the north end of the Taylorsville fault (Solomon, 1998; unpublished UGS data; appendix H), and is also similar to the displacement range of 0.2–0.7 m predicted by a master–antithetic fault relation determined by two-dimensional boundary-element modeling (Bruhn and Schultz, 1996). By comparison, Keaton and others (1987) estimated an average per-event vertical displacement of 1.2–1.5 m for the WVFZ, but this estimate was based on cross-cutting geomorphic relations and a single vertical displacement measurement from a trench exposure. Also, the displacement data of Keaton and others are from near the middle of the WVFZ, whereas the Baileys Lake site and the consultant's trench site on the Taylorsville fault are near the northern end of the mapped traces of those faults. Displacement may increase toward the middle of the fault zone if the along-strike distribution of slip on the WVFZ has an ellipsoidal shape, and a displacement of 1.2–1.5 m may be more representative of maximum displacement than average displacement.

## COMPARISON OF SURFACE-FAULTING CHRONOLOGIES FOR THE WEST VALLEY FAULT ZONE AND SALT LAKE CITY SEGMENT OF THE WASATCH FAULT ZONE

A major goal of this study was to compare surface-faulting chronologies of the WVFZ and SLCS and thus clarify the seismogenic relation between the two fault zones (i.e., to what extent the WVFZ is seismically independent of, or moves coseismically with, the SLCS). Kinematic modeling of a normal fault system comprising a master fault and antithetic fault that intersect in a weak, partly ductile zone at a depth of about

**Table 5.** *Summary of displacement, recurrence, and slip-rate data for the West Valley fault zone.*

| Time Interval[1] | Vertical Displacement | Number of Events[2] | Site and Reference | Evidence/Comments | Ave. RI (kyr) | Ave. SR[3] (mm/yr) |
|---|---|---|---|---|---|---|
| **Granger fault:** | | | | | | |
| 11–0 ka | 1.4–1.5 m | 1 | Goggin Drain (Keaton and Currey, 1989) | Boreholes; offset of post-Bonneville red beds calculated from horizontal projection and first-order trend surfaces | NA | 0.1 |
| 12–0 ka | 0.7–1.1 m | 2 | Baileys Lake (this study) | Trenches; faulted post-Bonneville sediments | 6.0 | 0.06–0.09 |
| 12.5-9 – 0 ka | 0.7 m | 1 | Three Flags (Keaton and Currey, 1989) | Boreholes; offset of post-Bonneville red beds calculated from horizontal projection | NA | 0.06–0.08 |
| 12.5-11.5 – 0 ka | ≤ 3 m | 2 | 1300 South (Keaton and Currey, 1989) | Boreholes; offset of post-Bonneville red beds calculated from horizontal projection and first-order trend surfaces | 5.8–6.3 | 0.3 |
| 13–0 ka | 5.2–6.7 m | 2 | UDOT (Keaton and others, 1987) | Boreholes; playa formation (event 1), burial by scarp-derived colluvium (event 2) | 6.5 | 0.4–0.5 |
| 13–0 ka | — | 3 | Central part of Granger fault traces (Keaton and others, 1987) | Geomorphic; depositional features and paleochannels | — | — |
| 13–0 ka | — | 5 | Central to southern Granger fault (Keaton and others, 1987) | Combined borehole and geomorphic | 2.6 | 0.4–0.5 |
| 18–0 ka | 1.7–2.1 m | 4 | Baileys Lake (this study) | Trenches; faulted Bonneville and post-Bonneville sediments | 3.4 | 0.1 |
| 28-22 – 0 ka | 3–4 m | 2 | Goggin Drain (Keaton and Currey, 1989) | Boreholes; offset of Fielding Geosol calculated from horizontal projection and first-order trend surfaces | 11.0–14.0 | 0.1–0.2 |
| 28-22 – 0 ka | 4.5 m | 3 | 1300 South (Keaton and Currey, 1989) | Boreholes; offset of Fielding Geosol calculated from horizontal projection and first-order trend surfaces | 7.3–9.3 | [0.2] |
| 26–13 ka | 0 m | 0 | UDOT (Keaton and others, 1987) | Boreholes; top and bottom of Bonneville Alloformation displaced same amount | NA | 0 |
| 60–26 ka | ≥ 7.6 m | >2 (est. 5-6) | UDOT (Keaton and others, 1987) | Boreholes; colluvium underlying and overlying Cutler Dam Alloformation in hanging wall | [5.7–6.8] | [≥ 0.2] |
| 60–0 ka | ≥ 12.8–14.3 m | — | UDOT (Keaton and others, 1987) | Boreholes; cumulative post-Cutler Dam (60 ± 20 ka) displacement | — | ≥ 0.2–0.4 |
| 140–60 ka | 3.1–6.1 m | (est. 3–4) | UDOT (Keaton and others, 1987) | Boreholes; colluvium between Cutler Dam and Little Valley Alloformations in hanging wall | [20.0–27.0] | 0.03–0.1 |
| 140–0 ka | 17.4–18.9 m | (est. 11–16) | UDOT (Keaton and others, 1987) | Boreholes; cumulative post-Little Valley (140 ± 10 ka) displacement | [8.8–12.7] | 0.1 |
| **Taylorsville fault:** | | | | | | |
| ~6–0 ka | 0.5–0.7 m | 1 | AGRA site (1300 N 2200 W) (Solomon, 1998; unpublished UGS data) | Trench; faulted post-Bonneville sediments | NA | 0.1 |
| 12–0 ka | >1.2–1.5 m | 2 | Pioneer Industrial Park (Keaton and others, 1987) | Trench; deformed Bonneville sediments | 6.0 | >0.1 |
| **Entire West Valley fault zone:** | | | | | | |
| 13–0 ka | >6.4–8.2 m | 6–7 | NA (Keaton and others, 1987) | Combined data for Granger and Taylorsville faults | 1.8– 2.2 | 0.5–0.6 |
| 18–0 ka | >2.3–2.8 m | 6 | NA (this study) | Combined data for Granger and Taylorsville faults | 2.0–3.6 | — |

[1] Time intervals based on correlation of marker beds with the time of pluvial lake-cycle events.
[2] For Keaton and others (1987) and Keaton and Currey (1989) data, number of events is estimated based on assumption of 1.2–1.5 m vertical offset per event.
[3] Reported values rounded to one significant figure.
NA, not applicable; RI, recurrence interval; SR, slip rate; UDOT, Utah Department of Transportation; est. = estimate.
Brackets indicate value derived from data in Keaton and others (1987) or Keaton and Currey (1989) but not given in the original report.

15 km (Bruhn and Schultz, 1996) has shown that movement on the master fault can trigger slip on the antithetic fault, and in the case of a listric master fault, produce antithetic-fault surface rupture. Applying this model to the SLCS (master fault)–WVFZ (antithetic fault) pair, we used our comparison of the timing of surface-faulting earthquakes on the two fault zones to test the hypothesis of seismogenic dependence of the WVFZ on the SLCS.

In this discussion, *independent* refers to antithetic fault rupture that does not contribute seismic moment to an earthquake initiated by slip on a master fault, but has its own moment release in a distinct, separate earthquake. Independent ruptures include triggered events related to but occurring sometime after slip on the master fault (e.g., as part of an aftershock sequence) as well as events that lack a clear relation to slip on the master fault. In contrast, *coseismic* refers to the synchronous rupture of both the master and antithetic faults, where both ruptures contribute seismic moment to a single earthquake. The $M_S$ 6.9 Campania–Basilicata (Italy) earthquake in 1980 is an example of coseismic faulting, where an antithetic fault ruptured 40 s after an earthquake nucleated on the master fault but before the end of the overall rupture episode (Bernard and Zollo, 1989; Westaway, 1992). In contrast, the 1984 Devil Canyon (Idaho) earthquake is an example of independent, triggered rupture, where antithetic faulting on the Lone Pine fault produced an $M_L$ 5.0 aftershock two and a half weeks after the $M_L$ 5.8 main shock on the master Challis fault (Payne and others, 2004). We do not know of a clear example of completely independent rupture of an antithetic fault paired with a major, range-bounding master normal fault. The $M_L$ 6.6 Hansel Valley (Utah) earthquake in 1934 (Walter, 1934; Shenon, 1936; dePolo and others, 1989) may be an example of this, where surface faulting occurred on possible antithetic intrabasin faults but no rupture occurred on the nearby range-bounding North Promontory fault, which may be a master fault. However, a strike-slip focal mechanism has been determined for this earthquake (Doser, 1989), and the vertical offsets on the floor of Hansel Valley could have a non-tectonic origin (e.g., lateral spread), so whether this earthquake is really an example of an independent antithetic faulting event is unclear.

The inherent limitations of paleoseismic earthquake chronologies—primarily related to the uncertainty in earthquake times—make confident determinations of prehistoric coseismic (i.e., synchronous) rupture on a master-antithetic fault pair virtually impossible. Also, the incomplete chronology for the WVFZ complicates direct comparison with the more complete record of the SLCS. Still, a comparison of WVFZ and SLCS chronologies can provide insight into whether an earthquake on the WVFZ may have been, or clearly was not, coseismic with an earthquake on the SLCS. Such a comparison can also show to what degree earthquakes on the WVFZ may be linked to fault activity on the SLCS.

Table 6 and figure 15 show several significant similarities in the times of specific earthquakes on the WVFZ and SLCS (see DuRoss and others [2014] for discussion of the SLCS chronology based on correlation of earthquakes documented at different sites). In particular, the mean times and two-sigma ranges for WVFZ earthquakes W1, W2, W3, and W4 are very similar to those for SLCS earthquakes S1, S2, S4, and S8, respectively (although the earthquake times of W1 and W2 are somewhat less robust given the caveats discussed above in the "Earthquake Timing and Recurrence" section). As figure 15 shows, the mean time of W2 is identical to that of SLCS earthquake S2 as documented at South Fork Dry Creek/Dry Gulch, and differs from the S2 mean time documented at Little Cottonwood Canyon by only 100 yr (~5%). Likewise, the mean time of W3 is identical to that of SLCS earthquake S4 as documented at Little Cottonwood Canyon, and differs from the S4 mean times documented at Penrose Drive and South Fork Dry Creek by ≤500 yr (≤10%). SLCS earthquake S8 has been documented at only one site (Penrose Drive), but its mean time differs from that of W4 by only 200 yr (2%). The mean time and two-sigma range for W5 do not indicate a clear temporal association with a SLCS earthquake; perhaps the relatively short W5-W4 inter-event recurrence interval (0.7 kyr) indicates two WVFZ earthquakes associated with a single SLCS earthquake (S8), or one associated earthquake and one independent earthquake (unlikely, in our opinion). Alternatively, evidence for an SLCS earthquake around the time of W5 may have been removed by erosion or otherwise not documented in the SLCS trench exposures (DuRoss and others, 2014). Finally, the mean time of W6 is similar to that of

*Table 6. Comparison of earthquake times on the West Valley fault zone and Salt Lake City segment.*

| Preliminary WVFZ Chronology | | | Preliminary SLCS Chronology | |
|---|---|---|---|---|
| Earthquake | Mean Time (ka) | 2σ Range (ka) | Earthquake | Min–Max Range[1] (ka) |
| **W1[2]** | 1.4 | 0.7–2.1 | **S1** | 1.1–1.5 |
| **W2[2]** | 2.2 | 2.0–2.4 | **S2** | 1.8–2.6 |
| – | – | – | **S3** | 3.2–4.9 |
| **W3** | 5.5 | 4.7–6.3 | **S4** | 4.5–6.6 |
| – | – | – | **S5** | 6.7–8.5 |
| – | – | – | **S6** | 8.6–10.8 |
| – | – | – | **S7** | 10.7–11.1 |
| **W4** | 12.3 | 11.2–13.4 | **S8** | 10.5–13.7 |
| **W5** | 13.0 | 11.9–14.1 | – | – |
| **W6** | 15.7 | 12.3–19.1 | **S9** | 13.8–19.2 |

[1] Salt Lake City segment chronology represented by minimum and maximum earthquake times derived generally from 2σ ranges for earthquakes at different sites that are considered to correlate with each other based on OxCal modeling (DuRoss and others, 2014). See figure 15 for a graphical representation of mean times and 2σ ranges for earthquakes at the different sites on the West Valley fault zone and Salt Lake City segment.

[2] Earthquake time poorly constrained; see appendix H.
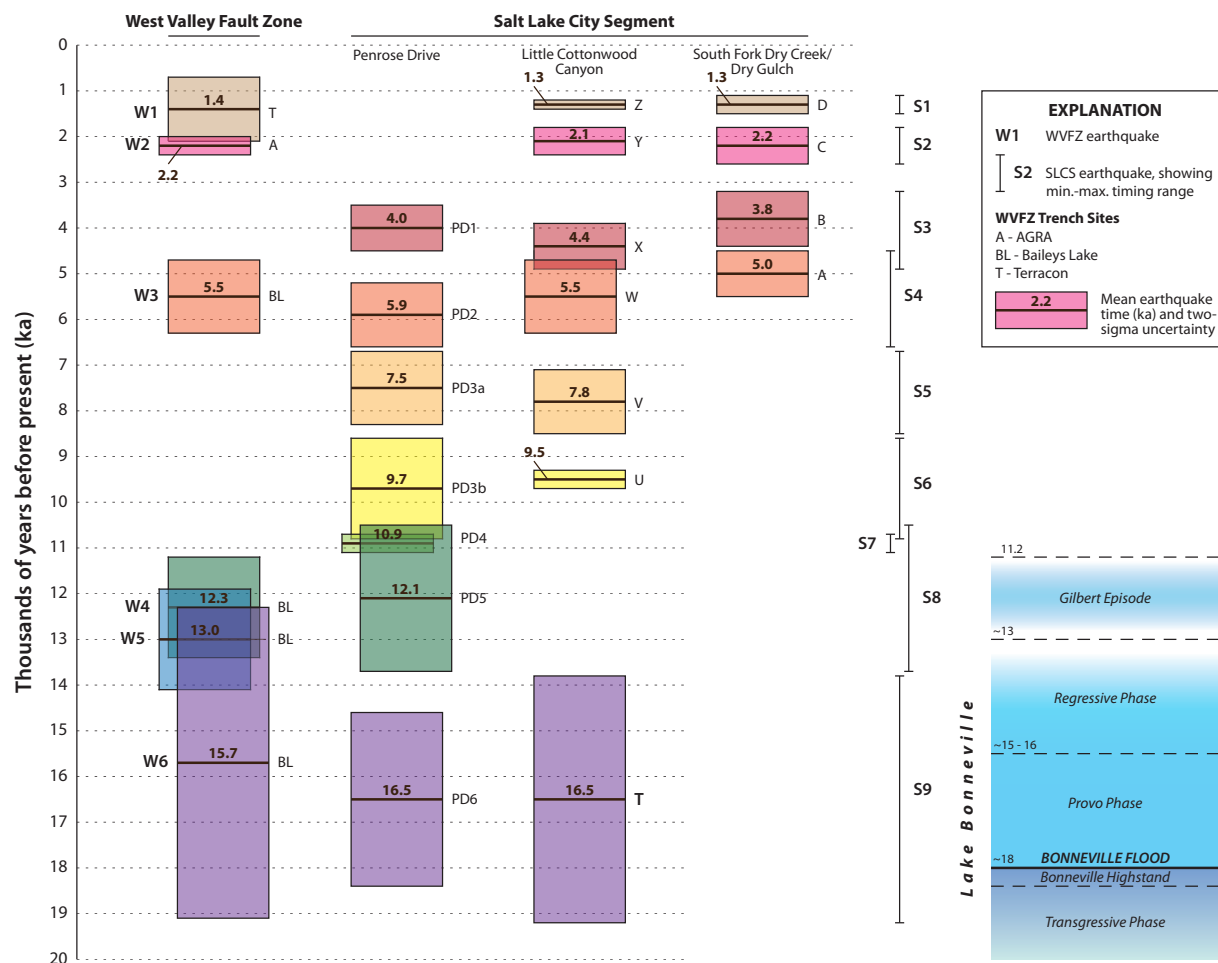
**Figure 15.** *Comparison of surface-faulting chronologies for the West Valley fault zone and Salt Lake City segment (modified from DuRoss and others, 2014). Note that the time of earthquake W1 is based on a single limiting age (see discussion in text, and appendix H). Schematic Lake Bonneville and Gilbert-episode chronologies shown at the same temporal scale for comparison with late Pleistocene earthquake times. Sources of earthquake timing information: West Valley fault zone—this study; Penrose Drive site—DuRoss and others (2014); Little Cottonwood Canyon site—McCalpin (2002), modified by OxCal modeling (DuRoss and others, 2014); South Fork Dry Creek/Dry Gulch site—Black and others (1996), modified by OxCal modeling (DuRoss and others, 2014).*

SLCS earthquake S9 as documented at Penrose Drive and Little Cottonwood Canyon; the 800-yr difference in mean times between these late Pleistocene (~15–16 ka) events represents a difference of only ~5%.

The paleoseismic timing data are consistent with displacement modeling and a general structural model that suggests seismogenic dependence of the WVFZ on SLCS activity. Five of six paleoearthquakes documented on the WVFZ have mean earthquake times and two-sigma ranges that are similar to those of SLCS earthquakes; the one WVFZ earthquake that does not have a clear temporal association with a SLCS earthquake (W5) occurred in the latest Pleistocene (~13 ka), a period in which the SLCS record may be incomplete (DuRoss and others, 2014). Additionally, per-event vertical displacements on the WVFZ (generally 0.4–0.7 m, but perhaps as large as 1.5 m) are similar to those predicted by two-dimensional boundary-element modeling of antithetic faulting triggered by slip on a listric master fault (0.2–0.7 m;

after Bruhn and Schultz, 1996). Finally, although the precise subsurface geometry of the WVFZ–SLCS fault system is unknown, the modeling of Bruhn and Schultz (1996) and seismic reflection profiles across the SLCS and elsewhere across the Wasatch fault zone (Bashore and others, 1981; Bashore, 1982; Smith and Bruhn, 1984; Velasco and others, 2010) indicate the potential for a listric geometry for the SLCS, or at least a flattening of dip at some depth within the seismogenic crust. This structural geometry suggests that the antithetic WVFZ has formed in response to rollover and collapse in the SLCS hanging wall (after the model of Xiao and Suppe, 1992; see also Withjack and others, 1995), and therefore WVFZ movement is likely coseismic (i.e., synchronous) with SLCS movement. Based on comparison of WVFZ and SLCS paleoearthquake timing and displacement data, we infer that large earthquakes on the WVFZ are more likely to be synchronous with or triggered by fault movement on the SLCS than occurring independently of movement on the SLCS. Kinematic and geometric model-

ing of the fault system also indicates a high likelihood for synchronous rupture.

## SUMMARY AND CONCLUSIONS

We conducted a fault-trench investigation at the Baileys Lake site on the WVFZ to answer significant questions regarding the timing, displacement, and recurrence of large (M ~6.5) surface-faulting earthquakes on the WVFZ. We also compared WVFZ earthquake timing and displacement data with data from the SLCS, including new data from the Penrose Drive site on the northern SLCS, to determine whether the WVFZ is seismically independent of, or moves coseismically with, the SLCS.

At the Baileys Lake site, we excavated three trenches across two small (<1-m-high) east-facing fault scarps near the northern end of the Granger fault, which comprises the westernmost traces of the WVFZ. Our trenches exposed late Quaternary geologic deposits consisting of Holocene loess, a nearly complete Lake Bonneville section, and pre-Bonneville wetland/alluvial-marsh sediments dated at 35.8 ± 0.8 ka. Fault-zone deformation exposed at the western scarp includes monoclinal warping and discrete shear offset, whereas we observed only broad, monoclinal warping at the eastern scarp. Stratigraphic and structural relations provide evidence for four surface-faulting earthquakes on the western fault trace, and at least one folding event on the eastern fault trace that may or may not correlate with the most recent surface faulting on the western trace. Seven radiocarbon ages, 14 OSL ages, and 13 ostracode samples provide temporal constraints on earthquake times, which we modeled using OxCal calibration and analysis software. The earliest earthquake, BL4, has a clear event horizon and associated seismite, and occurred at 15.7 ± 3.4 ka (2σ); BL4 was a sublacustrine event (Provo phase of Lake Bonneville). Earthquake BL3, evidenced by fault terminations and timing constraints on deformation of lacustrine strata in the fault zone, occurred at 13.0 ± 1.1 ka, after Lake Bonneville's regression to very low levels and before transgression of the Gilbert lake across the site. Earthquakes BL2 and BL1, the only earthquakes at the Baileys Lake site for which scarp-derived colluvium has been preserved, occurred at 12.3 ± 1.1 ka (during the Gilbert episode) and 5.5 ± 0.8 ka (post-Gilbert), respectively. Average per-event vertical displacement for the Granger fault at the Baileys Lake site is 0.5 ± 0.1 m.

Combining the Baileys Lake data with previous paleoseismic data yields a paleoearthquake chronology comprising six earthquakes for the WVFZ as a whole: five on the Granger fault and one on the Taylorsville fault. Mean recurrence over different time intervals ranges from 3.6 to 5.4 kyr for the Granger fault, and from 2.0 to 3.6 kyr for the WVFZ as a whole. Given the distributed nature of surface faulting on the WVFZ, the variability in recurrence intervals likely results from differences in surface-faulting activity on different fault strands, as well as from an incomplete earthquake chronology for the fault zone as a whole.

Our calculated slip rates for the Granger fault of 0.09–0.12 mm/yr (post-Bonneville highstand) and 0.06–0.09 mm/yr (Holocene), based on data from the Baileys Lake site, fall within the previously determined range for the fault of 0.03–0.5 mm/yr (Keaton and others, 1987; Keaton and Currey, 1989). Because of the small number of earthquakes documented in paleoseismic trenching studies and the likelihood of an incomplete paleoseismic record for the WVFZ, we do not attempt to evaluate changes in slip rate over time for the WVFZ as a whole based on inter-event times and per-event displacements.

All but one of the earthquakes documented on the WVFZ have mean times and two-sigma ranges that are very similar to those of SLCS earthquakes. The one WVFZ earthquake that does not have a clear temporal association with a SLCS earthquake occurred in the latest Pleistocene (~13 ka), a period in which the SLCS record may be incomplete. Also, per-event vertical displacements on the WVFZ (generally 0.4–0.7 m from trench data) are similar to those predicted by two-dimensional boundary-element modeling of antithetic faulting triggered by slip on a listric master fault (0.2–0.7 m; after Bruhn and Schultz, 1996). Based on comparison of WVFZ and SLCS earthquake timing and displacement data, large earthquakes on the WVFZ that are coseismic with or triggered by fault movement on the SLCS have a higher likelihood than WVFZ earthquakes that occur independently of movement on the SLCS. When considered together with mechanical and geometric models of the fault system, the paleoseismic data support a high likelihood for synchronous rupture of the WVFZ with the SLCS.

## ACKNOWLEDGMENTS

# REFERENCES

Agnon, A., Migowski, C., and Marco, S., 2006, Intraclast breccias in laminated sequences reviewed—recorders of paleo-earthquakes, *in* Enzel, Y., Agnon, A., and Stein, M., editors, New frontiers in Dead Sea paleoenvironmental research: Geological Society of America Special Paper 401, p. 195–214 (doi: 10.1130/2006.2401(13)).

Agricultural Stabilization and Conservation Service, 1937, Aerial photography, Project AAL frames 1-29 to 1-30, dated 9-19-1937, and frames 4-8 to 4-10, dated 9-21-1937, black and white, approximate scale 1:20,000. (Available online in the UGS Aerial Imagery Collection at<http://geology.utah.gov/databases/imagery/index.php>.)

Aitken, M.J., 1994, Optical dating—a non-specialist review: Quaternary Geochronology (Quaternary Science Reviews), v. 13, p. 503–508.

Automated Geographic Reference Center (AGRC), 2012, Utah GIS Portal: Online, <http://agrc.its.state.ut.us/>, accessed January 2012.

Balch, D.P., Cohen, A.S., Schnurrenberger, D.W., Haskell, B.J., Valero Garces, B.L., Beck, J.W., Cheng, H., and Edwards, R.L., 2005, Ecosystem and paleohydrological response to Quaternary climate change in the Bonneville basin, Utah: Palaeogeography, Palaeoclimatology, Palaeoecology, v. 221, p. 99–122 (doi: 10.1016/j.palaeo.2005.01.013).

Bashore, W.M., 1982, Upper crustal structure of the Salt Lake Valley and the Wasatch fault from seismic modeling: Salt Lake City, University of Utah, M.S. thesis, 95 p.

Bashore, W.M., Smith, R.B., Zandt, G., and Ansorge, J., 1981, Upper crustal structure of the Salt Lake Valley and the Wasatch Front from seismic modeling: Eos, Transactions of the American Geophysical Union, v. 62, p. 961.

Benson, L.V., Lund, S.P., Smoot, J.P., Rhode, D.E., Spencer, R.J., Verosub, K.L., Louderback, L.A., Johnson, C.A., Rye, R.O., and Negrini, R.M., 2011, The rise and fall of Lake Bonneville between 45 and 10.5 ka: Quaternary International, v. 235, p. 57–69.

Bernard, P., and Zollo, A., 1989, The Irpina (Italy) 1980 earthquake—detailed analysis of complex normal faulting: Journal of Geophysical Research, v. 94, p. 1631–1647.

Birkeland, P.W., Machette, M.N., and Haller, K.M., 1991, Soils as a tool for applied Quaternary geology: Utah Geological and Mineral Survey Miscellaneous Publication 91-3, 63 p.

Black, B.D., Hecker, S., Hylland, M.D., Christenson, G.E., and McDonald, G.N., 2003, Quaternary fault and fold database and map of Utah: Utah Geological Survey Map 193DM, scale 1:50,000, CD.

Black, B.D., Lund, W.R., Schwartz, D.P., Gill, H.E., and Mayes, B.H., 1996, Paleoseismic investigation on the Salt Lake City segment of the Wasatch fault zone at the South Fork Dry Creek and Dry Gulch sites, Salt Lake County, Utah—Paleoseismology of Utah, Volume 7: Utah Geological Survey Special Study 92, 22 p., 1 plate.

Bowman, S.D., Beisner, K., and Unger, C., 2009, Compilation of 1970s Woodward-Lundgren & Associates Wasatch fault investigation reports and oblique aerial photography, Wasatch Front and Cache Valley, Utah and Idaho: Utah Geological Survey Open-File Report 548, 3 p., 6 plates.

Bronk Ramsey, C., 1995, Radiocarbon calibration and analysis of stratigraphy—the OxCal program: Radiocarbon, v. 37, no. 2, p. 425–430.

Bronk Ramsey, C., 2001, Development of the radiocarbon program OxCal: Radiocarbon, v. 43, no. 2a, p. 355–363.

Bronk Ramsey, C., 2008, Depositional models for chronological records: Quaternary Science Reviews, v. 27, no. 1-2, p. 42–60.

Bronk Ramsey, C., 2009, Bayesian analysis of radiocarbon dates: Radiocarbon, v. 51, no. 1, p. 337–360.

Bruhn, R.L., and Schultz, R.A., 1996, Geometry and slip distribution in normal fault systems—implications for mechanics and fault-related hazards: Journal of Geophysical Research, v. 101, no. B2, p. 3401–3412.

Cluff, L.S., Brogan, G.E., and Glass, C.E., 1970, Wasatch fault, northern portion—earthquake fault investigation and evaluation, a guide to land-use planning: Oakland, California, Woodward-Clyde and Associates, unpublished consultant report for the Utah Geological and Mineralogical Survey, variously paginated.

Colman, S.M., Kelts, K.R., and Dinter, D.A., 2002, Depositional history and neotectonics in Great Salt Lake, Utah, from high-resolution seismic stratigraphy: Sedimentary Geology, v. 148, p. 61–78.

Currey, D.R., 1982, Lake Bonneville—selected features of relevance to neotectonic analysis: U.S. Geological Survey Open-File Report 82-1070, 30 p., 1 plate, scale 1:500,000.

Currey, D.R., 1990, Quaternary paleolakes in the evolution of semidesert basins, with special emphasis on Lake Bonneville and the Great Basin, U.S.A.: Palaeogeography, Palaeoclimatology, Palaeoecology, v. 76, p. 189–214.

Currey, D.R., Berry, M.S., Douglass, G.E., Merola, J.A., Murchison, S.B., Ridd, M.K., Atwood, G., Bills, B.G., and Lambrechts, J.R., 1988a, The highest Holocene stage of Great Salt Lake, Utah [abs.]: Geological Society of America Abstracts with Programs, v. 20, no. 6, p. 411.

Currey, D.R., Berry, M.S., Green, S.A., and Murchison, S.B., 1988b, Very late Pleistocene red beds in the Bonneville basin, Utah and Nevada [abs.]: Geological Society of America Abstracts with Programs, v. 20, no. 6, p. 411.

dePolo, C.M., Clark, D.G., Slemmons, D.B., and Aymard, W.H., 1989, Historical Basin and Range Province surface faulting and fault segmentation, *in* Schwartz, D.P., and Sibson, R.H., editors, Fault segmentation and controls of rupture initiation and termination, Proceedings of Workshop XLV: U.S. Geological Survey Open-File Report 89-315, p. 131–162.

Doser, D.I., 1989, Extensional tectonics in northern Utah–southern Idaho, U.S.A., and the 1934 Hansel Valley sequence: Physics of the Earth and Planetary Interiors, v. 54, p. 120–134.

Duller, G.A.T., 2008, Luminescence dating—guidelines on using luminescence dating in archaeology: Swindon, United Kingdom, English Heritage Publishing, 45 p., online, <http://www.aber.ac.uk/en/media/departmental/iges/english_heritage_luminescence_dating.pdf>.

DuRoss, C.B., and Hylland, M.D., 2012, Paleoseismic investigation to compare surface faulting chronologies of the West Valley fault zone and Salt Lake City segment of the Wasatch fault zone, Salt Lake County, Utah: Utah Geological Survey, Final Technical Report to the U.S. Geological Survey, National Earthquake Hazards Reduction Program, award no. G10AP00068, 61 p. + 9 tables, 28 figures, 12 appendices, and 2 plates.

DuRoss, C.B., Hylland, M.D., McDonald, G.N., Crone, A.J., Personius, S.F., Gold, R.D., and Mahan, S.A., 2014, Holocene and latest Pleistocene paleoseismology of the Salt Lake City segment of the Wasatch fault zone, Utah, at the Penrose Drive trench site, *in* DuRoss, C.B., and Hylland, M.D., Evaluating surface faulting chronologies of graben-bounding faults in Salt Lake Valley, Utah—new paleoseismic data from the Salt Lake City segment of the Wasatch fault zone and the West Valley fault zone—Paleoseismology of Utah, Volume 24: Utah Geological Survey Special Study 149, p. 1–39, 6 appendices, 1 plate, CD.

DuRoss, C.B., Personius, S.F., Crone, A.J., Olig, S.S., and Lund, W.R., 2011, Integration of paleoseismic data from multiple sites to develop an objective earthquake chronology—application to the Weber segment of the Wasatch fault zone: Bulletin of the Seismological Society of America, v. 101, no. 6, p. 2765–2781.

Eardley, A.J., 1962, Glauber's salt bed west of Promontory Point, Great Salt Lake: Utah Geological and Mineralogical Survey Special Study 1, 12 p.

Eardley, A.J., Shuey, R.T., Gvosdetsky, V., Nash, W.P., Picard, M.D., Grey, D.C., and Kukla, G.J., 1973, Lake cycles in the Bonneville basin, Utah: Geological Society of America Bulletin, v. 84, p. 211–216.

Forester, R.M., 1987, Late Quaternary paleoclimate records from lacustrine ostracodes, *in* Ruddiman, W.F., and Wright, H.E., editors, North America and adjacent oceans during the last deglaciation: Boulder, Colorado, Geological Society of America, The Geology of North America, v. K-3, chapter 12, p. 261–276.

Forman, S.L., Nelson, A.R., and McCalpin, J.P., 1991, Thermoluminescence dating of fault-scarp-derived colluvium—deciphering the timing of earthquakes on the Weber segment of the Wasatch fault zone, north-central Utah: Journal of Geophysical Research, v. 96, no. B1, p. 595–605.

Friedrich, A.M., Wernicke, B.P., Niemi, N.A., Bennett, R.A., and Davis, J.L., 2003, Comparison of geodetic and geologic data from the Wasatch region, Utah, and implications for the spectral character of Earth deformation at periods of 10 to 10 million years: Journal of Geophysical Research, v. 108, no. B4, 2199 (doi:10.1029/2001JB000682).

Gilbert, G.K., 1890, Lake Bonneville: U.S. Geological Survey Monograph 1, 438 p.

Godsey, H.S., Currey, D.R., and Chan, M.A., 2005, New evidence for an extended occupation of the Provo shoreline and implications for regional climate change, Pleistocene Lake Bonneville, Utah, USA: Quaternary Research, v. 63, no. 2, p. 212–223.

Godsey, H.S., Oviatt, C.G., Miller, D.M., and Chan, M.A., 2011, Stratigraphy and chronology of offshore to nearshore deposits associated with the Provo shoreline, Pleistocene Lake Bonneville, Utah: Palaeogeography, Palaeoclimatology, Palaeoecology, v. 310, no. 3–4, p. 442–450 (doi: 10.1016/j.palaeo.2011.08.005).

Huntley, D.J., Godfrey-Smith, D.I., and Thewalt, M.L.W., 1985, Optical dating of sediments: Nature, v. 313, p. 105–107.

Hylland, M.D., DuRoss, C.B., McDonald, G.N., Olig, S.S., Oviatt, C.G., Mahan, S.A., Crone, A.J., and Personius, S.F., 2012, Basin-floor Lake Bonneville stratigraphic section as revealed in paleoseismic trenches at the Baileys Lake site, West Valley fault zone, Utah, *in* Hylland, M.D., and Harty, K.M., editors, Selected topics in engineering and environmental geology in Utah: Utah Geological Association Publication 41, p. 175–193, DVD.

Hylland, M.D., DuRoss, C.B., McDonald, G.N., and Oviatt, C.G., 2011, Basin-floor Lake Bonneville stratigraphic section as revealed in paleoseismic trenches on the West Valley fault zone, Salt Lake Valley, Utah [abs.]: Geological Society of America Abstracts with Programs, v. 43, no. 4, p. 80.

Janecke, S.U., and Oaks, R.Q., Jr., 2011, Reinterpreted history of latest Pleistocene Lake Bonneville—geologic setting of threshold failure, Bonneville flood, deltas of the Bear River, and outlets for two Provo shorelines, southeastern Idaho, USA, *in* Lee, J., and Evans, J.P., editors, Geologic field trips to the Basin and Range, Rocky Mountains, Snake River Plain, and terranes of the U.S. Cordillera: Geological Society of America Field Guide 21, p. 195–222 (doi:10.1130/2011.0021(09)).

Keaton, J.R., 1987, Potential consequences of earthquake-induced regional tectonic deformation along the Wasatch

Front, north-central Utah, *in* McCalpin, J., editor, Proceedings of the 23rd Symposium on Engineering Geology and Soils Engineering: Boise, Idaho Department of Transportation, p. 19–34.

Keaton, J.R., and Currey, D.R., 1989, Earthquake hazard evaluation of the West Valley fault zone in the Salt Lake City urban area, Utah: Salt Lake City, Dames & Moore, Final Technical Report prepared for U.S. Geological Survey, contract no. 14-08-0001-G1397, 69 p. (Subsequently published in 1993 as Utah Geological Survey Contract Report 93-7.)

Keaton, J.R., Currey, D.R., and Olig, S.J., 1987, Paleoseismicity and earthquake hazards evaluation of the West Valley fault zone, Salt Lake City urban area, Utah: Salt Lake City, Dames & Moore and University of Utah Department of Geography, Final Technical Report prepared for U.S. Geological Survey, contract no. 14-08-0001-22048, 55 p. + 33 p. appendix. (Subsequently published in 1993 as Utah Geological Survey Contract Report 93-8.)

Lienkaemper, J.J., and Bronk Ramsey, C., 2009, OxCal—versatile tool for developing paleoearthquake chronologies—a primer: Seismological Research Letters, v. 80, no. 3, p. 431–434.

Lund, W.R., 2005, Consensus preferred recurrence-interval and vertical slip-rate estimates—review of Utah paleoseismic-trenching data by the Utah Quaternary Fault Parameters Working Group: Utah Geological Survey Bulletin 134, 109 p., CD.

Lund, W.R., 2007, Summary—Utah Quaternary Fault Parameters Working Group annual meeting—Wednesday, February 28, 2007: Unpublished working group meeting minutes, 13 p., available online at <http://geology.utah.gov/ghp/workgroups/pdf/uqfpwg/UQFPWG-2007_Summary.pdf>.

Machette, M.N., 1985, Calcic soils of the southwestern United States, *in* Weide, D.L., editor, Soils and Quaternary geology of the southwestern United States: Geological Society of America Special Paper 203, p. 1–21.

Machette, M.N., Personius, S.F., and Nelson, A.R., 1992, Paleoseismology of the Wasatch fault zone—a summary of recent investigations, interpretations, and conclusions, *in* Gori, P.L., and Hays, W.W., editors, Assessment of regional earthquake hazards and risk along the Wasatch Front, Utah: U.S. Geological Survey Professional Paper 1500-A-J, p. A1–A71.

Marco, S., and Agnon, A., 1995, Prehistoric earthquake deformations near Masada, Dead Sea graben: Geology, v. 23, no. 8, p. 695–698.

Marco, S., and Agnon, A., 2005, High-resolution stratigraphy reveals repeated earthquake faulting in the Masada fault zone, Dead Sea transform: Tectonophysics, v. 408, p. 101–112.

McCalpin, J.P., editor, 1996, Paleoseismology: San Diego, California, Academic Press, International Geophysics Series, Volume 62, 588 p.

McCalpin, J.P., 2002, Post-Bonneville paleoearthquake chronology of the Salt Lake City segment, Wasatch fault zone, from the 1999 "megatrench" site—Paleoseismology of Utah, Volume 10: Utah Geological Survey Miscellaneous Publication 02-7, 37 p.

McKean, A.P., and Hylland, M.D., 2013, Interim geologic map of the Baileys Lake quadrangle, Salt Lake County, Utah: Utah Geological Survey Open-File Report 624, scale 1:24,000.

Miller, D.M., Oviatt, C.G., and McGeehin, J.P., 2013, Stratigraphy and chronology of Provo shoreline deposits and lake-level implications, late Pleistocene Lake Bonneville, eastern Great Basin, USA: Boreas, v. 42, p. 342–361. (Article first published online October 25, 2012, doi:10.1111/j.1502-3885.2012.00297.x.)

Miller, R.D., 1980, Surficial geologic map along part of the Wasatch Front, Salt Lake Valley, Utah: U.S. Geological Survey Miscellaneous Field Studies Map MF-1198, 13 p., scale 1:100,000.

Murchison, S.B., 1989, Fluctuation history of Great Salt Lake, Utah, during the last 13,000 years: Salt Lake City, University of Utah, Ph.D. dissertation, 137 p.

National Aeronautics & Space Administration (NASA), 2006, Visible Earth—a catalog of NASA images and animations of our home planet: Online, <http://visibleearth.nasa.gov/>, accessed July 2006.

Nelson, A.R., Lowe, M., Personius, S., Bradley, L.A., Forman, S.L., Klauk, R., and Garr, J., 2006, Holocene earthquake history of the northern Weber segment of the Wasatch fault zone, Utah—Paleoseismology of Utah, Volume 13: Utah Geological Survey Miscellaneous Publication 05-8, 39 p., 2 plates.

O'Connor, J.E., 1993, Hydrology, hydraulics, and geomorphology of the Bonneville Flood: Geological Society of America Special Paper 274, 83 p.

Oviatt, C.G., 1991, Stratigraphy of Lake Bonneville deposits along Grouse Creek, northwestern Utah: U.S. Geological Survey Open-File Report 91-342, 22 p., 2 plates.

Oviatt, C.G., 1997, Lake Bonneville fluctuations and global climate change: Geology, v. 25, p. 155–158.

Oviatt, C.G., 2014, The Gilbert episode in the Great Salt Lake basin, Utah: Utah Geological Survey Miscellaneous Publication 14-3, 20 p., CD.

Oviatt, C.G., Currey, D.R., and Sack, D., 1992, Radiocarbon chronology of Lake Bonneville, eastern Great Basin, USA: Palaeogeography, Palaeoclimatology, Palaeoecology, v. 99, p. 225–241.

Oviatt, C.G., and Miller, D.M., 1997, New explorations along the northern shores of Lake Bonneville, *in* Link, P.K., and

Kowallis, B.J., editors, Mesozoic to Recent geology of Utah—Geological Society of America field trip guidebook, 1997 annual meeting, Salt Lake City, Utah, Part 2: Brigham Young University Geology Studies, v. 42, pt. 2, p. 345–371.

Oviatt, C.G., Miller, D.M., McGeehin, J.P., Zachary, C., and Mahan, S., 2005, The Younger Dryas phase of Great Salt Lake, Utah, USA: Palaeogeography, Palaeoclimatology, Palaeoecology, v. 219, p. 263–284.

Oviatt, C.G., Miller, D.M., Zachary, C., and McGeehin, J.P., 2001, Refining the age of the lake transgression to the Gilbert shoreline in the Bonneville basin, Utah, USA [abs.]: EOS, Transactions, American Geophysical Union, Fall Meeting Supplement 82, no. 47, p. F755, abstract #PP22A-0496.

Oviatt, C.G., and Thompson, R.S., 2005, Late Quaternary history of Great Salt Lake and Lake Bonneville from sediment cores [abs.]: Geological Society of America Abstracts with Programs, v. 37, no. 7, p. 335.

Oviatt, C.G., Thompson, R.S., Kaufman, D.S., Bright, J., and Forester, R.M., 1999, Reinterpretation of the Burmester core, Bonneville basin, Utah: Quaternary Research, v. 52, p. 180–184.

Payne, S.J., Zollweg, J.E., and Rodgers, D.W., 2004, Stress triggering of conjugate normal faulting—late aftershocks of the 1983 $M_s$ 7.3 Borah Peak, Idaho, earthquake: Bulletin of the Seismological Society of America, v. 94, no. 3, p. 828–844.

Personius, S.F., and Scott, W.E., 1992, Surficial geologic map of the Salt Lake City segment and parts of adjacent segments of the Wasatch fault zone, Davis, Salt Lake, and Utah Counties, Utah: U.S. Geological Survey Miscellaneous Investigations Series Map I-2106, scale 1:50,000. (Digital version published by the Utah Geological Survey, 2009, Map 243DM, CD.)

Prescott, J.R., and Hutton, J.T., 1994, Cosmic ray contributions to dose rates for luminescence and ESR dating—large depths and long-term time variations: Radiation Measurements, v. 23, p. 497–500.

Puseman, K., and Cummings, L.S., 2005, Separation and identification of charcoal and organics from bulk sediment samples for improved radiocarbon dating and stratigraphic correlations, *in* Lund, W.R., editor, Western States Seismic Policy Council Proceedings Volume of the Basin and Range Province Seismic Hazards Summit II: Utah Geological Survey Miscellaneous Publication 05-2, 10 p., CD.

Reheis, M.C., Adams, K.D., Oviatt, C.G., and Bacon, S.N., in press, Pluvial lakes in the western United States—a view from the outcrop: Quaternary Science Reviews.

Reimer, P.J., Baillie, M.G.L., Bard, E., Bayliss, A., Beck, J.W., Blackwell, P.G., Bronk Ramsey, C., Buck, C.E., Burr, G.S., Edwards, R.L., Friedrich, M., Grootes, P.M., Guilderson, T.P., Hajdas, I., Heaton, T.J., Hogg, A.G., Hughen, K.A., Kaiser, K.F., Kromer, B., McCormac, F.G., Manning, S.W., Reimer, R.W., Richards, D.A., Southon, J.R., Talamo, S., Turney, C.S.M., van der Plicht, J., and Weyhenmeyer, C.E., 2009, IntCal09 and Marine09 radiocarbon age calibration curves, 0–50,000 years cal BP: Radiocarbon, v. 51, no. 4, p. 1111–1150.

Rhodes, E.J., 2011, Optically stimulated luminescence dating of sediments over the past 200,000 years: Annual Review of Earth and Planetary Sciences, v. 39, p. 461–488 (doi: 10.1146/annurev-earth-040610-133425).

Schwartz, D.P., and Coppersmith, K.J., 1984, Fault behavior and characteristic earthquakes—examples from the Wasatch and San Andreas fault zones: Journal of Geophysical Research, v. 89, p. 5681–5698.

Shenon, P.J., 1936, The Utah earthquake of March 12, 1934, *in* Neumann, F., United States earthquakes, 1934: U.S. Department of Commerce, serial no. 593, p. 43–48.

Smith, R.B., and Bruhn, R.L., 1984, Intraplate extensional tectonics of the eastern Basin-Range—inferences on structural style from seismic reflection data, regional tectonics, and thermal-mechanical models of brittle-ductile deformation: Journal of Geophysical Research, v. 89, no. B7, p. 5733–5762.

Solomon, B.J., 1998, New evidence for the age of faulting on the West Valley fault zone: Utah Geological Survey, Survey Notes, v. 30, no. 3, p. 8 and 13.

Spencer, R.J., Baedecker, M.J., Eugster, H.P., Forester, R.M., Goldhaber, M.B., Jones, B.F., Kelts, K., Mckenzie, J., Madsen, D.B., Rettig, S.L., Rubin, M., and Bowser, C.J., 1984, Great Salt Lake, and precursors, Utah—the last 30,000 years: Contributions to Mineralogy and Petrology, v. 86, p. 321–334.

Swan, F.H., III, Schwartz, D.P., and Cluff, L.S., 1980, Recurrence of moderate to large magnitude earthquakes produced by surface faulting on the Wasatch fault zone, Utah: Bulletin of the Seismological Society of America, v. 70, p. 1431–1462.

Thompson, R.S., Toolin, L.J., Forester, R.M., and Spencer, R.J., 1990, Accelerator-mass spectrometer (AMS) radiocarbon dating of Pleistocene lake sediments in the Great Basin: Palaeogeography, Palaeoclimatology, Palaeoecology, v. 78, p. 301–313.

Trumbore, S.E., 2000, Radiocarbon geochronology, *in* Noller, J.S., Sowers, J.M., and Lettis, W.R., editors, Quaternary geochronology—methods and applications: Washington, D.C., American Geophysical Union, AGU Reference Shelf 4, p. 41–60.

U.S. Department of Agriculture, 2012, Aerial Photography Field Office, National Agriculture Imagery Program: Online, <http://www.fsa.usda.gov/FSA/apfoapp?area=home&subject=prog&topic=nai>, accessed January 2012.

Velasco, M.S., Bennett, R.A., Johnson, R.A., and Hreinsdót-
tir, S., 2010, Subsurface fault geometries and crustal ex-
tension in the eastern Basin and Range Province, west-
ern U.S.: Tectonophysics, v. 488, p. 131–142.

Walter, H.G., 1934, Hansel Valley, Utah, earthquake: The
Compass of Sigma Gamma Epsilon, v. 14, no. 4, p. 178–
181.

Westaway, R., 1992, Revised hypocentre and fault rupture
geometry for the 1980 November 23 Campania-Basili-
cata earthquake in southern Italy: Geophysical Journal
International, v. 109, p. 376–390.

Wheeler, R.L., and Krystinik, K.B., 1992, Persistent and
nonpersistent segmentation of the Wasatch fault zone,
Utah—statistical analysis for evaluation of seismic haz-
ard, *in* Gori, P.L., and Hays, W.W., editors, Assessment of
regional earthquake hazards and risk along the Wasatch
front, Utah: U.S. Geological Survey Professional Paper
1500-A-J, p. B1–B47.

Withjack, M.O., Islam, Q.T., and La Pointe, P.R., 1995, Nor-
mal faults and their hanging-wall deformation—an ex-
perimental study: American Association of Petroleum
Geologists Bulletin, v. 79, no. 1, p. 1–18.

Woodward, L., Harvey, J.L., Donaldson, K.M., Shiozaki, J.J.,
Leishman, G.W., and Broderick, J.H., 1974, Soil survey
of Salt Lake area, Utah: U.S. Department of Agricul-
ture, Soil Conservation Service, 132 p., 58 sheets, scale
1:20,000.

Xiao, H., and Suppe, J., 1992, Origin of rollover: American
Association of Petroleum Geologists Bulletin, v. 76, no.
4, p. 509–529.

Yeats, R.S., Sieh, K., and Allen, C.R., 1997, The geology of
earthquakes: New York, Oxford University Press, 568 p.

# APPENDIX A

# DESCRIPTION OF STRATIGRAPHIC UNITS IN TRENCHES AT THE BAILEYS LAKE SITE

| Unit[1] | USCS[2] | Texture (wt. %)[3] | Plast.[4] | Dens./ Consist.[5] | Carb. Morph.[6] | Rxn w/HCl[7] | Clast Ang.[8] | Bedding[9] | Lower Bound.[10] | Color, dry (moist)[11] | Soil Development | Comments and Genesis |
|---|---|---|---|---|---|---|---|---|---|---|---|---|
| 11 | ML | 99/1/0 | M–H | VSt | none | M | — | NS | Ab–Cl | 10YR 6/2 (10YR 4/2) | Modern platy A horizon (soil unit S2); burrowed/root-mixed; pinhole structure, root pores | Organic-rich clayey silt; discontinuous, locally filling in topographic depressions; massive, overprinted by modern A horizon; *Loess* |
| 10 | ML, OL | 95/5/0 | M | VSt | none | M–S | — | NS | Cl | 10YR 6/2 (10YR 4/2) | Organics throughout deposit; locally root-penetrated and burrowed | Disaggregated soil with silt; colluvium composed of small granular soil blocks eroded from prismatic soil (soil unit S1); massive; may be in part contemporaneous with unit 11; *Scarp-Derived Colluvium (BL1 wedge)* |
| 9 | ML | 99/1/0 | M | VSt | none–II | S | — | NS | Ab–Cl | 10YR 8/1 (10YR 7/2) | Prismatic soil (buried; soil unit S1); abundant carbonate (both primary and pedogenic); minor Fe staining; abundant root pores, heavily burrowed | Massive silt with clay; *Loess* |
| 8 | CL | 98/2/0 | L–M | VSt | none–II | S | — | WS | Ab–Cl | 5Y 7/1 (2.5Y 6/2) | Vertical jointing; root pores, locally burrowed | Finely laminated clay, silt, and carbonate (marl); bedding locally wavy; locally cemented with carbonate (depositional); *Lacustrine (Gilbert episode)* |
| 7 | SP | 2/98/0 | NP | H | none | S | SA | WS | Ab | 10YR 5/1 (10YR 3/2) | No soil development; minor burrowing | Dark gray, medium to coarse sand and minor silt; clast-supported texture; locally thinly bedded, fining upward, and cemented with carbonate (likely depositional); thins westward; *Lacustrine (Gilbert episode [shorezone sand])* |

| Unit[1] | USCS[2] | Texture (wt. %)[3] | Plast.[4] | Dens./ Consist.[5] | Carb. Morph.[6] | Rxn w/HCl[7] | Clast Ang.[8] | Bedding[9] | Lower Bound.[10] | Color, dry (moist)[11] | Soil Development | Genesis and Comments |
|---|---|---|---|---|---|---|---|---|---|---|---|---|
| 6 | ML | 99/1/0 | M | VSt | none–II | M–S | — | V | Ab–Cl | 10YR 6/2 (10YR 5/3) to 10YR 8/1 (10YR 6/2) | Organics throughout fine-grained "soil stringers"; some organics mixed with fine-grained colluvium; burrowed; local carbonate cementation | Colluvium comprising disaggregated fragments (fine gravel size) of clay, silt, and sand eroded from scarp, interbedded with 0.5–3 cm thick, organic-rich, fine grained "soil stringers" that thicken to the east and have slope-parallel geometry; *Scarp-Derived Colluvium (BL2 wedge)* |
| 5 | CL | 99/1/0 | L | VSt | none | S | — | WS | Cl | 10YR 7/1 (2.5Y 6/3) | Vertical jointing; root pores with minor Fe staining; minor burrowing | Laminated clay and silt with carbonate (marl); conformably drapes pre-existing topography; locally differentiated as 5a and 5b; upper unit (5b)— finely laminated; lower unit (5a)— laminated to thin bedded, locally massive; few ostracodes, mostly unidentifiable fragments; *Lacustrine (Gilbert episode)* |
| 4 | SW, CH | 10/80/10 | NP, H | M, VSt | none | S | A–SA | WS–V | Ab | 10YR 8/1 (10YR 8/2) | No soil development | Primarily carbonate fragments (reworked "hash") with local in situ precipitated carbonate (locally well-cemented, wavy tufa mats); locally includes clay, silt, and fine to coarse sand; clast-supported texture; *Lacustrine (Gilbert episode, transgressive [shorezone tufa])* |
| 3 | CH | 90/10/0 | H | VSt | none | W–M | — | WS | Ab | 2.5Y 7/2 (5Y 5/2) | Root pores; Fe and Mn staining; pervasive vertical jointing | Finely laminated greenish clay and silt; blocky weathering due to joints and silt partings; prominent parting observed locally 25–30 cm above base; few ostracodes, most broken; *Lacustrine (Bonneville, regressive phase)* |

| Unit[1] | USCS[2] | Texture (wt. %)[3] | Plast.[4] | Dens./ Consist.[5] | Carb. Morph.[6] | Rxn w/HCl[7] | Clast Ang.[8] | Bedding[9] | Lower Bound.[10] | Color, dry (moist)[11] | Soil Development | Genesis and Comments |
|---|---|---|---|---|---|---|---|---|---|---|---|---|
| 2e | CH, ML | 99/1/0 | H | VSt | none | W, S | — | WS | Ab | 7.5YR 7/3 (7.5YR 5/4) | Root pores and Fe staining; vertical jointing | Massive red clay with 2–3-cm-thick silty clay (upper) and sandy silt (lower) interbeds exhibiting open, upright folds; red color grades to gray in uppermost 10–18 cm; few to abundant ostracodes; *Lacustrine (Bonneville, mid- to late transgressive phase)* |
| 2d | CL–SP | 50/50/0 | M–NP | VSt–H | none | M | — | WS | Ab | 2.5Y 6/2 (2.5Y 5/3) | No soil development; local Fe staining | Upper part: ~10-cm-thick clay with silt and fine sand; Lower part: ~10-cm-thick fine sand with thin, red and green clay fragments (rip-up clasts); *Turbidite Marker Bed (Bonneville, mid- to late transgressive phase)* |
| 2c | CH | 99/1/0 | H | St | none | W | — | WS | Ab | 7.5YR 7/2 (7.5YR 5/3) | Root pores and minor filaments; minor Fe staining | Red clay with gray, 2–10-cm-thick silt and fine sand interbeds; clay beds contain ostracodes, some broken; *Lacustrine (Bonneville, transgressive phase with turbidites)* |
|  | ML–SP | 50/50/0 | NP | M–H | none | W | — | WS | Ab | 2.5Y 7/3 (2.5Y 5/3) |  |  |
| 2b | CH | 99/1/0 | H | St | none | W–S | — | PS | Ab | U: 5YR 8/2 (5YR 4/3) L: 2.5Y 8/2 (2.5Y 7/2) | Root pores, decayed filaments, and considerable oxidation (Fe and Mn) in upper ~0.5 m, where red clay grades to gray with depth; minor carbonate nodules | Massive light gray clay (red in upper ~0.5 m) with few laterally continuous silt partings; prominent parting 15 cm below top; few to abundant ostracodes; *Lacustrine (Bonneville, transgressive phase)* |

| Unit[1] | USCS[2] | Texture (wt. %)[3] | Plast.[4] | Dens./ Consist.[5] | Carb. Morph.[6] | Rxn w/HCl[7] | Clast Ang.[8] | Bedding[9] | Lower Bound.[10] | Color, dry (moist)[11] | Soil Development | Genesis and Comments |
|---|---|---|---|---|---|---|---|---|---|---|---|---|
| 2a | SM | 40/60/0 | NP–H | M | none | M | — | WS | Ab | 10YR 6/3 (10YR 4/2) | No soil development; local weak to moderate Fe staining; locally cemented with nodular carbonate, especially near fault zone | Ripple-laminated, locally cross-bedded (westerly apparent dip) silty sand with clay interbeds; generally fining upward; gastropod shells and shell fragments and few ostracodes in clay; ***Lacustrine (Bonneville, early transgressive phase)*** |
| 1 | CH | 99/1/0 | H | St | none | W–M | — | V | NE | 5Y 6/2 (5Y 4/2) to 2.5Y 7/0 (2.5Y 5/0) | Root pores with minor oxidation (mottling), decayed filaments; ≥30-cm-thick oxidized zone; weak vertical structure (fractures); local burrowing | Gray to brown clay thinly interbedded with white fine sand; ***Pre-Bonneville Wetland/Alluvial Marsh*** |

[1] Units as shown on plate 1, listed in stratigraphic order (top to bottom).
[2] Unified Soil Classification System (ASTM D2488).
[3] Percentages of fines/sand/gravel fractions are field estimates.
[4] Plasticity: NP – nonplastic, L – low, M – medium, H – high.
[5] Density: Ls – loose, L – low, M – medium, H – high; Consistency: Vsf – very soft, S – soft, St – stiff, VSt, very stiff.
[6] Pedogenic carbonate morphology; stage designations after Machette (1985) and Birkeland and others (1991).
[7] Reaction with HCl: W – weak, M – moderate, S – strong.
[8] Clast angularity: A – angular, SA – subangular, SR – subrounded, R – rounded.
[9] Bedding: NS – nonstratified, PS – poorly stratified, WS – well stratified, V – variable.
[10] Lower boundary: Ab – abrupt, Cl – clear, Gr – gradual, NE – not exposed.
[11] Munsell color of matrix. L, lower part of unit; U, upper part of unit.

# APPENDIX B

## DESCRIPTION OF PEDOGENIC SOIL UNITS IN TRENCHES AT THE BAILEYS LAKE SITE

| Unit[1] | Horizon | Depth (cm) | Color, dry (moist)[2] | Structure (type, grade, size)[3] | Gravel (%) | Consistence, dry (wet)[4] | Texture | Clay Films (amount, distinctness, location) | Lower Boundary[5] | Comments |
|---|---|---|---|---|---|---|---|---|---|---|
| **Site 1: West(N) trench, south wall, horizontal meter mark 34.0** | | | | | | | | | | |
| S2 | A | 0–13 | 10YR 6/2 (10YR 4/2) | gr–pl, moderate, fine to medium | 0 | sh (ss, ps) | Silty clay loam | None | a, w | Root penetrated, abundant pores; no visible carbonate. |
| S2 | AB | 13–20 | 10YR 6/2 (10YR 4/2) | massive | 0 | h (ss, ps) | Silty clay loam | None | a–c, w | Soil developed on loess; abundant roots, root pores, burrowing; no visible carbonate. |
| S1 | Bt | 20–40 | 10YR 6/2 (10YR 4/2) | pr–abk, moderate, fine | 0 | h (ss, ps) | Silty clay loam to silty clay | Few, faint, clay films line tubular or interstitial pores | c–g, w | Abundant roots, root pores, minor burrowing; minor carbonate, likely inherited from parent material (loess and playa clays). |
| **Site 2: West(N) trench, south wall, horizontal meter mark 15.8** | | | | | | | | | | |
| S2 | A | 0–20 | 10YR 6/2 (10YR 4/2) | gr–pl, moderate, fine to medium | 0 | sh (ss, ps) | Silty clay loam | None | a, w | Root penetrated, abundant pores, burrowed; no visible carbonate. |
| S2 | AB | 20–32 | 10YR 6/2 (10YR 4/2) | massive | 0 | h (ss, ps) | Silty clay loam | None | a–c, w | Soil developed on loess; abundant roots, root pores, burrowing; no visible carbonate. |
| S1 | Bt | 32–47 | 10YR 6/2 (10YR 4/2) | pr–abk, moderate, fine | 0 | h (ss, ps) | Silty clay loam to silty clay | Few, faint, clay films line tubular or interstitial pores | c–g, w | Abundant roots, root pores, minor burrowing; minor carbonate, likely inherited from parent material (loess and playa clays). |

Note: Abbreviations and symbols used to describe soil properties after Birkeland and others (1991).
[1] Units as shown on plate 1.
[2] Munsell color of matrix.
[3] Structure type: gr – granular, abk – angular blocky, sbk – subangular blocky, pr – prismatic, cpr – columnar, pl – platy.
[4] Dry consistence: lo – loose, so – weakly coherent, sh – slightly hard, h – hard, vh – very hard, eh – extremely hard. Wet consistence (stickiness): so – nonsticky, ss – slightly sticky, s – sticky, vs – very sticky. Wet consistence (plasticity): po – nonplastic, ps – slightly plastic, p – plastic, vp – very plastic.
[5] Boundary distinctness: a – abrupt (<2 cm), c – clear (2–5 cm), g – gradual (5–15 cm), d – diffuse (>15 cm). Topography: s – smooth, w – wavy, i – irregular, b – broken.

# APPENDIX C

## PROCESSING AND ANALYSIS OF RADIOCARBON SAMPLE MATERIAL FROM THE BAILEYS LAKE SITE BY PALEORESEARCH INSTITUTE

Table C.1. Correlation of original and final sample identification numbers.

| Original Field ID[1] | Final ID[2] | Comments |
|---|---|---|
| BL-R1 | BL-R1 | – |
| BL-R2a | BL-R2-1 | – |
| BL-R2b | BL-R2-2 | – |
| BL-R3a | – | Possible contamination from burrowing; not submitted for processing |
| BL-R3b | BL-R3-1 | 7 fragments unidentified hardwood (PRI) |
|  | BL-R3-2 | 45 fragments unidentifiable charcoal and stems (PRI) |
| BL-R4 | BL-R4 | – |
| BL-R5 | BL-R5 | – |

[1] Sample identification used in PaleoResearch Institute (PRI) report (this appendix).
[2] Sample identification used in this report.

EXAMINATION OF BULK SEDIMENT AND MICROCHARCOAL EXTRACTION FOR
SAMPLES FROM THE BAILEYS LAKE TRENCH SITE,
SALT LAKE CITY, UTAH


By

Kathryn Puseman

With Assistance from
Peter Kováčik,
R. A. Varney,
and
Thomas Lux

PaleoResearch Institute
Golden, Colorado


PaleoResearch Institute Technical Report 10-151


Prepared For

Utah Geological Survey
Salt Lake City, Utah

January 2011

# INTRODUCTION

Six bulk soil samples from two paleoseismic trenches were floated to recover organic fragments suitable for radiocarbon analysis. These samples were collected from the Baileys Lake trench site on the Granger fault in Salt Lake City, Utah, as part of the Utah Geological Survey's efforts to develop detailed information on the timing and recurrence of paleoearthquakes in the West Valley fault zone. Botanic components and detrital charcoal were identified, and potentially radiocarbon datable material was separated. Four of the samples yielded sufficient charred material that can be submitted for AMS radiocarbon analysis. In the absence of larger-sized charred remains, one of the samples was extracted to recover microscopic charcoal/particulate soil organics for dating. Samples for AMS radiocarbon dating will be submitted to Woods Hole Institute.

# METHODS

## Flotation and Charcoal Identification

The samples were water-screened a 150 micron mesh sieve, taking care to retain all material that passed through the screen for possible microcharcoal and/or humate extraction. The water-screened portion was floated using a modification of the procedures outlined by Matthews (1979). Each sample was added to approximately 3 gallons of water, then stirred until a strong vortex formed. The floating material (light fraction) was poured through a 150 micron mesh sieve. Additional water was added and the process repeated until all floating material was removed from the sample (a minimum of five times). The material that remained in the bottom (heavy fraction) was poured through a 0.5-mm mesh screen. The floated portions were allowed to dry. The light fractions were weighed, then passed through a series of graduated screens (US Standard Sieves with 2-mm, 1-mm, 0.5-mm and 0.25-mm openings) to separate charcoal debris and to initially sort the remains. The contents of each screen then were examined.

Charcoal fragments, when present, were separated and broken to expose fresh cross, radial, and tangential sections, then examined under a binocular microscope at a magnification of 70x and under a Nikon Optiphot 66 microscope at magnifications of 320-800x. The weights of each charcoal type were recorded. The material that remained in the 2-mm, 1-mm, 0.5-mm, and 0.25-mm sieves was scanned under a binocular stereo microscope at a magnification of 10x, with some identifications requiring magnifications of up to 70x. The material that passed through the 0.25-mm screen was not examined. Remains were recorded as charred and/or uncharred, whole and/or fragments. The term "seed" is used to represent seeds, achenes, caryopses, and other disseminules. Macrofloral remains, including charcoal, are identified using manuals (Carlquist 2001; Hoadley 1990; Martin and Barkley 1961; Musil 1963; Panshin and de Zeeuw 1980; Schopmeyer 1974) and by comparison with modern and archaeological references. Because charcoal and possibly other botanic remains were to be submitted for radiocarbon dating, clean laboratory conditions were used during flotation and identification to avoid contamination. All instruments were washed between samples, and samples were protected from contact with modern charcoal.

## Microcharcoal Recovery

Now it is possible to recover microscopic charcoal (microcharcoal) from sediments for the purpose of obtaining an AMS radiocarbon age.  Microscopic charcoal fragments are far superior to humates because they provide dates with the same precision as those obtained from larger pieces of charcoal, with the single exception that the individual pieces of microscopic charcoal are not identified to taxon.

A chemical extraction technique based on that used for pollen, and relying upon heavy liquid extraction, has been modified to recover microcharcoal for the purpose of obtaining an AMS radiocarbon age.  After removing calcium carbonates and iron with hydrochloric acid (10%), the sample was screened through 150 micron mesh.  The material remaining in the screen was examined for the presence of macroscopic charcoal.  Since no macroscopic charcoal was found, the screened sample then was rinsed until neutral, and a small quantity of sodium hexametaphosphate was added.  The sample then was filled with reverse osmosis, deionized (RODI) water and allowed to settle according to Stoke's Law.  After two hours the supernatant, containing clay, was poured off and the sample was rinsed with RODI water three more times, being allowed to settle according to Stoke's Law after each rinse to remove more clays.  This settling process was repeated until the supernatant was clear of clays.  Once the clays had been removed, the sample was freeze-dried using a vacuum system, freezing out all moisture at -107 °C.  Sodium polytungstate (SPT), with a density of 1.8, was used for the flotation process.  The sample was mixed with SPT and centrifuged at 1500 rpm for 10 minutes to separate organic from inorganic remains.  The supernatant containing pollen, organic remains, and microcharcoal was decanted.  Sodium polytungstate again was added to the inorganic fraction to repeat the separation process until all visible microcharcoal had been recovered.  The microcharcoal was recovered from the sodium polytungstate and rinsed thoroughly with RODI water.  Following this step, the sample was examined using a binocular microscope at a magnification of up to 30x to check the matrix for microscopic charcoal and other debris.  Each sample received a treatment with hot hydrofluoric acid (40%) to remove all visible silica.  RODI water rinses followed, with another examination with the binocular microscope.  The hydrofluoric acid treatments were repeated, but it still was not possible to remove all of the inorganic remains.

## DISCUSSION

The Bailey's Lake Site consists of three trenches excavated across two parallel strands of the Granger Fault, located within Salt Lake City in Utah's West Valley fault zone.  The West Valley fault zone (WVFZ), previously termed the Jordan Valley fault zone, trends north-northeast through an urbanized area three miles southwest of downtown Salt Lake City.  The Granger Fault in the southern WVFZ presents as an east-facing scarp with heights of as great as 6.1 meters.  The site lies at the approximate elevation of the Late Holocene highstand of Great Salt Lake and below the elevation of the Gilbert shoreline of Lake Bonneville.

Modern surface vegetation in this area includes saltbush (*Atriplex*), rabbitbrush, (*Chrysothamnus*), and grasses (Poaceae) (Michael Hylland, personal communication, November 2010).  This area has experienced modifications from the excavation of canals,

ditches, and pipeline trenches, as well as introduction of fill for roadside embankments and footings for powerline towers.  The site also has been intermittently grazed by livestock.  Excavations at the Bailey's Lake trench site exposed possible pre-Bonneville marsh deposits, sandy to clayey Bonneville lake-cycle deposits, fine-grained wetland and/or Gilbert lake-cycle deposits, sandy fluvial sediment, loess, and fault-scarp-derived colluvium.  Six bulk soil samples from these excavations were submitted for macrofloral analysis prior to radiocarbon dating.

### West(N) Trench

Sample BL-R1 was collected from the north wall of the northern-most of the two western trenches from soil S3 and was buried by P1 colluvium (Table 1).  This sample will provide a broad minimum date for P2.  Several fragments of charcoal too small and vitrified for identification were present in this sample, as well as several small, unidentified charred stem fragments (Table 2, Table 3).  Vitrified charcoal has a shiny, glassy appearance due to fusion by heat.  The charred stem fragments and the charcoal fragments were noted only in the 0.25 mm screen and were so small that it was difficult and time consuming to try and separate these remains; therefore the charred material was left combined and yielded a total weight of 0.0112 g.  Four charred *Scirpus*-type seeds also were noted and suggest the presence of bulrush growing along the lake margin.  Uncharred bark scale fragments, an uncharred *Erodium* seed, and uncharred roots and rootlets reflect modern plants in the area.  The sample also yielded a few, small uncharred bone fragments, two insect chitin fragments, a few snail shell fragments, and a small amount of muscovite.

Sample BL-R2 was processed as two separate samples, designated BL-R2a and BL-R2b.  Sample BL-R2a is a fragmented bulk soil sample collected from dark, inclined beds in P2 colluvium in the north wall of the northern West trench.  This sample will provide a possible minimum age for P2 and a broad maximum age for P1.  A charred Cheno-am perisperm and six charred *Scirpus*-type seed fragments were noted in sample BL-R2a, each weighing less than 0.0001 g.  Cheno-am seed perisperm (similar to endosperm) consists of the nutritive tissue of the seed, surrounding and absorbed by the embryo.  It represents a mature seed that has lost the outer seed coat (testa).  Charred unidentified stem fragments and charcoal fragments too small and vitrified for identification from the 0.25 mm screen weighed a total of 0.0052 g.  In addition, the sample contained a few root fragments, numerous rootlets, a few small bone fragments, an insect chitin fragment, and a moderate amount of snail shells.

Sample BL-R2b was recovered from dark, inclined beds in P2 colluvium as an intact block and will provide a possible minimum age for P2 and a broad maximum age for P1.  Charred unidentified stem fragments and small, vitrified charcoal fragments from the 0.25 mm screen of sample BL-R2b yielded a total weight of 0.0043 g.  A charred unidentified fruit fragment weighing less than 0.0001 g, a few uncharred rootlets, a few snail shells, and a small amount of muscovite also were noted.

Sample BL-R3b was taken from P1 colluvium in the north wall of the northern-most of the two western trenches and will provide a possible minimum age for P1.  This sample yielded seven fragments of hardwood charcoal too small for further identification weighing 0.0055 g.  Charcoal too small for identification and several charred unidentified stem fragments from the 0.25 mm screen weighed a total weight of 0.0077 g.

## West(S) Trench

Sample BL-R4 was collected from the upper part of Unit 1a, a possible pre-Bonneville marsh deposit, in the south wall of the southern-most of the two western trenches. This sample will act as an age control for the lacustrine sequence and will provide a broad maximum age for P4. Recovery of three charred *Scirpus*-type seed fragments weighing less than 0.0001 g again note the presence of bulrush. A single piece of charcoal noted in the 0.25 mm screen weighing less than 0.0001 g was too small and vitrified for identification and too small for radiocarbon dating. As a result, the sediment that passed through the 150 micron mesh sieve during water-screening was processed to recover microcharcoal or particulate soil organics. Microcharcoal extraction resulted in a total weight of 0.0025 g, approximately 25-30% of which is insoluble microminerals. This microcharcoal sample is sufficient for AMS radiocarbon dating.

Sample BL-R5 is a bulk soil sample collected from Unit 3, a late Pleistocene-early Holocene wetland or shallow lacustrine deposit, in the south wall of the southern-most of the two western trenches to provide the maximum age for P3 and a broad minimum age for P4. No organic material was noted in this sample, which contained only clay and muscovite.

## SUMMARY AND CONCLUSIONS

Macrofloral analysis of sediment samples from paleoseismic trenches at the Baileys Lake trench site on the Granger fault in Salt Lake City, Utah, yielded charred organic remains that can be submitted for AMS radiocarbon dating. All four samples from the West(N) trench contained small charred stem fragments and charcoal too small and vitrified for identification in sufficient quantities for dating. Sample BL-R4 from the West(S) trench did not yield sufficient macroscopic charred remains; however, a sufficient quantity of microscopic charcoal fragments were recovered for dating. Sample BL-R5 yielded no organic remains.

TABLE 1

PROVENIENCE DATA FOR SAMPLES FROM THE BAILEYS LAKE SITE, SALT LAKE CITY, UTAH

| Sample Number | Trench | Wall | Sample location (horiz., vert.) | Provenience/ Description | Analysis |
|---|---|---|---|---|---|
| BL-R1 | West(N) | North | 22.1-22.4m, 3.3m | Bulk sample from soil S3 buried by P1 colluvium; maximum age for P1, broad minimum for P2 | Macrofloral |
| BL-R2a | | | 22.1m, 3.1-3.2m | Bulk sample from dark, inclined beds in P2 colluvium; minimum(?) age for P2, broad maximum for P1 | Macrofloral |
| BL-R2b | | | 22.1m, 3.1-3.2m | Bulk sample from dark, inclined beds in P2 colluvium; minimum(?) age for P2, broad maximum for P1 | Macrofloral |
| BL-R3b | | | 22.2m, 3.5m | Bulk sample from P1 colluvium; minimum (?) age for P1 | Macrofloral |
| BL-R4 | West(S) | South | 25.8m, 1.1m | Bulk sample from upper part of unit 1a (possible pre-Bonneville marsh deposits); age control for lacustrine sequence, broad maximum age for P4 | Macrofloral Microcharcoal |
| BL-R5 | | | 17.4m, 2.2m | Bulk sample from unit 3 (latest Pleistocene-early Holocene wetland or shallow lacustrine deposits); maximum age for P3, broad minimum for P4 | Macrofloral |

TABLE 2
MACROFLORAL REMAINS FROM THE BAILEYS LAKE SITE, SALT LAKE CITY, UTAH

| Sample No. | Identification | Part | Charred W | Charred F | Uncharred W | Uncharred F | Weights/Comments |
|---|---|---|---|---|---|---|---|
| BL-R1 | Liters Floated | | | | | | 1.00 L |
| West(N) | Light Fraction Weight | | | | | | 0.445 g |
| trench | FLORAL REMAINS: | | | | | | |
| North wall | *Scirpus*-type | Seed | | 4 | | | < 0.0001 g |
| | Unidentified | Bark scale | | | 2 | | |
| | *Erodium* | Seed | | | 1 | | |
| | Roots | | | | | X | Few |
| | Rootlets | | | | | X | Numerous |
| | CHARCOAL/WOOD: | | | | | | |
| | Total charcoal ≥ 0.25 mm | | | | | | 0.0112 g |
| | Unidentifiable charcoal - vitrified, small + Unidentified charred stem fragments | Charcoal/ Stem | | X | | | 0.0112 g |
| | NON-FLORAL REMAINS: | | | | | | |
| | Bone < 2 mm | | | | | X | Few |
| | Gravel | | | | | X | Few |
| | Insect | Chitin | | | | 2 | |
| | Muscovite | | | | | X | Few |
| | Snail shell < 2 mm | | | | | X | Few |
| BL-R2a | Liters Floated | | | | | | 0.40 L |
| West(N) | Light Fraction Weight | | | | | | 0.468 g |
| trench | FLORAL REMAINS: | | | | | | |
| North wall | Cheno-am | Perisperm | 1 | | | | < 0.0001 g |
| | *Scirpus*-type | Seed | | 6 | | | < 0.0001 g |
| | Roots | | | | | X | Few |
| | Rootlets | | | | | X | Numerous |
| | CHARCOAL/WOOD: | | | | | | |
| | Total charcoal ≥ 0.25 mm | | | | | | 0.0052 g |
| | Unidentifiable charcoal - vitrified, small + Unidentified charred stem fragments | Charcoal/ Stem | | X | | | 0.0052 g |

TABLE 2 (Continued)

| Sample No. | Identification | Part | Charred | | Uncharred | | Weights/ |
|---|---|---|---|---|---|---|---|
| | | | W | F | W | F | Comments |
| BL-R2a | NON-FLORAL REMAINS: | | | | | | |
| West(N) trench North wall | Bone < 2 mm | Chitin | | | | X | Few |
| | Gravel | | | | | X | Few |
| | Insect | | | | | 1 | |
| | Muscovite | | | | | X | Few |
| | Snail shell ≥ 2 mm | | | | | 1 | 0.003 g |
| | Snail shell < 2 mm | | | | 10 | X | Moderate |
| BL-R2b | Liters Floated | | | | | | 0.10 L |
| West(N) trench North wall | Light Fraction Weight | | | | | | 0.788 g |
| | FLORAL REMAINS: | | | | | | |
| | Unidentified | Fruit | | 1 | | | < 0.0001 |
| | Rootlets | | | | | X | Few |
| | CHARCOAL/WOOD: | | | | | | |
| | Total charcoal ≥ 0.25 mm | | | | | | 0.0043 g |
| | Unidentifiable charcoal - vitrified, small + Unidentified charred stem fragments | Charcoal/ Stem | | X | | | 0.0043 g |
| | NON-FLORAL REMAINS: | | | | | | |
| | Gravel | | | | | X | Few |
| | Muscovite | | | | | X | Few |
| | Snail shell < 2 mm | | | | | X | Few |
| BL-R3b | Liters Floated | | | | | | 0.90 L |
| West(N) trench North wall | Light Fraction Weight | | | | | | 3.073 g |
| | FLORAL REMAINS: | | | | | | |
| | Unidentified | Bark scale | | | 3 | | |
| | Rootlets | | | | | X | Few |
| | CHARCOAL/WOOD: | | | | | | |
| | Total charcoal ≥ 0.5 mm | | | | | | 0.0132 g |
| | Unidentified hardwood | Charcoal | | 7 | | | 0.0055 g |
| | Unidentifiable charcoal - vitrified, small + Unidentified charred stem fragments | Charcoal/ Stem | | 45 | | | 0.0077 g |

TABLE 2 (Continued)

| Sample No. | Identification | Part | Charred W | Charred F | Uncharred W | Uncharred F | Weights/ Comments |
|---|---|---|---|---|---|---|---|
| BL-R3b | NON-FLORAL REMAINS: | | | | | | |
| West(N) trench North wall | Bone ≥ 2 mm | | | | | 2 | 0.035 g |
| | Bone < 2 mm | | | | | X | Few |
| | Bone | Vertebra | | | 1 | | < 0.001 g |
| | Gravel | | | | | X | Few |
| | Insect | Chitin | | | | 2 | |
| | Snail shell < 2 mm | | | | 2 | X | Moderate |
| Bl-R4 | Liters Floated | | | | | | 1.10 L |
| West(S) trench South wall | Light Fraction Weight | | | | | | 0.787 g |
| | FLORAL REMAINS: | | | | | | |
| | *Scirpus*-type | Seed | | 3 | | | < 0.0001 g |
| | CHARCOAL/WOOD: | | | | | | |
| | Total charcoal ≥ 0.25 mm | | | | | | < 0.0001 g |
| | Unidentifiable - small, vitrified | Charcoal | | 1 | | | < 0.0001 g |
| | NON-FLORAL REMAINS: | | | | | | |
| | Insect | Chitin | | | | 5 | |
| | Light orange clay clumps | | | | | X | Few |
| | Muscovite | | | | | X | Moderate |
| BL-R5 | Volume Water-screened | | | | | | 0.10 L |
| West(S) trench South wall | Water-screened Sample Weight | | | | | | 0.853 g |
| | NON-FLORAL REMAINS: | | | | | | |
| | Clay | | | | | X | Few |
| | Muscovite | | | | | X | Few |

W = Whole
F = Fragment
X = Presence noted in sample
L = Liter
g = grams
mm = millimeters
L = liters

TABLE 3
INDEX OF MACROFLORAL REMAINS RECOVERED FROM THE BAILEYS LAKE SITE, SALT LAKE CITY, UTAH

| Scientific Name | Common Name |
| --- | --- |
| FLORAL REMAINS: | |
| Cheno-am | Includes goosefoot and amaranth families |
| *Erodium* | Storksbill, Filaree |
| *Scirpus*-type (includes *Amphiscirpus*, *Bolboshoenus*, *Isolepis*, *Shoenoplectus*, and *Scirpus*) | Bulrush |
| CHARCOAL/WOOD: | |
| Unidentified hardwood | Wood from a broad-leaved flowering tree or shrub |
| Unidentifiable - vitrified | Charcoal exhibiting a shiny, glassy appearance due to fusion by heat |
| NON-FLORAL REMAINS: | |
| Muscovite | The most common mica, found in granites, pegmatites, gneisses and schists, with a layered structure of aluminum silicate sheets weakly bonded together by layers of potassium ions |

# REFERENCES CITED

Carlquist, Sherwin
    2001   *Comparative Wood Anatomy: Systematic, Ecological, and Evolutionary Aspects of Dicotyledon Wood*. Springer Series in Wood Science. Springer, Berlin.

Hoadley, R. Bruce
    1990   *Identifying Wood: Accurate Results with Simple Tools*. The Taunton Press, Inc., Newtown, Connecticut.

Martin, Alexander C. and William D. Barkley
    1961   *Seed Identification Manual*. University of California, Berkeley.

Matthews, Meredith H.
    1979   Soil Sample Analysis of 5MT2148: Dominguez Ruin, Dolores, Colorado. Appendix B. In *The Dominguez Ruin: A McElmo Phase Pueblo in Southwestern Colorado*, edited by A. D. Reed. Bureau of Land Management Cultural Resource Series. vol. 7. Bureau of Land Management, Denver, Colorado.

Musil, Albina F.
    1963   *Identification of Crop and Weed Seeds*. Agricultural Handbook no. 219. U.S. Department of Agriculture, Washington D.C.

Panshin, A. J. and Carl de Zeeuw
    1980   *Textbook of Wood Technology*. McGraw-Hill Book, Co., New York.

Schopmeyer, C. S.
    1974   *Seeds of Woody Plants in the United States*. Agricultural Handbook No. 450. U.S. Department of Agriculture, Washington, D.C.

# APPENDIX D

## SUMMARY OF RADIOCARBON DATING, BAILEYS LAKE SITE

| Sample No. | NOSAMS[1] Accession No. | Trench, wall | Station[2] (m) | Depth[3] (m) | Unit Sampled[4] | Material Sampled | Organic Material Dated[5] | Pre-Treatment Method | δ13C[6] | Relation to Earthquake[7] | Age[8] (14C yr B.P.) | Age[9] (cal yr B.P.) |
|---|---|---|---|---|---|---|---|---|---|---|---|---|
| BL-R1 | OS-86493 | West(N), north | 21.8, 3.3 | 0.48 | S1 (top) | Paleosol | Unidentifiable charcoal (vitrified, small) and unidentified stem fragments (charred) (11.2 mg) | Acid-base-acid | -25 | Max – BL1 | 5400 ± 30 | 6220 ± 100 |
| BL-R2-1 | OS-86491 | West(N), north | 22.1, 3.1 | 0.82 | 6 | Scarp-derived colluvium (organic interbed) (BL2) | Unidentifiable charcoal (vitrified, small) and unidentified stem fragments (charred) (5.2 mg) | Acid-base-acid | -25 | Min – BL2 | 675 ± 30 | 620 ± 80 |
| BL-R2-2 | OS-86573 | West(N), north | 22.1, 3.1 | 0.82 | 6 | Scarp-derived colluvium (organic interbed) (BL2) | Unidentifiable charcoal (vitrified, small) and unidentified stem fragments (charred) (4.3 mg) | Acid-base-acid | -25 | Min – BL2 | 1800 ± 25 | 1740 ± 100 |
| BL-R3-1 | OS-86492 | West(N), north | 22.3, 3.5 | 0.40 | 10 | Scarp-derived colluvium (BL1) | 7 fragments unidentified hardwood charcoal (5.5 mg) | Acid-base-acid | -25 | Min – BL1 | 3890 ± 30 | 4330 ± 100 |
| BL-R3-2 | OS-86494 | West(N), north | 22.3, 3.5 | 0.40 | 10 | Scarp-derived colluvium (BL1) | 45 fragments unidentifiable charcoal (vitrified, small) and unidentified stem fragments (charred) (7.7 mg) | Acid-base-acid | -25 | Min – BL1 | 4280 ± 30 | 4850 ± 60 |
| BL-R4 | OS-86572 | West(S), south | 25.8, 1.1 | 2.97 | 1 | Wetland clay | 1 fragment unidentifiable charcoal (vitrified, small) and microcharcoal (1.7 mg) | Acid-base-acid | -25 | — | 31,400 ± 350 | 35,780 ± 820 |
| BL-R5 | — | West(S), south | 17.4, 2.2 | 1.38 | 3 (base) | Lacustrine clay and silt | None; sample lacked organic material | — | — | Min – BL4 | — | — |

[1] National Ocean Sciences Accelerator Mass Spectrometry Facility, Woods Hole Oceanographic Institution (Woods Hole, Massachusetts).
[2] Station coordinates are horizontal and vertical meter marks along arbitrary reference grid for trench (see plate 1).
[3] Depth below ground surface.
[4] See appendix A for descriptions of stratigraphic units, and appendix B for description of pedogenic soil unit S1.
[5] Separation and identification by Paleo Research Institute (Golden, Colorado); see appendix C.
[6] Assumed delta 13C value.
[7] Min (max) indicates minimum (maximum) limiting time constraint for a surface-faulting earthquake (e.g., BL1).
[8] Laboratory-reported radiocarbon age with one standard deviation uncertainty. B.P. is before present (AD 1950).
[9] Mean calendar-calibrated age and 2σ uncertainty, rounded to nearest decade, determined using OxCal calibration software (v. 4.1.7; Bronk Ramsey, 2009) and the IntCal09 atmospheric data set (Reimer and others, 2009).

# SUMMARY OF LUMINESCENCE DATING, BAILEYS LAKE SITE

| Sample No.[1] | Trench, wall | Station[2] (m) | Depth[3] (m) | Unit Sampled[4] | Material Sampled | Water Content[5] (%) | Water Saturation History[6] (%) | K[7] (%) | U[7] (ppm) | Th[7] (ppm) | Cosmic Dose Additions[8] (Gy/kyr) | Total Dose Rate OSL[9] (IRSL)[10] (Gy/kyr) | Equivalent Dose OSL[9] (IRSL)[10] (Gy) | n[11] | Relation to Earthquake[12] | Laboratory Age OSL[9] (IRSL)[10] (yr before 2011) |
|---|---|---|---|---|---|---|---|---|---|---|---|---|---|---|---|---|
| BL-L1 | West (S), south | 25.7, 1.3 | 2.65 | 2a | Fine lacustrine sand | 2 (23) | 85 | 1.28 ± 0.03 | 1.83 ± 0.12 | 5.18 ± 0.26 | 0.19 ± 0.02 | 1.64 ± 0.05 (2.31 ± 0.07) | 51.8 ± 2.28 (72.0 ± 3.71) | 19 (21) | — | 31,590 ± 1670 (31,150 ± 1930) |
| BL-L2 | West (S), south | 25.7, 1.6 | 2.35 | 2a | Fine lacustrine sand | 20 (25) | 85 | 1.49 ± 0.04 | 1.89 ± 0.14 | 5.93 ± 0.34 | 0.20 ± 0.02 | 1.79 ± 0.06 (2.49 ± 0.09) | 55.8 ± 2.85 (68.8 ± 2.22) | 20 (20) | — | 31,170 ± 1940 (27,620 ± 1310) |
| BL-L3 | West (S), south | 19.6, 0.9 | 2.75 | 2c | Lacustrine silt | 2 (18) | 85 | 2.28 ± 0.04 | 2.91 ± 0.11 | 11.3 ± 0.35 | 0.19 ± 0.02 | 3.01 ± 0.06 (4.33 ± 0.09) | 73.4 ± 7.34 (115 ± 4.54) | 13 (30) | — | 24,440 ± 2,500 (26,470 ± 1,200) |
| BL-L4 | West (S), south | 19.7, 1.2 | 2.40 | 2c | Fine lacustrine sand | 7 (22) | 85 | 2.14 ± 0.03 | 3.08 ± 0.11 | 10.4 ± 0.29 | 0.20 ± 0.02 | 2.95 ± 0.05 (4.27 ± 0.08) | 131 ± 15.3 (83.0 ± 2.19) | 6 (28) | — | 43,380 ± 5,140 (19,440 ± 620) |
| BL-L5 | West (S), south | 19.6, 1.4 | 2.20 | 2d | Fine to medium lacustrine sand | 19 (29) | 85 | 2.39 ± 0.04 | 3.12 ± 0.15 | 13.2 ± 0.40 | 0.20 ± 0.02 | 3.42 ± 0.07 (4.98 ± 0.10) | 67.8 ± 8.07 (136 ± 4.65) | 5 (24) | — | 19,810 ± 2,380 (27,390 ± 1,080) |
| BL-L7 | West (N), south | 21.7, 1.9 | 1.80 | 2e | Lacustrine silt | 15 (39) | 85 | 2.21 ± 0.05 | 3.15 ± 0.22 | 10.6 ± 0.55 | 0.21 ± 0.02 | 3.20 ± 0.10 (4.64 ± 0.15) | 61.8 ± 1.01 (94.6 ± 2.01) | 20 (20) | Max – BL4 | 19,300 ± 380 (20,380 ± 570) |
| BL-L8 | West (N), south | 21.4, 2.2 | 1.55 | 3 | Fine lacustrine sand | 19 (46) | 70 | 1.18 ± 0.02 | 2.49 ± 0.08 | 8.17 ± 0.28 | 0.22 ± 0.02 | 1.93 ± 0.04 (2.89 ± 0.07) | 27.2 ± 0.053 (41.1 ± 1.93) | 20 (20) | Min – BL4 | 14,070 ± 820 (14,220 ± 740) |
| BL-L9 | West (N), south | 20.7, 2.4 | 1.25 | 3 | Lacustrine clay, silt, and fine sand | 18 (50) | 70 | 1.31 ± 0.02 | 2.75 ± 0.09 | 7.89 ± 0.29 | 0.23 ± 0.02 | 2.02 ± 0.05 (2.99 ± 0.07) | 26.2 ± 1.11 (37.8 ± 2.12) | 19 (20) | Max – BL3 | 12,960 ± 620 (12,660 ± 770) |
| BL-L10 | West (N), south | 22.2, 3.5 | 0.15 | 11 | Loess | 6 (29) | 90 | 1.54 ± 0.02 | 2.82 ± 0.08 | 8.26 ± 0.27 | 0.32 ± 0.02 | 2.51 ± 0.06 (3.66 ± 0.08) | 8.05 ± 0.61 (11.9 ± 0.55) | 16 (20) | Min – BL1 | 3210 ± 250 (3240 ± 160) |
| BL-L11 | West (N), north | 19.8, 2.8 | 0.80 | 9 | Loess | 9 (37) | 70 | 1.00 ± 0.03 | 1.65 ± 0.11 | 3.87 ± 0.36 | 0.25 ± 0.02 | 1.57 ± 0.05 (2.21 ± 0.07) | 19.6 ± 0.90 (29.2 ± 1.49) | 16 (16) | — | 12,470 ± 700 (13,200 ± 810) |
| BL-L12 | West (N), north | 22.0, 3.3 | 0.55 | S1 | Paleosol | 7 (34) | 70 | 1.61 ± 0.03 | 2.48 ± 0.12 | 8.28 ± 0.28 | 0.25 ± 0.02 | 2.89 ± 0.07 (4.25 ± 0.13) | 17.4 ± 1.36 (28.5 ± 1.03) | 18 (20) | Max – BL1 | 6020 ± 500 (6710 ± 310) |
| BL-L13 | West (N), north | 21.4, 2.8 | 1.00 | 5 | Lacustrine clay, silt, and fine sand | 4 (29) | 70 | 1.01 ± 0.02 | 1.92 ± 0.07 | 3.93 ± 0.23 | 0.24 ± 0.02 | 1.68 ± 0.09 (2.41 ± 0.12) | 21.0 ± 1.10 (29.9 ± 0.75) | 19 (20) | Max – BL2 Min – BL3 | 12,530 ± 910 (12,390 ± 710) |
| BL-L14 | West (N), south | 18.7, 2.6 | 1.00 | 7 | Fine to coarse lacustrine sand | 2 (27) | 70 | 1.37 ± 0.03 | 1.83 ± 0.09 | 5.41 ± 0.31 | 0.24 ± 0.02 | 2.07 ± 0.07 (2.90 ± 0.10) | 23.8 ± 5.36 (31.3 ± 1.96) | 13 (13) | Min – BL2 | 11,510 ± 2610 (10,800 ± 770) |
| BL-L16 | West (S), south | 27.9, 2.0 | 2.15 | 2a | Fine lacustrine sand | 6 (34) | 85 | 1.33 ± 0.03 | 1.86 ± 0.15 | 6.07 ± 0.35 | 0.20 ± 0.02 | 1.94 ± 0.07 (2.76 ± 0.10) | 60.2 ± 3.14 (57.4 ± 1.70) | 24 (24) | — | 31,030 ± 1960 (20,790 ± 970) |

[1] Analyses by U.S. Geological Survey Luminescence Dating Laboratory (Denver, Colorado); samples BL-L6 and BL-L15 collected as duplicates (not analyzed) of samples BL-L7 and BL-L10, respectively.

[2] Station coordinates are horizontal and vertical meter marks along arbitrary reference grid for trench (see plate 1).

[3] Depth below ground surface.

[4] See appendix A for descriptions of stratigraphic units, and appendix B for description of pedogenic soil unit S1.

[5] Field moisture; complete sample saturation percent in parentheses.

[6] Estimated water saturation history (i.e., time below water table) of sampled material.

[7] Analyses obtained using laboratory gamma spectrometry (high-resolution Ge detector), and readings were delayed after 21 days of being sealed in the planchet (used for dose rates).

[8] Cosmic doses and attenuation with depth were calculated using the methods of Prescott and Hutton (1994); Gy – gray.

[9] Dose rate and optically stimulated luminescence (OSL) age for fine-grained (90–125 microns) quartz sand; linear + exponential fit used on equivalent dose, single aliquot regeneration; ages rounded to nearest decade, errors to 1σ.

[10] Dose rate and infrared stimulated luminescence (IRSL) age for fine grains (4–11 microns) of polymineral silt; exponential fit used for equivalent dose, multiple aliquot additive dose; ages rounded to nearest decade, errors to 1σ; fade tests indicate no correction.

[11] Number of replicated equivalent dose (De) estimates used to calculate the mean; total number of measurements made, including failed runs with unusable data, in parentheses.

[12] Min (max) indicates minimum (maximum) limiting time constraint for a surface-faulting earthquake (e.g., BL1).

# APPENDIX F

## OSTRACODE IDENTIFICATION AND INTERPRETATION, BAILEYS LAKE SITE

| Sample No.[1] | Trench, wall | Station[2] (m) | Unit Sampled[3] | Ostracodes | Comments[4] | Interpretation |
|---|---|---|---|---|---|---|
| O-13 | West(N), south | 19.6, 2.4 | 5 | None identifiable | Few ostracodes, mostly unidentifiable fragments (probably *Candona* sp.); some ostracode fragments carbonate-coated | Gilbert episode |
| O-12 | West(N), south | 18.4, 2.2 | 3 | *Limnocythere ceriotuberosa* *Candona caudata*(?) *Candona adunca* *Cytherissa lacustris* | Few ostracodes, most broken; sediment lumps, sand | Bonneville, regressive phase |
| O-11 | West(S), south | 17.7, 2.1 | 2e | *Limnocythere ceriotuberosa* *Candona adunca* | Abundant clean ostracodes; sand | Bonneville, mid- to late transgressive phase |
| O-10 | West(S), south | 17.7, 1.9 | 2e | *Limnocythere ceriotuberosa* *Candona caudata*(?) *Candona adunca* | Few ostracodes, some clean, some carbonate-coated; sand | |
| O-9 | West(S), south | 20.8, 1.7 | 2e | *Limnocythere ceriotuberosa* *Candona adunca* | Abundant clean ostracodes; sand; few redox lumps | |
| O-8 | West(S), south | 19.3, 1.3 | 2c | *Limnocythere ceriotuberosa* *Candona caudata*(?) *Candona adunca* | Clean ostracodes; sand | Bonneville, transgressive phase |
| O-7 | West(S), south | 19.4, 1.1 | 2c | *Limnocythere staplini* *Limnocythere ceriotuberosa* *Candona caudata*(?) | Sand; black sulfide lumps | |
| O-6 | West(S), south | 26.4, 2.6 | 2b | *Limnocythere staplini* *Limnocythere ceriotuberosa* *Candona caudata*(?) | Clean ostracodes; sand; redox lumps | |
| O-5 | West(S), south | 26.4, 2.5 | 2b | *Limnocythere staplini* | Few ostracodes, some clean, some carbonate-coated; broken *Candona* sp.; carbonate-coated redox lumps; sand | |
| O-4 | West(S), south | 26.0, 1.6 | 2a | *Limnocythere staplini* *Candona rawsoni* | Abundant curved flakes of carbonate, some with linear impressions on smooth concave sides, convex sides are rough (flakes appear to be leaf or stem encrustations); redox lumps; snail-shell fragments and whole shells; hollow tubes of redox-cemented sand | Bonneville, early transgressive phase |
| O-3 | West(S), south | 25.6, 1.4 | 2a | *Limnocythere staplini* *Candona rawsoni* *Cytherissa lacustris* | Few ostracodes; snail-shell fragments; sediment lumps, sand | |
| O-2 | West(S), south | 25.6, 1.2 | 1 | *Candona rawsoni* | Few ostracodes (fragments); charophyte stem encrustations; redox lumps | Pre-Bonneville wetland/alluvial marsh |
| O-1 | West(S), south | 25.6, 0.8 | 1 | *Candona rawsoni* | Few ostracodes, some shells carbonate-coated; charophyte stem encrustations; sulfide lumps, sand | |

[1] Samples listed in stratigraphic order (top to bottom).
[2] Station coordinates are horizontal and vertical meter marks along arbitrary reference grid for trench (see plate 1).
[3] See appendix A for descriptions of stratigraphic units.
[4] Redox lumps = iron minerals, some oxidized (yellow colors), some reduced (black), mostly cementing sand; sulfide lumps = lumps of black iron sulfide minerals.

# APPENDIX G

# OXCAL MODEL FOR THE GRANGER FAULT AT THE BAILEYS LAKE SITE

An OxCal model for the Granger fault at the Baileys Lake site was created using OxCal calibration and analysis software (version 4.1.7; Bronk Ramsey, 2009; using the IntCal09 calibration curve of Reimer and others, 2009). The models include *C_Date* for luminescence ages, *R_Date* for radiocarbon ages, and *Boundary* for undated events (paleoearthquakes). These components are arranged into ordered sequences based on the relative stratigraphic positions of the samples. The sequences may contain *phases*, or groups where the relative stratigraphic ordering information for the individual radiocarbon ages is unknown. The model is presented here in reverse stratigraphic order, following the order in which the ages and events are evaluated in OxCal.

**Model Input**

```
Plot()
 {
  Sequence("Baileys Lake, full chronology")
  {
   Boundary("Start");
   R_Date("BL-R4, C14 31,400 +/-350",31400,350);
   C_Date("BL-L1, OSL 31,590 +/-1670",-29580,1670);
   C_Date("BL-L2, OSL 31,170 +/-1940",-29160,1940);
   C_Date("BL-L16, OSL 31,030 +/-1960",-29020,1960);
   C_Date("BL-L3, OSL 24,440 +/-2500",-22430,2500);
   C_Date("BL-L5, OSL 19,810 +/-2380",-17800,2380);
   C_Date("BL-L7, OSL 19,300 +/-380",-17290,380);
   Boundary("BL4");
   C_Date("BL-L8, OSL 14,070 +/-820",-12060,820);
   C_Date("BL-L9, OSL 12,960 +/-620",-10950,620);
   Boundary("BL3");
   C_Date("BL-L13, OSL 12,530 +/-910",-10520,910);
   Boundary("BL2");
   C_Date("BL-L14, OSL 11,510 +/-2610",-9500,2610);
   C_Date("BL-L11, OSL 12,470 +/-700",-10460,700);
   Phase("Soil S1");
   {
    C_Date("BL-L12, OSL 6020 +/-500",-4010,500);
    R_Date("BL-R1, C14 5400+/-30",5400,30);
   };
   Boundary("BL1");
   Phase("Unit 10, P1 Colluvium");
   {
    R_Date("BL-R3-2, C14 4280+/-30",4280,30);
    R_Date("BL-R3-1, C14 3890+/-30",3890,30);
   };
   C_Date("BL-L10, OSL 3210 +/-250",-1200,250);
   Boundary("Begin historical record",1847 AD);
  };
 };
```

## Model Output

| Baileys Lake Full Chronology | Unmodelled (BP) | | Modelled (BP) | | Agreement |
|---|---|---|---|---|---|
| | mean | sigma | mean | sigma | |
| Boundary Start | 38450 | 3010 | | | |
| R_Date BL-R4, C14 31,400 ±350 | 35850 | 420 | 35780 | 410 | 99.7 |
| C_Date BL-L1, OSL 31,590 ±1670 | 31530 | 1670 | 32660 | 1250 | 97.5 |
| C_Date BL-L2, OSL 31,170 ±1940 | 31110 | 1940 | 31090 | 1240 | 119 |
| C_Date BL-L16, OSL 31,030 ±1960 | 30970 | 1960 | 29470 | 1400 | 95.6 |
| C_Date BL-L3, OSL 24,440 ±2500 | 24380 | 2500 | 24730 | 1990 | 109.3 |
| C_Date BL-L5, OSL 19,810 ±2380 | 19750 | 2380 | 21050 | 1340 | 112.5 |
| C_Date BL-L7, OSL 19,300 ±380 | 19240 | 380 | 19210 | 380 | 100.3 |
| **Boundary BL4** | | | **15700** | **1690** | |
| C_Date BL-L8, OSL 14,070 ±820 | 14010 | 820 | 14080 | 630 | 112.5 |
| C_Date BL-L9, OSL 12,960 ±620 | 12900 | 620 | 13360 | 460 | 95 |
| **Boundary BL3** | | | **12960** | **530** | |
| C_Date BL-L13, OSL 12,530 ±910 | 12470 | 910 | 12640 | 520 | 121.2 |
| **Boundary BL2** | | | **12340** | **570** | |
| C_Date BL-L14, OSL 11,510 ±2610 | 11450 | 2610 | 11890 | 580 | 136.2 |
| C_Date BL-L11, OSL 12,470 ±700 | 12410 | 700 | 11450 | 560 | 62.6 |
| Phase Soil S1 | | | | | |
| C_Date BL-L12, OSL 6020 ±500 | 5960 | 500 | 6540 | 260 | 76.8 |
| R_Date BL-R1, C14 5400±30 | 6220 | 50 | 6220 | 50 | 98 |
| **Boundary BL1** | | | **5540** | **400** | |
| Phase Unit 10, P1 Colluvium | | | | | |
| R_Date BL-R3-2, C14 4280±30 | 4850 | 30 | 4850 | 30 | 98.9 |
| R_Date BL-R3-1, C14 3890±30 | 4330 | 50 | 4330 | 50 | 99.9 |
| C_Date BL-L10, OSL 3210 ±250 | 3150 | 250 | 3150 | 250 | 100 |
| Boundary Begin historical record, 1847 | 100 | 0 | 100 | 0 | 100 |

WEST VALLEY FAULT ZONE EARTHQUAKE TIMING CONSTRAINTS FROM
CONSULTANTS' TRENCHES

Two trenches excavated by consultants (as part of pre-development fault-setback investigations required by local governments) have yielded useful earthquake timing data for the West Valley fault zone where the Utah Geological Survey was able to sample organic sediment for radiocarbon dating. One trench was near the north end of the Taylorsville fault at about 2100 West and 1300 North (between the Salt Lake City International Airport and Interstate 215), and was excavated by AGRA Earth and Environmental, Inc. in September 1997 (figures H1 through H4). The other trench was on the middle part of the westernmost trace of the Granger fault in the northeastern quadrant of the intersection of 4800 West and California Avenue (1300 South), near the "1300 South" site of Keaton and Currey (1989), and was excavated by Terracon Consultants, Inc. in March 1998 (figures H5 through H7); see figure 4 in the main report for site locations. These trenches were open only briefly, precluding detailed logging, so the geologic context of the samples is not well established. Because of this, as well as the nature of the radiocarbon ages (apparent mean residence time [AMRT] ages from bulk-soil samples, with applied mean residence correction [MRC] and carbon age span [CAS] factors; see discussion in Machette and others, 1992, appendix), relatively large uncertainty exists in the relation between the radiocarbon ages and earthquake timing. Also, we must assume that the soil samples were not contaminated by young organic material. Notwithstanding these caveats, the radiocarbon ages provide constraints on the timing of two surface-faulting earthquakes that are younger than the most recent surface-faulting earthquake documented at the Baileys Lake site.

UGS geologists collected two bulk-soil samples from the AGRA trench on the Taylorsville fault: sample AGRA-RC1 was collected from crack-fill sediment/fault-zone colluvium and yielded an AMRT radiometric age of $2350 \pm 80$ [14]C yr B.P., and sample AGRA-RC2 was collected from sag pond deposits beneath the possible colluvial wedge and yielded an AMRT age of $2520 \pm 70$ [14]C yr B.P. (unpublished UGS data; figure H4). Applying a 200-yr MRC and 200-yr CAS, these radiocarbon ages calendar calibrated to 2110 +210/-200 cal yr B.P. (AGRA-RC1) and 2330 +120/-170 cal yr B.P. (AGRA-RC2) (unpublished UGS data). Solomon (1998) reported the earthquake time as "roughly 2200 years" (the average of the two ages).

UGS geologists collected a single bulk-soil sample from the Terracon site on the Granger fault. Sample GFT-RC1 was interpreted as being from scarp-derived colluvium and yielded an AMRT radiometric age of $1880 \pm 80$ [14]C yr B.P. (unpublished UGS data). Applying a 300-yr MRC and 200-yr CAS, the radiocarbon age calendar calibrated to 1460 +170/-130 cal yr B.P. (unpublished UGS data). If the sample indeed came from the heel of the colluvial wedge as described in unpublished UGS file information, the radiocarbon age may provide a close minimum time constraint for the earthquake, as an age from scarp-derived colluvium can generally be interpreted as a minimum limit on earthquake timing (e.g., McCalpin, 1996; Yeats and others, 1997). However, our review of site photographs (figures H6 and H7) raises the possibility that the sample may have been obtained from a faulted soil A horizon that was buried on the hanging wall by scarp-derived colluvium. Extensive burrowing and soil carbonate and/or

evaporite mineral precipitation (associated with a shallow, fluctuating water table) appear to obscure geologic contacts within the fault zone. If sample GFT-RC1 came from a buried soil beneath the colluvial wedge, it would provide a maximum time constraint for the earthquake.

We used OxCal calibration and analysis software (version 4.1.7; Bronk Ramsey, 2009; using the IntCal09 calibration curve of Reimer and others, 2009) to provide updated calendar calibration of the radiocarbon ages and to model earthquake times. The models include *R_Date* for radiocarbon ages, *Delta_R* for MRC factors, and *Boundary* for undated events (paleoearthquakes). As noted in appendix G, these components are arranged into ordered sequences based on the relative stratigraphic positions of the samples. The models are presented in reverse stratigraphic order (table H1), following the order in which the ages and events are evaluated in OxCal. Because of the uncertainty as to whether sample GFT-RC1 provides a minimum or maximum limiting time constraint, we constructed two models to account for both possibilities (table H1 and figure H8).

The OxCal models indicate two paleoearthquakes. The older earthquake occurred around 2.2 ± 0.2 ka (2σ), consistent with the time estimated by Solomon (1998). The modeled age of the younger earthquake is 1.7 ± 0.3 ka if sample GFT-RC1 is considered to provide a minimum limiting time constraint; if GFT-RC1 provides a maximum limiting time constraint, the modeled age of the younger earthquake is 1.2 ± 0.6 ka (2σ). Lacking a solid basis for interpreting GFT-RC1 as either a minimum or maximum time constraint, we combined the modeled earthquake times to yield a mean time of 1.4 ± 0.7 ka. Both of these earthquakes are younger than the most recent paleoearthquake documented at the Baileys Lake site (see tables 3 and 4, and figure 15 in the main report).

Figure H1. Fault trench on the Taylorsville fault between the Salt Lake City International Airport and Interstate 215, excavated by AGRA Earth and Environmental, Inc. in September 1997; view looking east. Photo by UGS staff.

Figure H2. Fault-zone exposure, north wall of AGRA trench on the Taylorsville fault, September 1997. See figure H4 for interpretation. Photo by UGS staff.

Figure H3. Exposed stratigraphy immediately to the right (east) of the fault zone, north wall of AGRA trench on the Taylorsville fault, September 1997. See figure H4 for interpretation. Photo by UGS staff.
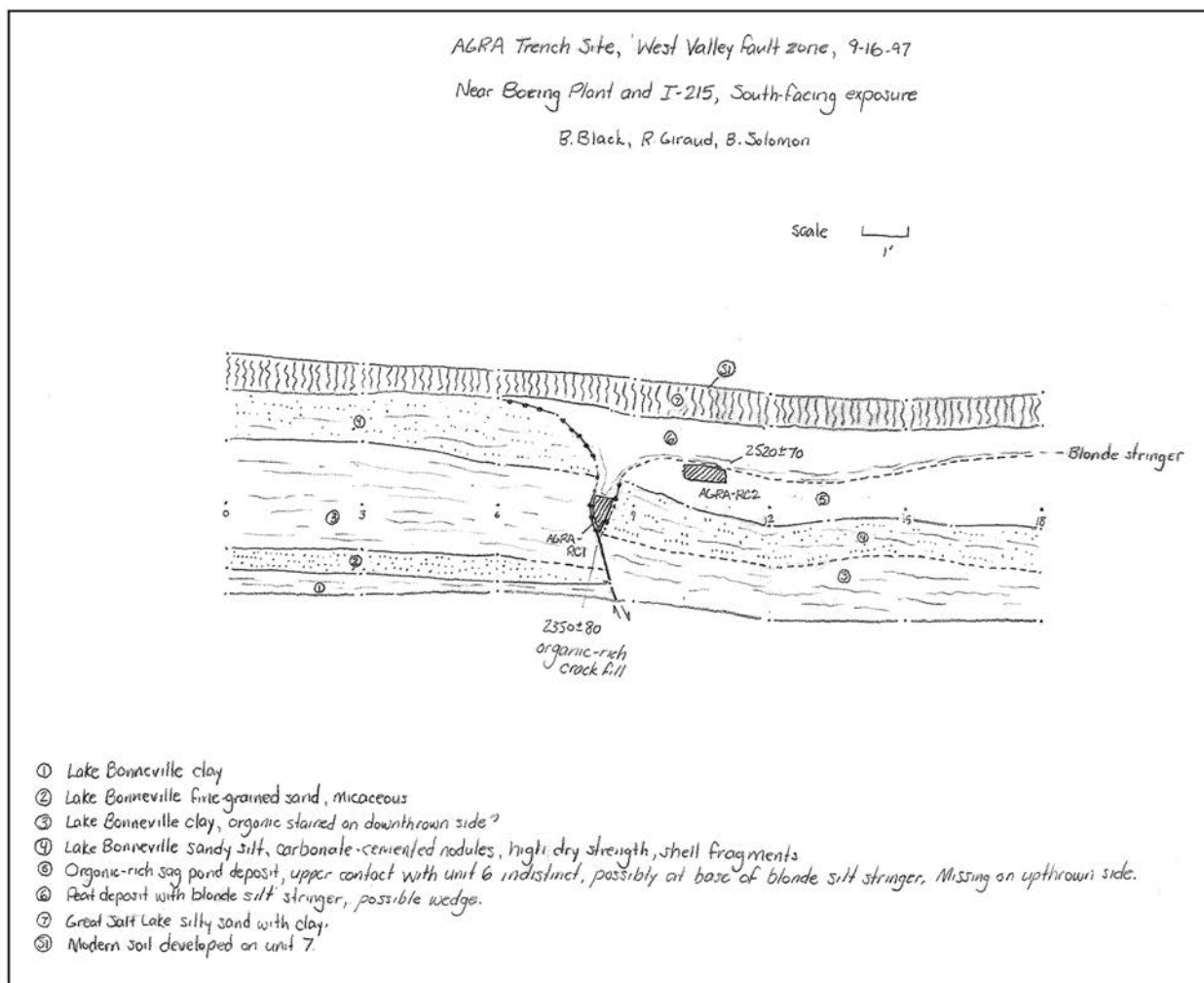
Figure H4. Trench log of north wall of the AGRA trench on the Taylorsville fault (from unpublished UGS files).

Figure H5. Fault trench on the Granger fault at 4800 West and California Avenue (1300 South), excavated by Terracon Consultants, Inc. in March 1998; view looking east. Photo by UGS staff.

Figure H6. Fault-zone exposure, north wall of Terracon trench on the Granger fault, March 1998. Photo by UGS staff.
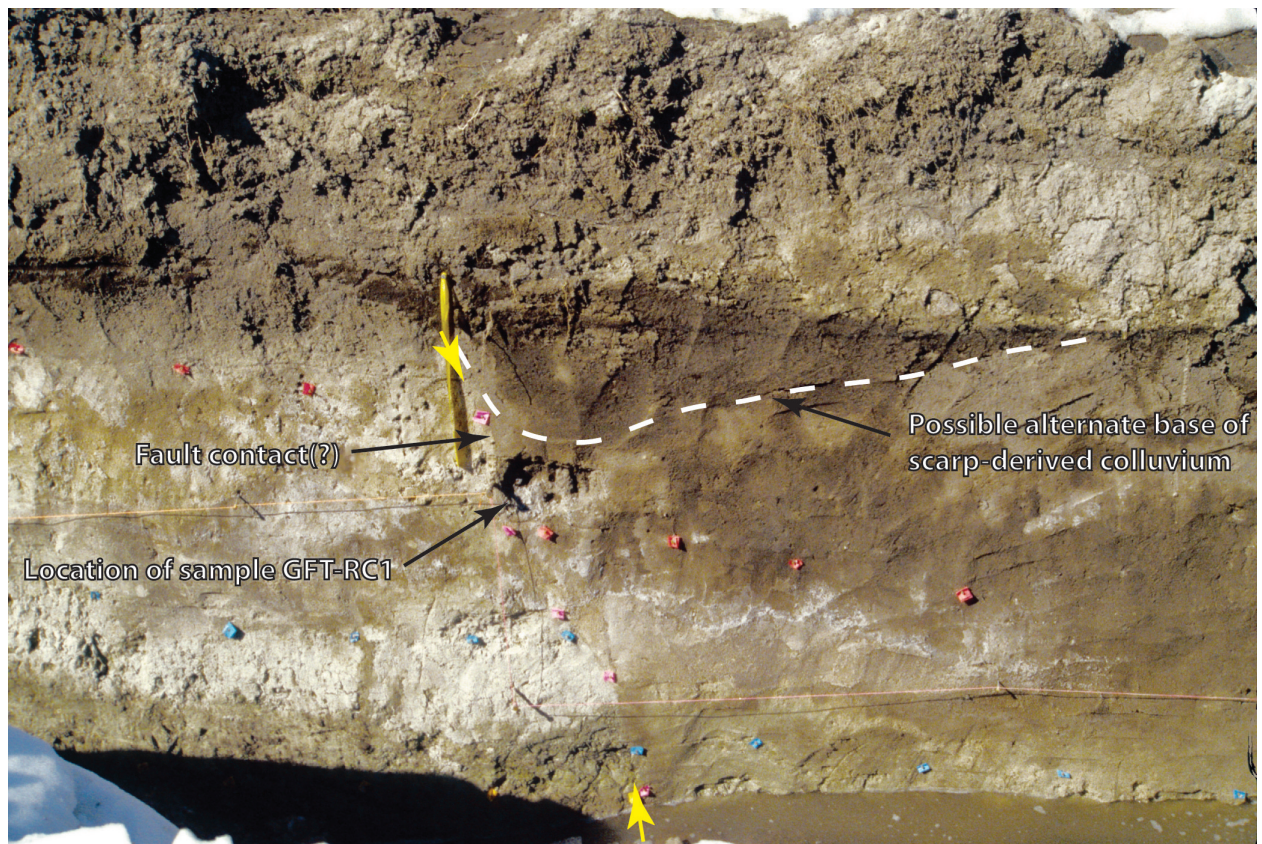
Figure H7. Detail of fault zone exposed in Terracon trench on the Granger fault, March 1998; fault between yellow arrows. Sample GFT-RC1 was originally interpreted as being from the "heel of the MRE [most recent event] colluvial wedge" (unpublished UGS file information), in which case the sampled sediment's age of $1880 \pm 80$ [14]C yr B.P. may provide a close minimum constraint on earthquake timing. An alternate interpretation is that the sample was from a soil that was faulted and subsequently buried by scarp-derived colluvium, in which case the age may provide a close maximum constraint on earthquake timing. Photo by UGS staff, annotation added for this study.
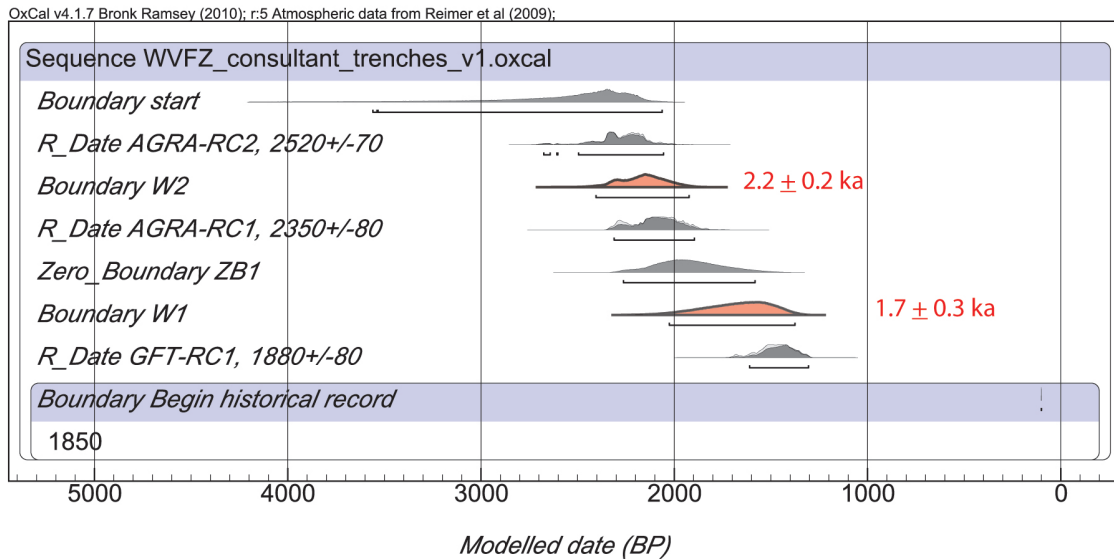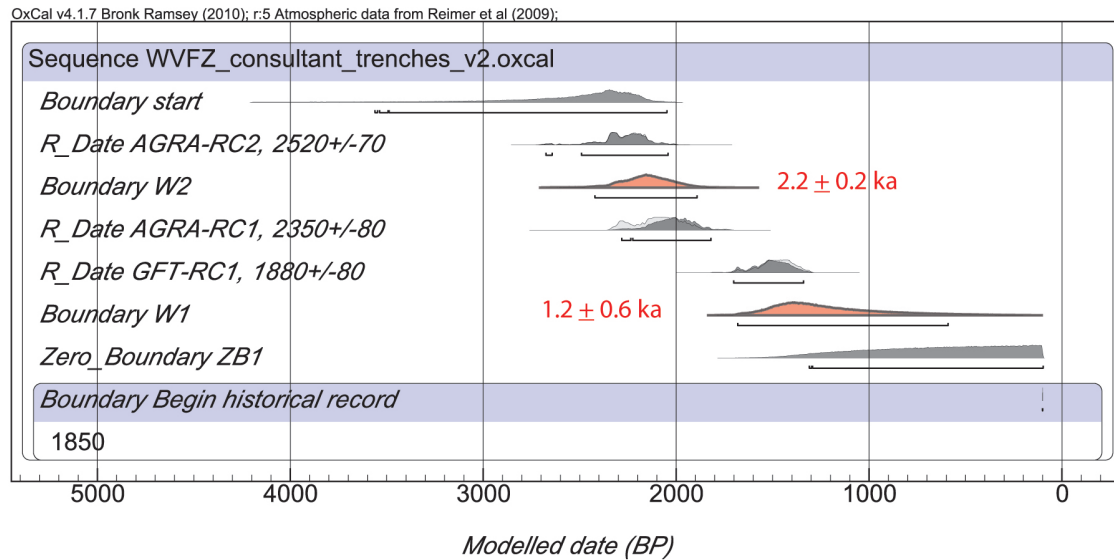
Figure H8. OxCal models for West Valley fault zone earthquake timing based on consultant trench data, showing stratigraphic ordering of ^{14}C ages and probability density functions (PDFs) for the timing of earthquakes W1 and W2 (red). Models constructed using OxCal version 4.1.7 (Bronk Ramsey, 2009) and the IntCal09 radiocarbon calibration curve (Reimer and others, 2009). Brackets below PDFs indicate 2σ time ranges. A and B show sample GFT-RC1 modeled as minimum and maximum age constraint, respectively, for earthquake W1 timing.

Table H1. OxCal model output for West Valley fault zone earthquake timing based on consultant trench data.

| WVFZ_consultant_trench_v1.oxcal Version 1[1] | Unmodelled (BP) | | Modelled (BP) | | Agreement |
|---|---|---|---|---|---|
| | mean | sigma | mean | sigma | |
| Boundary start | | | 2590 | 400 | |
| Delta_R MRT-200yr | 250 | 50 | 251 | 52 | 98 |
| R_Date AGRA-RC2, 2520±70 | 2270 | 130 | 2280 | 120 | 101 |
| **Boundary W2**[2] | | | **2170** | **120** | |
| R_Date AGRA-RC1, 2350±80 | 2090 | 120 | 2090 | 110 | 104 |
| Zero_Boundary ZB1 | | | 1920 | 170 | |
| **Boundary W1**[2] | | | **1680** | **170** | |
| Delta_R MRT-300yr | 300 | 0 | 300 | 0 | 100 |
| R_Date GFT-RC1, 1880±80 | 1480 | 90 | 1460 | 80 | 102 |
| Boundary Begin historical record - 1850 AD | 100 | 0 | 100 | 0 | 100 |

| WVFZ_consultant_trench_v2.oxcal Version 2[3] | Unmodelled (BP) | | Modelled (BP) | | Agreement |
|---|---|---|---|---|---|
| | mean | sigma | mean | sigma | |
| Boundary start | | | 2580 | 400 | |
| Delta_R MRT-200yr | 250 | 50 | 266 | 52 | 95 |
| R_Date AGRA-RC2, 2520±70 | 2270 | 130 | 2270 | 120 | 103 |
| **Boundary W2** | | | **2150** | **130** | |
| R_Date AGRA-RC1, 2350±80 | 2090 | 120 | 2020 | 110 | 96 |
| Delta_R MRT-300yr | 300 | 0 | 300 | 0 | 100 |
| R_Date GFT-RC1, 1880±80 | 1480 | 90 | 1510 | 90 | 94 |
| **Boundary W1** | | | **1210** | **290** | |
| Zero_Boundary ZB1 | | | 660 | 360 | |
| Boundary Begin historical record - 1850 AD | 100 | 0 | 100 | 0 | 100 |

| **Combined W1 (ver. 1) and W1 (ver. 2)**[4] | | |
|---|---|---|
| | mean: | 1445 cal yr. B.P. |
| | 2 sigma: | 659 cal yr. B.P. |
| | 5th percent: | 805 cal yr. B.P. |
| | 50th percent: | 1490 cal yr. B.P. |
| | 95th percent: | 1920 cal yr. B.P. |
| | mode: | 1510 cal yr. B.P. |

[1] Sample GFT-RC1 modeled as minimum age constraint for earthquake W1 timing.
[2] "W1" and "W2" correspond to West Valley fault zone earthquakes W1 and W2 as given in tables 4 and 6, and figure 15 in the main report.
[3] Sample GFT-RC1 modeled as maximum age constraint for earthquake W1 timing.
[4] Mean modeled earthquake time and 2σ uncertainty used for earthquake W1 in preliminary West Valley fault zone chronology (see tables 3, 4, and 6, and figure 15 in the main report).

Plate 1
Utah Geological Survey Special Study 149
Late Quaternary Paleoseismology of the West Valley Fault Zone—
Insights from the Baileys Lake Trench Site

## Explanation
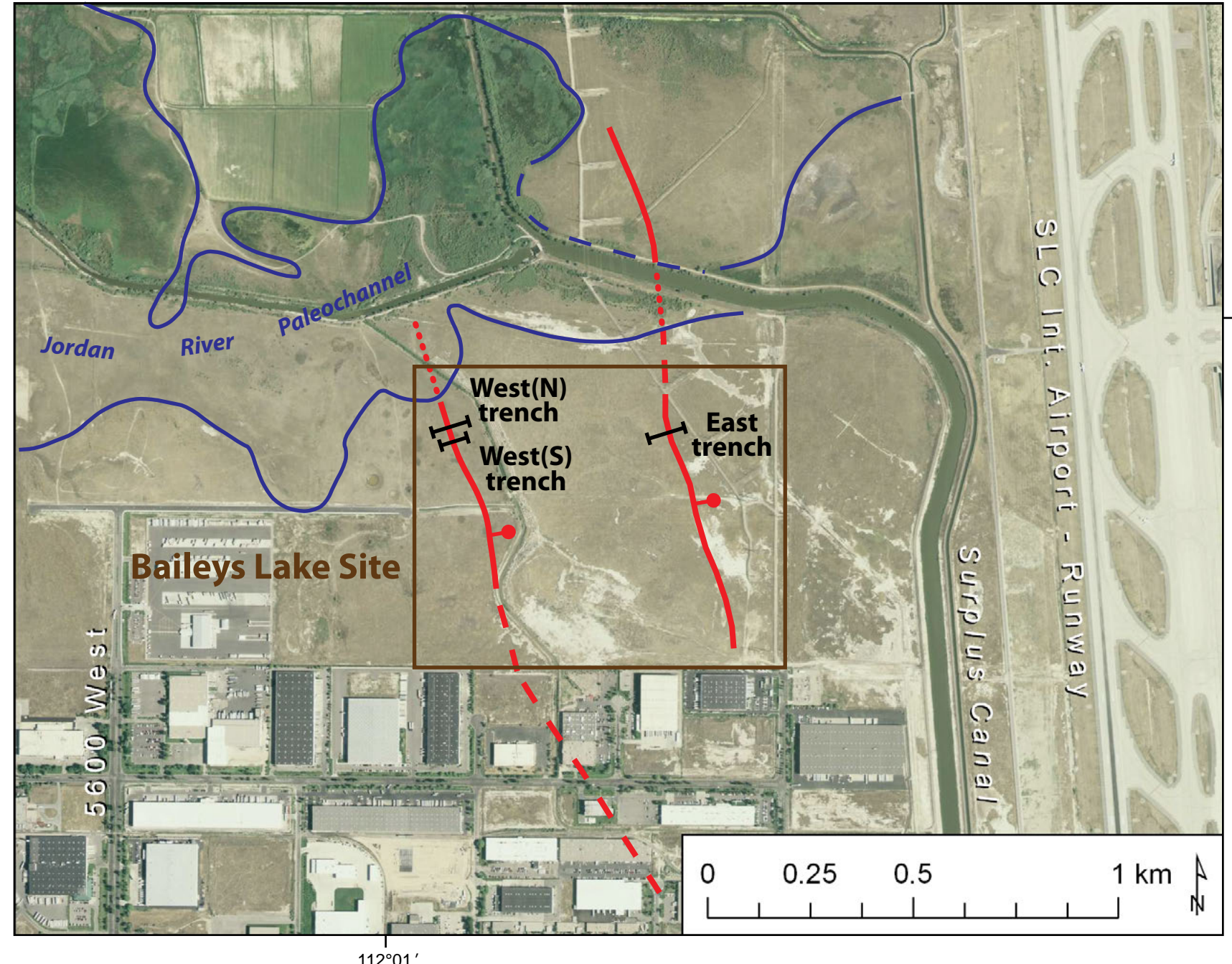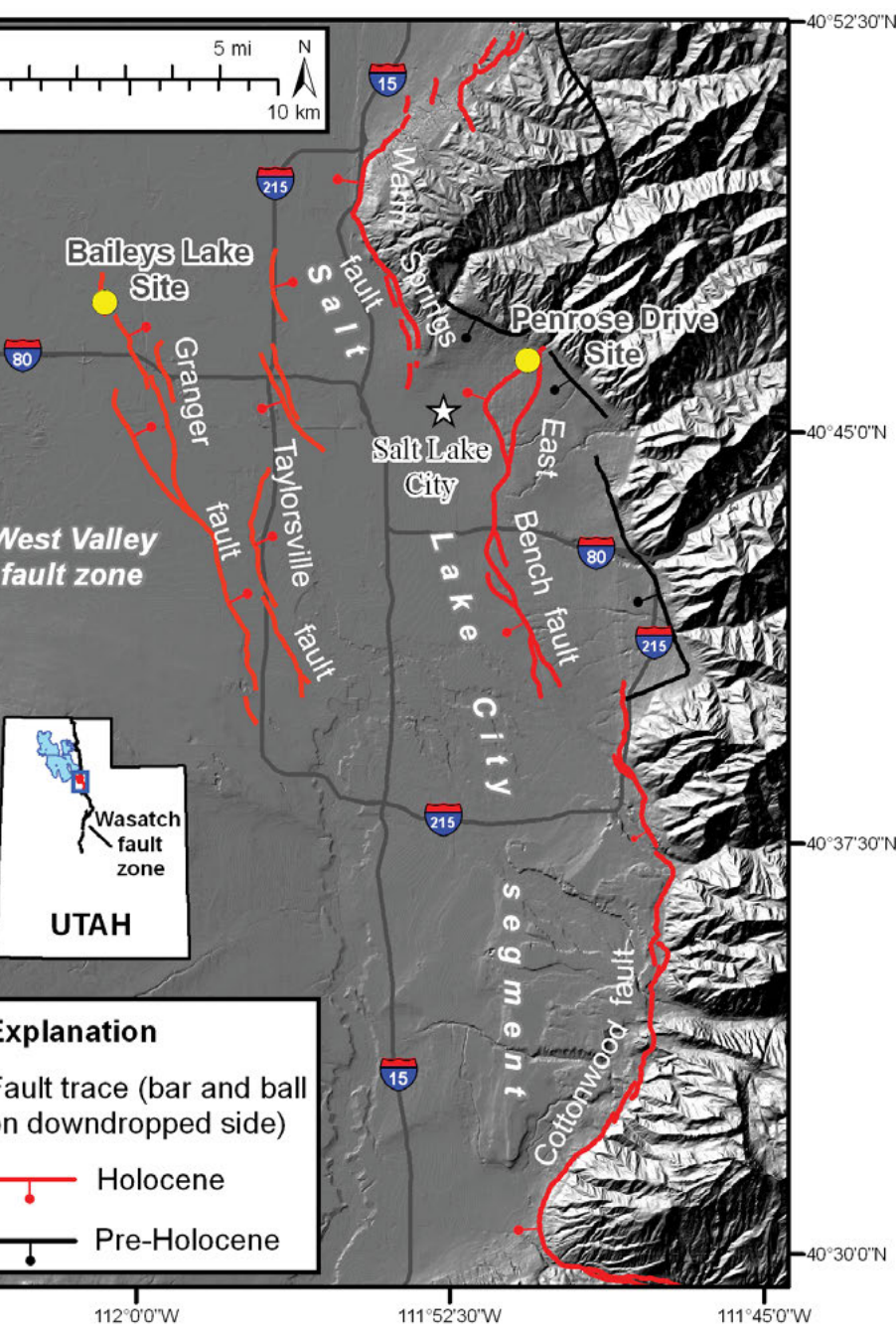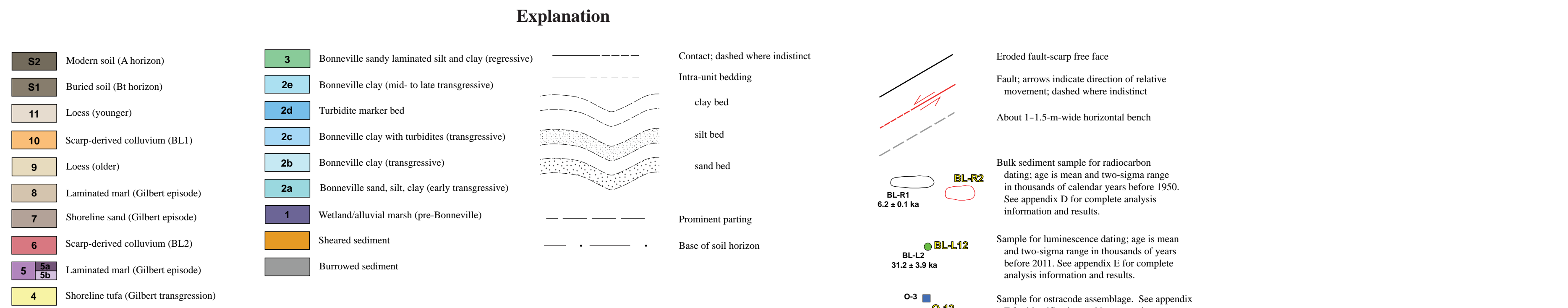


Summary of dating results for the Baileys Lake site.



### NOTES

n1  Well-sorted, non-stratified (liquefied) sand injected horizontally along bedding plane

n2  Relatively large clay rip-up clast within graded sand interbed (turbidite)

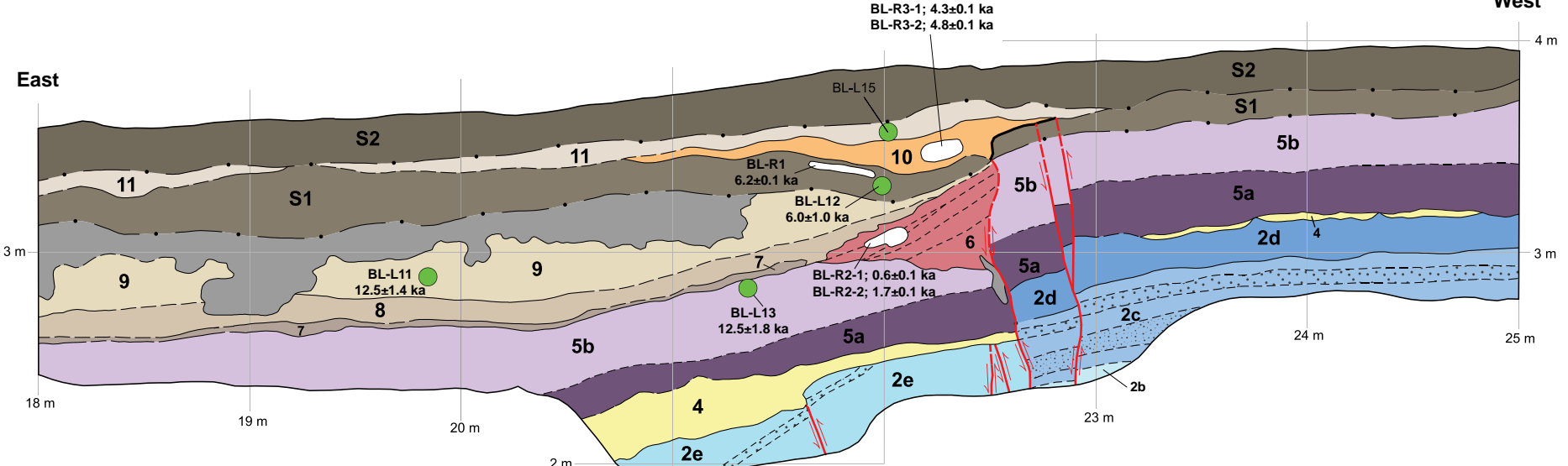n3  Angular cobble (9 x 7 x 2 cm) of dark gray micrite (dropstone)
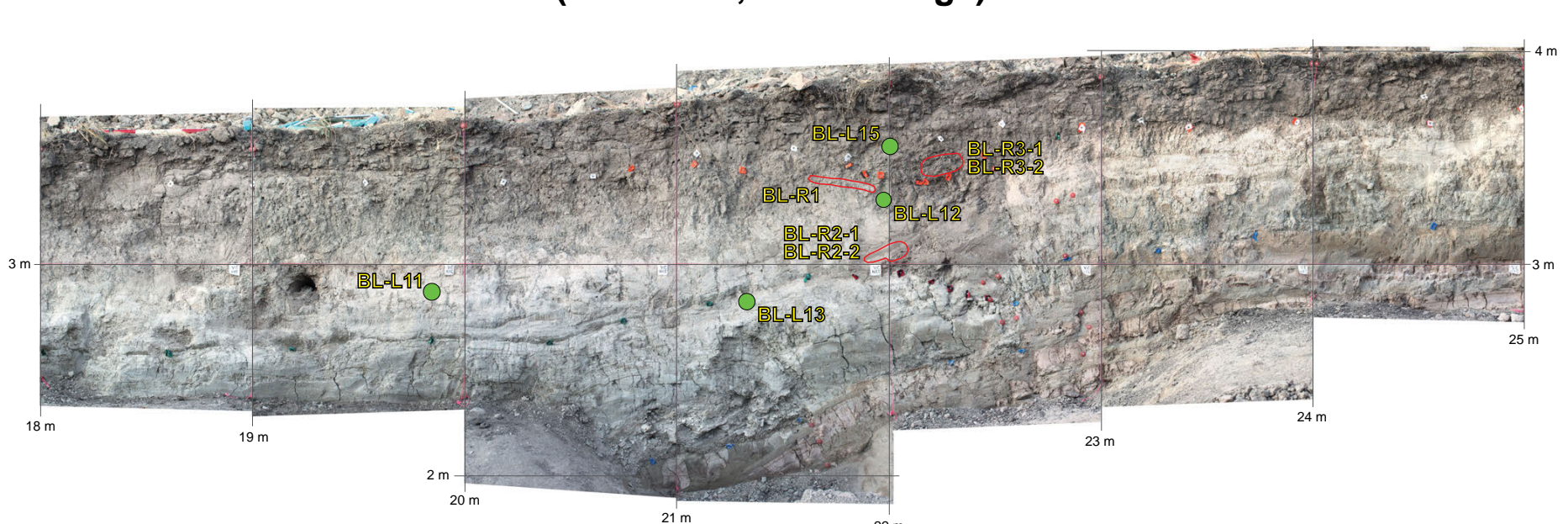
## Baileys Lake West(S) Trench (south wall)
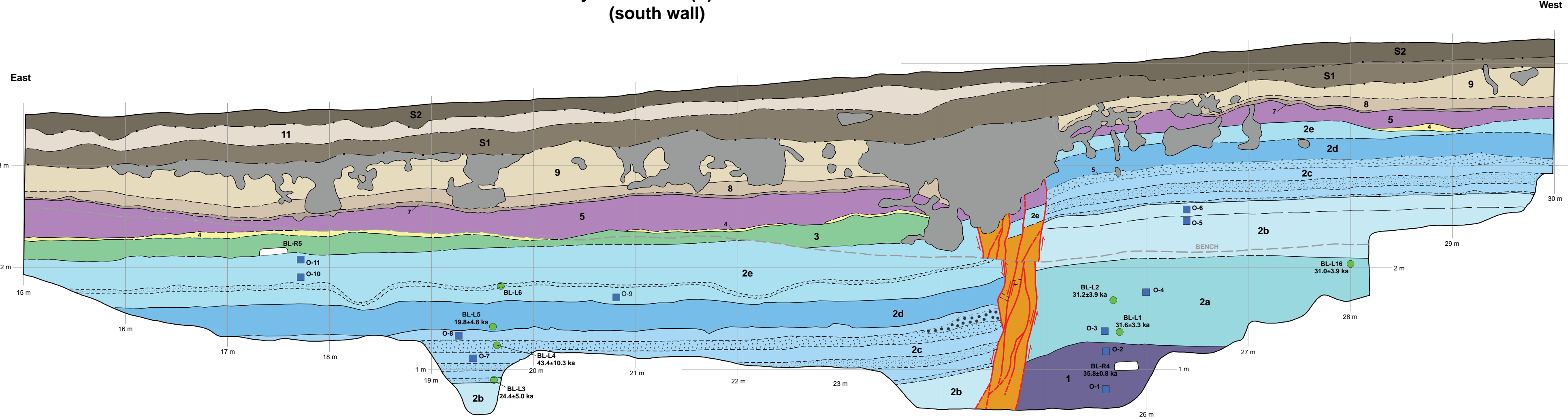


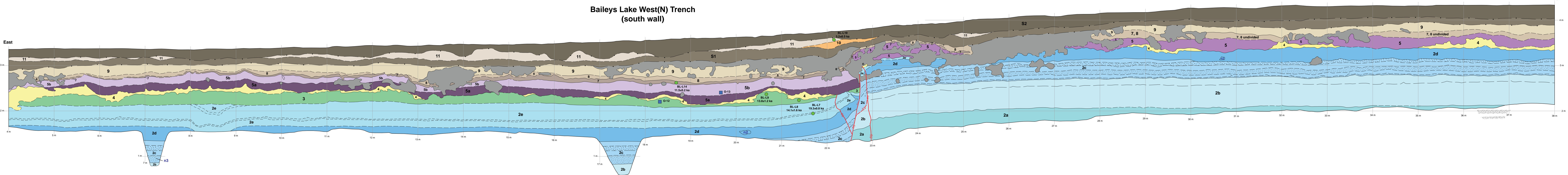### Photomosaic of Baileys Lake West(S) Trench (south wall)



## Baileys Lake West(N) Trench (south wall)



### Photomosaic of Baileys Lake West(N) Trench (south wall)



## Baileys Lake West(N) Trench (north wall, mirror image)
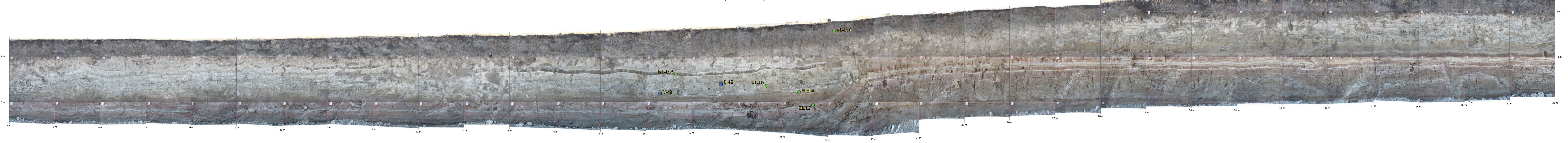


### Photomosaic of Baileys Lake West(N) Trench (north wall, mirror image)

## Baileys Lake East Trench (south wall)



### Photomosaic of Baileys Lake East Trench (south wall)



**STRATIGRAPHIC AND STRUCTURAL RELATIONS AT THE BAILEYS LAKE TRENCH SITE, GRANGER FAULT, WEST VALLEY FAULT ZONE**

by

Michael D. Hylland, Christopher B. DuRoss, Greg N. McDonald, Susan S. Olig, Charles G. Oviatt, Shannon A. Mahan, Anthony J. Crone, and Stephen F. Personius

2014